Forces and Stability in Ternary Colloidal Systems:

Evidence of Synergistic Effects

Shunxi Ji

Dissertation submitted to the faculty of the Virginia Polytechnic Institute and State University in partial fulfillment of the requirements for the degree of

Doctor of Philosophy

In

Chemical Engineering

John Y. Walz

William A. Ducker

Richey M. Davis

Stephen M. Martin

April 15, 2014

Blacksburg, VA

Keywords: Depletion forces, structural forces colloidal stability, depletion force model, nanoparticle halos

Forces and Stability in Ternary Colloidal Systems: Evidence of Synergistic Effects

Shunxi Ji

Abstract

Understanding and controlling the forces between colloidal particles in solution, along with the resulting stability of a dispersion of such particles, continues to be at topic of great interest. Although most laboratory studies focus on model systems in which the number of system species is kept to a minimum, real colloidal systems can be much more complex, consisting of multiple components that can vary greatly in size, charge, shape, etc. This dissertation focused on a topic that has received very little prior study, namely synergistic effects that can arise in mixed colloidal systems in which the resulting force and stability of the system cannot be predicted using results obtained in more idealized systems consisting of fewer components.

Two specific systems were studied. The first was a ternary system of particles in which micron-sized particles were in a dispersion containing both nanoparticles and submicron particles. It was shown through both computation modeling and direct force measurements that the nanoparticles can create attractive forces between the micron and submicron particles such that a halo of submicron particles is formed. This halo results in long range forces between the microparticles that cannot be predicted from measurements in systems containing only nanoparticles or only submicron particles. In addition, the forces can be large enough to alter the stability of a dispersion of these microparticles.

The second system consisted of microparticles in a solution containing nanoparticles and a polyelectrolyte, specifically poly(acrylic) acid. Again, through modeling and experimentation, it was found that complexation of the nanoparticles and polyelectrolyte molecules led to depletion and structural forces between the microparticles that were substantially greater than the sum of the forces measured in systems of only nanoparticles or only polyelectrolyte. It was also found that these greater forces could lead to destabilization of a dispersion of microparticles that was stable when only nanoparticles or only polyelectrolyte was present.

While these results clearly demonstrate the difficulty associated with predicting forces and stability in mixed colloidal systems, they also indicate that such systems offer new and interesting opportunities for controlling stability that clearly warrant additional study.

Table of Contents

List of Figures

List of Tables

1. Introduction

Colloidal suspensions have extensive applications in various fields. Researchers and scientists use them for ceramics processing, water purification, drug delivery systems, etc. As a result, predicting and controlling the stability of such dispersions, which is determined in large part by the interaction forces between the dispersed phases, continues to receive significant study. Traditionally, control of colloidal stability is achieved by manipulating the electrostatic repulsive force between charged particles, such as by adjusting the solution pH or ionic strength, or by creating repulsive steric forces via adsorbing polymer or surfactant[1,2].

Investigations of colloidal forces, either computationally or experimentally, have traditionally involved relatively ideal systems in which the number of components in the system have been kept to a minimum. For example, studies investigating the depletion force that arises when a negatively adsorbing species is added to a dispersion of colloidal particles typically assume that only one 'depletant' is present. Real colloidal systems however, either in nature or industry, are rarely so ideal. Instead, many different species may be present, each of which can have an impact on the depletion force and resulting dispersion stability.

In such systems, the simplest approach for predicting the net interparticle force would be to assume that each species acts independently, meaning that the resulting force would simply be the sum of the forces produced by each component. To date, however, there have been very few studies that address whether such assumption is even remotely valid.

This dissertation focused on understanding interparticle forces and stability in two different types of multi-component (ternary) colloidal systems. The specific goal was to determine whether synergistic effects were present in which the resulting forces and stability could not be determined from studies in simpler, binary-component systems.

The first system was a ternary particle system in which micron-sized particles (microparticles) were dispersed in a system in a liquid system containing two completely different types of particles, namely submicron particles and nanoparticles (i.e., one and two orders of magnitude smaller, respectively, than the microparticles). This investigation was motivated by earlier studies by Tohver *et al*.[3], who suggested that in a binary system containing only weakly-charged microparticles and highly charged nanoparticles, the nanoparticles could form a halo around the microparticles that could result in strong repulsive forces between the microparticles. In the work of Tohver *et al*., it was theorized that the haloing arises from either van der Waals or electrostatic forces between the nanoparticles and microparticles. Force measurements performed in this dissertation, however, showed that in these binary systems, the 'so-called' nanoparticle halo was most likely a result of simple irreversible deposition of the nanoparticles onto the microparticle surface.

By comparison, in the ternary system studied here, the halo (of submicron particles) arises from attractive depletion forces between the micron and submicron particles produced by the presence of the nanoparticles. Thus there is a clear synergistic effect that arises from having both nanoparticles and submicron particles present in the system.

The second system studied involved a different type of synergism, namely one that arises from the complexation of nanoparticles and polymers. The specific system consisted of silica microparticles dispersed in a solution of silica nanoparticles and poly(acrylic) acid polymer. Through modeling and experimentation, it was found that this complexation resulted in interparticle forces between the microparticles, specifically depletion and structural forces that were substantially greater than the sum of the forces measured in systems of only nanoparticles or only polyelectrolyte. It was also found that these greater forces could lead to destabilization of a dispersion of microparticles that was otherwise stable when only nanoparticles or only polyelectrolyte was present.

The results of these studies clearly demonstrate that predicting forces and stability in complex, mixed colloidal systems using only results from more ideal, binary component systems can lead to both quantitative and even qualitative errors. Nonetheless, the results also show that such multi-component systems offer new and interesting approaches to controlling the stability of a colloidal system.

2. LIterature Review

2.1. *Theoretical Prediction of Depletion Forces*

In a charged colloidal system, interactions between particles include van der Waals and electrostatic forces. However there are also attractive depletion forces existing in solutions of colloidal particles with asymmetric sizes. The origin of this force can be explained by the local osmotic pressure difference that can arise in such a solution. In a solution containing both large and small particles, small particles can be depleted from the gap between large particles when the large particle separation is small enough, such that the osmotic pressure induced by small particles is lower in the gap than that in the bulk. This osmotic pressure difference results in an attractive force between the larger particles, known as the depletion force. At a sufficiently high a concentration of small particles, an oscillatory small particle density profile around each large particle surface exists due to multi-particle interactions. This profile creates an oscillatory force between the larger particles that has been termed the structural force.

Theoretical prediction of depletion forces has been studied extensively by different researchers. The earliest and undoubtedly most famous analytical expression of depletion forces was proposed by Asakura and Oosawa[4, 5]. These authors first predicted depletion forces between two parallel plates immersed in a solution of negatively-adsorbing macromolecules. Their prediction was based on changes in the excluded volume of the system that arose when two particles approached significantly close that nanoparticles became depleted from the gap region. (When this occurs, the free volume of the system actually increases, which is energetically favorable.) They later predicted depletion forces between two large spherical particles in a solution of macromolecules using this same approach.

Although this represented the first theoretical (and satisfactory) explanation of the depletion effect, the model of Asakura and Oosawa still had a number of limitations. First, the model ignored interactions between macromolecules themselves. Second, interactions between particles in the model were assumed to be hard-wall interactions, meaning that the interaction force between the macromolecules and particles was equal to zero until they come into contact, at which point the force was infinitely repulsive.

The depletion force between two uncharged plates in a solution of non-adsorbing polymers was calculated by Feigin and Napper[6]. They first used a Monte-Carlo simulation method to obtain the polymer segment concentration profile between the plates. Then the profile was coupled with the Flory-Huggins expression so that the actual depletion force could be calculated. The Derjaguin approximation was also used to convert the depletion force between two plates into that between two spherical particles. Their model was capable of predicting a long-range repulsion, which was due to ordering of macromolecules in the gap region between the plates or particles.

Mao *et al*.[7] obtained the depletion forces in a solution system of hard spheres using the Henderson equation. The equation reduced the problem of calculation to simply finding the concentration profile of macromolecules within the gap between two large particles. Second and third order effects of macromolecule concentrations were also included, which resulted in the prediction of a long range structural repulsion and attraction.

Walz and Sharma[8] also developed a theoretical expression of depletion forces between large colloidal spherical particles in a solution of macromolecules. The model essentially sums equilibrium forces applied to each colloidal particle by all macromolecules in the solution. It also takes into account the interactions between macromolecules themselves. In this model, all species are assumed to interact through a hard wall interaction plus a long range electrostatic repulsion. Because interactions between the macromolecules were included, a long range repulsive force (the onset of the structural interaction) is also predicted. The results showed that the presence of charge could substantially increase both the magnitude and range of the depletion and structural forces. More detail about this model is given in the theory section.

Piech and Walz[9] investigated the effect of polydispersity in the macromolecule sizes and surface potentials on depletion attractions and structural repulsions between two charged large particles. They first incorporated log-normal distributions with the equilibrium force model of Walz and Sharma[8]. The model showed that polydispersity in surface potentials has only a very small effect on the force profile. However at a constant macromolecule volume fraction, polydispersity can decrease the magnitudes of both the depletion attraction and structural forces. At a constant macromolecule number density, polydispersity increases the magnitude of the depletion attraction but lowers that of the long range structural forces.

Later, Piech and Walz[10] modified the equilibrium force model in order to obtain the depletion force between two microparticles in a solution of nano-spheroids. They also developed analytical expressions for calculating the depletion forces induced by charged spheres and spheroids

Other work on depletion and structural forces can be found in references 11-23.

2.2. Experimental Measurements of Depletion Forces

Sharma and Walz[24] measured the interaction energy between a polystyrene microparticle and a glass plate in a solution of silica nanoparticles using total internal reflection microscopy (TIRM). The measured energy profile showed both a short-range attraction and long-range structural repulsion, even at nanoparticle concentrations as low as 0.05% vol. The experimental results also verified the force balance model of Walz and Sharma[8].

Odiachi and Prieve[25] also used TIRM to measure the depletion interaction between a 6 μm polystyrene particle and glass slide in a solution of laponite clay nanoparticles. The nanoparticle solution in the experiment contained 1mM NaCl. Their results showed an attractive depletion force between the microparticle and slide at separations as large as 200 nm, which greatly exceeded the average size of laponite nanoparticles (25 nm). With increasing nanoparticle concentrations, the magnitude of the depletion attraction increased, however the range remain unchanged. They also showed that increasing the salt concentration could decrease both the magnitude and range of the depletion force.

Piech and Walz[26] measured depletion and structural forces in charged systems with controlled levels of polydispersity. The force data was collected between a silica microparticle and slide in a solution of polystyrene/silica nanoparticles using the colloidal probe atomic force microscopy (CP-AFM) technique. The force profile showed clear oscillatory features in the presence of nanoparticles. If all the nanoparticles had

the same surface potentials, the magnitude of oscillation increased with an increasing portion of larger nanoparticles in the solution at a constant nanoparticle number density. On the other hand, the magnitude decreased with increasing portion of larger nanoparticles in the solution at a fixed nanoparticle volume fraction. If the size of nanoparticles was constant, the same trend could be obtained if the portion of more highly charged nanoparticles was increased. They also compared their experimental results to those predicted using the force balance model developed for systems with polydispersity[9]. The agreement between experimental and theoretical data was better at lower nanoparticle concentration because the model used only a 2nd order virial expansion to predict density distributions.

Piech *et al.*[15] investigated the depletion interaction between two microparticles next to a flat wall using the hydrodynamic force balance (HFB) technique. They used this technique to obtain the breakup force of a silica or polystyrene microparticle doublet in a solution of silica/polystyrene nanoparticles. The doublets formed in solution because of depletion attractions between the particles. The breakup forces were essentially that required to drag one of the particles away from the other one. The measured results matched the prediction obtained used the force balance model of Walz and Sharma[8].

Helden *et al.*[27] performed total reflection microscopy (TIRM) measurements and acquired the depletion potential between a polystyrene microparticle and silica plate in a solution of colloidal rods. The van der Waals interaction was negligible due to the use of DMF as the solvent. Their results showed that the magnitude of the depletion attraction increased with increasing concentration of rods when no salt was present in the solution. With the addition of salt, both the range and magnitude of the depletion attraction decreased. The reason they suggested was that the higher concentration of salt resulted in shorter Debye lengths, which decreased the effective size of the rods.

Other experimental measurement of the depletion and structural forces are provided in references 28-50.

In addition to these direct measurements of the force or energy of interaction, the effect of depletion interactions on destabilizing colloidal systems, frequently termed depletion flocculation, has also been heavily researched for many years. The earliest documented report can be traced to the work of Bondy,[51] who observed the creaming of natural rubbers by water-soluble polymers. Subsequent studies by Sharma *et al.*,[52] Cowell *et al.*[53] and Sperry *et al.*[54] have been performed to investigate both the critical flocculation and critical restabilization concentrations (i.e., minimum depletant concentrations needed for flocculation and restablization, respectively.) This restabilization arises from long-range structural repulsions that result from the ordering of the depletants in the gap region between interacting particles at increasing depletant concentrations. In addition to particles[55-58], depletion flocculation of liquid drops[32,33] and bacteria[59] have also been studied.

2.3. Nanoparticle Halos in Binary Systems

In 2001 Tohver *et al.*[3, 60] proposed a new mechanism of stabilization known as nanoparticle halos. These authors discovered that at pH 1.5, a colloidal solution of silica microspheres would undergo a series of phase transitions from flocculation → stable fluid → flocculation with increasing zirconia nanoparticle concentration in the system. At

this pH value, silica microparticles are negligibly positively charged and zirconia nanoparticles are highly positively charged. The flocculation in the beginning was due to the van der Waals attraction between the silica microparticles. The flocculation in the end was due to the depletion attraction induced by highly concentrated zirconia nanoparticles. However the stable fluid resulted from nanoparticle halos. Tohver *et al*. proposed that the zirconia nanoparticles could 'encircle' each microparticle when the nanoparticles were within a specific range of concentration. Instead of directly depositing on microparticle surfaces, nanoparticles would be slightly separated from microparticles. Those 'haloed' nanoparticles could increase the repulsion between silica microparticles.

The possible reason of this phenomenon was also proposed. Since the interaction between nanoparticles was highly repulsive and the one between nano- and microparticles was weakly repulsive, the nanoparticles were 'pushed' against the microparticles surfaces by the nanoparticles in the bulk. While the net repulsive interaction between the microparticles and nanoparticles was weak, it was believed to be sufficient to prevent strong deposition of the nanoparticle on to the microparticle surface.

Tohver *et al.*[60] also theoretically investigated nanoparticle halos with DLVO theory and the force balance model developed by Walz and Sharma[8]. They showed that the depletion attraction arising due to nanoparticles, which increased with increasing nanoparticle concentration, could be large enough to result in silica microparticle flocculation at nanoparticle concentrations above an upper critical value.

Chan and Lewis[61] studied nanoparticle halos in a solution of silica microparticles and polystyrene nanoparticles at pH 3, at which the interaction between micro- and nanoparticles was weakly repulsive. They first investigated the fluorescence intensity of fluorescently labeled polystyrene nanoparticles in the supernatant solution after microparticles settled under gravity so that the adsorption of nanoparticles on the microparticles could be analyzed. The result showed the adsorption reached a rather modest plateau with increasing nanoparticle concentration, which proved only rather weak adsorption existed in the system. The adsorption test result was consistent with the zeta potential measurements which showed that the zeta potential reached a quite low plateau value with increasing nanoparticle concentration. The sedimentation velocity of silica microparticles was also analyzed. The measurements showed that at nanoparticle concentrations large enough to induce nanoparticle halos, the sedimentation velocity was substantially lower than that without halos.

Luijten and coworkers[62-66] investigate halo effects in colloidal mixtures of silica microparticles and zirconia nanoparticles at pH 1.5 by using a Monte Carlo simulation method. The authors showed that at the very low concentrations of nanoparticles used in the experiments of Tohver *et al*., the repulsion between nanoparticles in the bulk was too weak to explain the formation of a halo. To overcome this, they proposed that a weak attraction existed between the nanoparticles and microparticles, which could arise from either truncated van der Waals forces, or an electrostatic attraction that can arise between surfaces with very different surface potentials (even though the sign of the potentials are the same). At high nanoparticle concentrations, the induced effective interaction between microparticles showed a primary energy well due to depletion forces that was large enough to cause flocculation of microparticle solutions.

The size ratio effects of particles in the solution on nanoparticle halos was studied by Chan and Lewis[67]. Increasing the nanoparticle size was found to narrow the window of stability at constant size of microparticles. On the contrary, smaller microparticles could broader the window of stability if the effective sizes of nanoparticles were kept constant.

Chavez-Paez[68] investigated the existence of nanoparticle halos using the Ornstein-Zernike integral equation coupled with the hyper-netted chain approximation closure. The model solution consisted of particles with high asymmetry of sizes and surface potentials. They showed an effective attraction could exist between nanoparticles and microparticles in the solution even when they were similarly charged. The results even predicted the oscillatory density profile of nanoparticles. However only electrostatic interactions between particles was considered.

The behavior of alumina microparticles in a solution of silica nanoparticles suggested the existence of nanoparticle halos in a different system as studied by Kong *et al.*[69]. They first investigated the interactions between microparticles and nanoparticles at pH 9.5. Their TEM pictures of the mixture showed no adsorption of silica particles on the alumina particle surfaces. The calculated DLVO energy profile, which consisted of a large primary energy barrier, also confirmed the lack of nanoparticle adsorption in the system. They experimentally proved that the sedimentation of alumina microparticles was much slower at a specific concentration of silica nanoparticles. Also by theoretically counting the number of silica particles forming halos around alumina particles, they justified that the slow sedimentation of alumina particles was due to nanoparticle halos.

Zhang *et al.*[70] investigated nanoparticle halos using ultrasmall-angle X-ray scattering (USAXS). They determined that the separation distance between a microparticle and halo nanoparticle was 2 nm in the system, which was also equivalent to the solution Debye length. They also showed that nanoparticle concentration within the halos was much higher than that in the bulk solution and determined that the lateral separation between halo particles greatly succeeded their effective sizes.

Hong and Willings[71] performed measurements on transition forces between a silica microparticle and plate in a solution of zirconia nanoparticles at pH 1.5. Their results showed the force between the silica microparticle and plate went from pure attraction to strong repulsion with increasing nanoparticle concentration in the system. They claimed that the repulsions were due to the presence of nanoparticle halos. Specifically with a nanoparticle volume fraction of $1x10^{-5}$, a 'meta-stabilization' peak existed at microparticle separation of 2.3nm, which was also the separation between microparticles and halo particles.

McKee and Walz[72] performed colloidal probe atomic force microscopy studies (CP-AFM) measurements to measure the force between a glass microparticle and plate in a solution of zirconia or polystyrene nanoaprticles. The radii of glass spheres, polystyrene and zirconia nanoparticles were 5 μm, 11nm and 6 nm respectively. Their results showed that upon addition of nanoparticles, the surface potentials of microparticle increased, which resulted in a substantially higher electrostatic repulsion between the silica microparticle and plate. The increasing surface potentials were due to the direct deposition of nanoparticles on microparticle surfaces. They claimed that the reason why the nanoparticles had direct contact with the microparticle surfaces instead

of forming halos was because of impurities on the glass surfaces. The metallic ions on the glass surfaces could form charges opposite to that on nanoparticle surfaces.

2.4. Depletion Forces in Complex Polymer Mixtures

In essentially all of these prior studies, the depletion force was created by a single component. Real systems, of course, are normally not so simple but can contain two or more components that can contribute to the force. For example, many commercial dispersions may contain various types of polymers, surfactants, and dispersed particles or droplets. While some studies on the effects of polydispersity in the size and charge of the depletant have been performed,[5,29-31] very few comprehensive studies of the depletion force arising from mixtures have been documented.

One exception is the work of Tulpar *et al*.,[73] who used colloidal probe atomic force microscopy (CP-AFM) to measure the force profile between a 5 μm diameter silica sphere and silica plate in mixtures of Pluronic F108, a neutral triblock copolymer, and sodium dodecylsulfate (SDS) surfactant. These authors found that no depletion forces could be detected between a silica microparticle and a silica plate in solutions of either only polymers or only surfactants with a surfactant concentration below the critical micelle concentration (CMC). However a significant depletion attraction was detected upon mixing the two materials, even if the surfactant concentration was still below the CMC. The onset of the depletion force was attributed to the adsorption of negatively charged surfactants on each neutral polymer molecule. As a result, large complex polyelectrolytes were formed that significantly increased the depletion force between two large silica surfaces.

As clearly demonstrated by Tulpar *et al*., the depletion interaction arising in mixtures of two components can be substantially greater than simply the sum of the interaction arising from each component independently. Specifically, such synergistic effects can arise when the depletants interact (e.g., aggregate) in a way such that substantially larger depletant complexes are created.

3. Theoretical Prediction of Depletion Forces in a Binary System

3.1. Interaction Forces between Two Colloidal Particles

Our goal in this section is to present the equations describing the interaction force between two colloidal particles in a solution containing a negatively adsorbing nanoparticle species. (For comparisons to the results from the CP-AFM measurements, which utilize a sphere-plate geometry, we utilize the Derjaguin approximation, which states that the force between a sphere and plate is approximately twice that between two equal spheres.)

We assume that in our systems, the force can be represented as the sum of an electrostatic repulsion, a van der Waals attraction, and a depletion/structural force. Thus

$$F_{total}(h)=F_{electro}(h)+F_{vdw}(h)+F_{depletion}(h) \quad [3.1]$$

Each of these contributions is described in greater detail below.

3.2. Electrostatic Interactions between Two Colloidal Particles

The linear superposition approximation (L.S.A) is used to predict electrostatic interactions between any two colloidal particles. It was developed by Bell *et al.*[74] in 1970. It is assumed that the surface potential at a point between two particles can be obtained by summing the potentials contributed by each particles at the same point. The resulting equation is

$$F=4\pi\varepsilon_0\varepsilon_n\left(\frac{kT}{e}\right)^2 Y_1 Y_2(1+\kappa R)\frac{a_1 a_2}{R^2}e^{-\kappa(R-a_1-a_2)} \quad [3.2]$$

where ε_0 and ε_n are the permittivity of free space and water, Y_1 and Y_2 are the effective reduced surface potentials, κ is the inverse Debye length, a_1 and a_2 represent the radii of the interacting particles, and R is the center to center distance between two particles.

After integration of the force as

$$E_{elec}=\int_{\infty}^{R} F(R')\,dR' \quad [3.3]$$

the electrostatic energy can be calculated as

$$E_{elec}=4\pi\varepsilon_0\varepsilon_n\left(\frac{kT}{e}\right)^2 Y_1 Y_2\frac{a_1 a_2}{R}e^{-\kappa(R-a_1-a_2)} \quad [3.4]$$

Although equations [3.2] and [3.4] are more accurate for a gap widths larger than several Debye lengths, Bell *et al.*[74] state that for absolute surface potentials of less than 100 mV, these two equations overestimate the actual values at a gap width of one Debye length by only about 10%. The Matlab programs used to calculate the effective surface potentials and electrostatic interactions are provided in Appendix A2.

3.3. *The Van der Waals Contribution to the Force*

The van der Waals interaction between two particles is calculated as

$$E_{VDW}(h)=-\frac{A_0}{6(1+14h/\lambda)}\left[\frac{2a_1a_2}{R^2-(a_1+a_2)^2}+\frac{2a_1a_2}{R^2-(a_1-a_2)^2}+\ln\frac{R^2-(a_1+a_2)^2}{R^2-(a_1-a_2)^2}\right] \quad [3.5]$$

where h is the separation distance, R is the center-to-center distance ($R = h+a_1+a_2$), A_0 is the non-retarded Hamaker constant, and λ is the retardation wavelength. This equation is the original expression of Hamaker[75] with a modification suggested by Gregory[76] to account for retardation effects.

The values of A_0 and λ were calculated by first using Lifshitz theory to calculate the Hamaker constant characterizing the interaction between two planar half spaces of the same materials as the spherical particles of interest versus separation distance between the half spaces. As described by Prieve and Russel[77], the Lifshitz equations needed to calculate the Hamaker constant between two half spaces of materials 1 and 2 separated by material 3 can be expressed as

$$A=-\frac{3}{2}kT\sum_{n=0}^{\infty}{}'\int_{r_n}^{\infty}x\left\{ln\left[1-\Delta_{13}\Delta_{23}e^{-x}\right]+ln\left[1-\bar{\Delta}_{13}\bar{\Delta}_{23}e^{-x}\right]\right\}dx \quad [3.6]$$

$$\Delta_{jk}=\frac{\varepsilon_j s_k-\varepsilon_k s_j}{\varepsilon_j s_k+\varepsilon_k s_j} \quad [3.7]$$

$$\bar{\Delta}_{jk}=\frac{s_k-s_j}{s_k+s_j} \quad [3.8]$$

$$s_k=\sqrt{x^2+\left(\frac{2\xi_n h}{c}\right)^2\left(\varepsilon_k-\varepsilon_3\right)} \quad [3.9]$$

$$r_n=\frac{2h\xi_n\sqrt{\varepsilon_3}}{c} \quad [3.10]$$

$$\xi_n=\frac{2\pi nkT}{\hbar} \quad [3.11]$$

$$\varepsilon(i\xi)=1+\sum_j\frac{d_j}{1+\xi\tau_j}+\sum_j\frac{f_j}{\omega_j^2+g_j\xi+\xi^2} \quad [3.12]$$

Note that the first term in the summation of equation [3.6] is multiplied by 0.5. Also h is the surface separation. c is the speed of light in vacuum. $\hbar$ is Planck's constant multiplied by 2π, and d_j, τ_j, f_j and ω_j are constants used in fitting the dielectric spectra data for the various materials. The values of the constants used in the calculation are listed in Table 3.1.

Table 3.1. The values of the constants used in calculating the Hamaker constant.

eV (1 electron volt)	1.601e-19 J
k (Boltzmann's constant)	8.6173e-5 eV/K
T (temperature)	298K
c (speed of light in vacuum)	2e8 m/s
$\hbar$ (adjusted Planck's constant)	6.5821e-16 eVs

The variable A_0 was set to be equal to the value of this Hamaker constant at zero separation, while λ was obtained by fitting the Hamaker constants to the expression $\frac{A_0}{(1+14h/\lambda)}$, which again is the retardation correction factor given by Gregory[76].

In the work described in this dissertation three materials were used in the measurements, which were silica, polystyrene and water. The spectra data for these materials is listed in Tables in Appendix A4. The results of calculation are listed in Table 3.2.

Table 3.2. Hamaker constants and retardation wavelengths of the materials in water.

	Silica-silica	Silica-polystyrene	Polystyrene-polystyrene
Hamaker constant (J)	0.76e-20	0.99e-20	1.36e-20
Retardation wavelength/nm	85	105	130

The Matlab programs that were used to perform the Lifshitz calculations are provided in Appendix A1.

3.4. Depletion/Structural Contribution to the Force

We describe here the force balance model of Walz and Sharma[8] to predict the depletion force between two charged microparticles in a solution of charged depletants at relative low depletant concentrations (e.g, order 1% vol. or less). More details of the model can also be found in Weronski and Walz[12].

The model system consists of two microparticles of radii of R_1 and R_2 immersed in a solution of nanoparticles with radii of a and bulk number density ρ_{nano}. A schematic is shown in Figure 3.1.

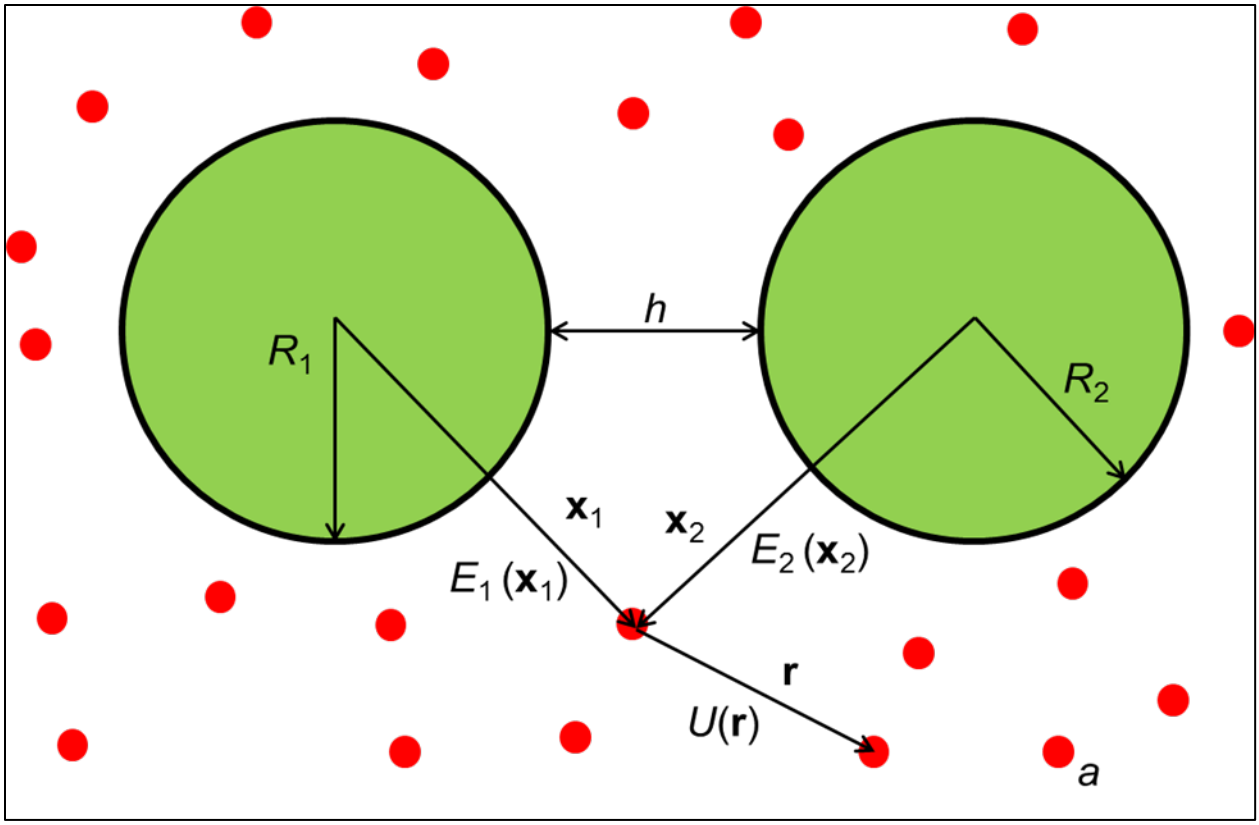

Figure 3.1. Schematic defining the variables in a system consisting of only microparticles and smaller particles (e.g., nanoparticles).

The depletion force exerted on particle 1 can be obtained by summing forces applied on particle 1 by all nanoparticles in the system. Mathematically this can be written as

$$\mathbf{F}_{depletion}(h) = -\int_{\boldsymbol{x}_1} \rho(\boldsymbol{x}_1, \rho_{nano}) \nabla E_1(\boldsymbol{x}_1, \rho_{nano})\, d\boldsymbol{x}_1 \qquad [3.13]$$

where $\rho(\mathbf{x}_1, \rho_{nano})$ is the local number density of nanoparticles at position $\mathbf{x}_1$, $-\nabla E_1(\mathbf{x}_1, \rho_{nano})$ is the force exerted on particle 1 by the nanoparticle at position $\mathbf{x}_1$, and the integration is performed over all space. Both of these parameters are functions of ρ_{nano}, which is the nanoparticle number density in bulk. The local number density of nanoparticles can be expressed as

$$\rho(\boldsymbol{x}_1, \rho_{nano}) = \rho_{nano} exp\left[-\frac{E_m(\boldsymbol{x}_1, \rho_{nano})}{kT}\right] \times \left[1 + b(\boldsymbol{x}_1, \rho_{nano})\rho_{nano}\right] \qquad [3.14]$$

where E_m is the local energy potential at position $\mathbf{x}_1$, and b is the secondary virial coefficient, which accounts for the interaction between nanoparticles.

The model assumes that local energy potential at any position of the solution can be calculated as the sum of interaction energies with particles 1 and 2. Thus combining equations [3.13] and [3.14] yields the following expression for the depletion force

$$\mathbf{F}_{depletion}(h) = -\int_{\mathbf{x}_1} \rho_{nano} exp\left[-\frac{E_1(\boldsymbol{x}_1)+E_2(\boldsymbol{x}_1)}{kT}\right] \times\left[1+b(\boldsymbol{x}_1)\rho_{nano}\right]\nabla E_1(\mathbf{x}_1)\, d\mathbf{x}_1 \quad [3.15]$$

where E_1 and E_2 are the pair potentials between a nanoparticle and two microparticles respectively.

Bellemans[78] and Fischer[79] developed a virial expansion for the distribution function for the case of planar boundaries and hard sphere-hard wall interactions. Anderson and Brannon[80] and Glandt[81] later applied this approach to the case of hard spheres inside rectangular, cylindrical and spherical pores. Walz and Sharma[8] simplified the results from Glandt and proposed that the calculation of the 2nd virial coefficient, *b*, can be obtained from superposition of effects of each interaction of nanoparticle and microparticle as

$$b = b_1(\boldsymbol{x}_1) + b_2(\boldsymbol{x}_2) \quad [3.16]$$

where b_1 and b_2 are the virial coefficients between a nanoparticle and corresponding microparticles at a specific position in the solution. A general expression for these virial coefficients is

$$b_i(\mathbf{x}_i) = \int_{\mathbf{r}} \left[\exp\left(\frac{-E_i(\mathbf{x}_i+\mathbf{r})}{kT}\right)-1\right] \times \left[\exp\left(\frac{-U(\mathbf{r})}{kT}\right)-1\right] d\mathbf{r} \quad [3.17]$$

where *i* is equal to 1 or 2, U(r) is the pair potential between a nanoparticle and another nanoparticle in the solution, and the integration is again over all volume.

Once the depletion force is calculated, the corresponding depletion energy between two interacting microparticles separated by distance *h* is calculated as

$$E(h) = -\int_{\infty}^{h} F(h')dh' \quad [3.18]$$

where $F(h')$ is the component of the force vector acting along the line of centers between the two particles.

The Matlab program used to calculate the depletion and structural interactions using this model is provided in Appendix A2.

3.5. Prediction of Depletion Forces Using an Approximate Square Well Model

In this project, a simplified depletion force model was also developed. The idea is using a square well energy model to simulate the interactions between microparticles and nanoparticles allow the development of analytical expressions for the depletion force between two large particles of equal size. Because the model ignores the higher-order concentration effects, the depletion results only depend on the nature of pair potentials between micro- and nanoparticles. The advantage of the square well model is that the program is able to run much faster than the rigorous model. In addition, it can be used as a check of the results from the more rigorous model.

In the square well model, the pair potentials between large and small particles are expressed as

$$E_{large\text{-}small}=\begin{cases}\infty & \text{if } d\le\tau_1\\ -kT\,ln(1+\varepsilon_1) & \text{if } \tau_1<d\le\tau_2\\ -kT\,ln(1-\varepsilon_2) & \text{if } \tau_2<d\le\tau_3\\ 0 & \text{if } d>\tau_3\end{cases} \qquad [3.19]$$

where the definitions of parameters are shown in figure 3.2.

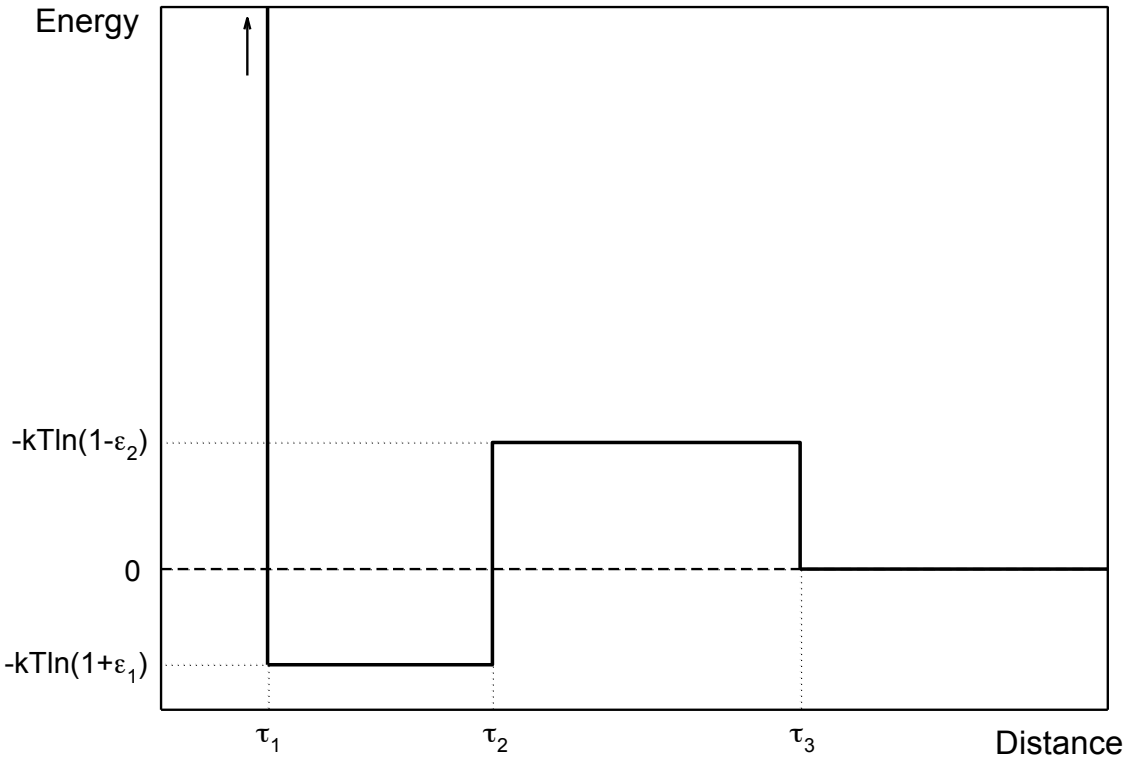

Figure 3.2. Definition of the parameters used in the approximate square-well model.

Here τ_1, τ_2 and τ_3 are the distance parameters, ε_1 and ε_2 are the parameters that determine the energies, and *d* represents surface separations between large and small particles. By setting pair potentials as Figure 3.7, we can simulate a wide variety of energy profiles between large and small particles. For example, by setting ε_1 and ε_2 to 0, a hard wall energy profile can be obtained.

By substituting equation [3.19] into equation [3.15] and setting the secondary varial coefficient to zero, an analytical solution for equation [3.19] can be obtained. After the calculation above, the total depletion force will be equal to the sum of each of the eleven terms in table 3.3 multiplied by $-2\pi\rho_\infty kT$. In other words

$$F_{total}=-2\pi\rho_\infty kT\sum_{i=1}^{11} Term\ i \qquad [3.20]$$

Note that for each term, the value of the term is zero when center-center distance *l* is outside of the indicated limits.

Table 3.3. The terms in the analytical solution for depletion forces.

Term	Contributions of the depletion force	Limits of l
1	$(1+\varepsilon_1)(R+a+\tau_1)^2\left(\frac{1}{2}\right)\left\{1-(1+\varepsilon_1)\left[\frac{l}{2(R+a+\tau_1)}\right]^2 + \varepsilon_1\left[\frac{(R+a+\tau_1)^2+l^2-(R+a+\tau_2)^2}{2(R+a+\tau_1)l}\right]^2\right\}$	$2R\le l\le 2(R+a+\tau_1)$
2	$\varepsilon_1(1+\varepsilon_1)(R+a+\tau_1)^2\left(-\frac{1}{2}\right)\left\{1-\left[\frac{(R+a+\tau_1)^2+l^2-(R+a+\tau_2)^2}{2(R+a+\tau_1)l}\right]^2\right\}$	$2(R+a+\tau_1)\le l\le 2R + 2a+\tau_1+\tau_2$
3	$\varepsilon_2(1+\varepsilon_1)(R+a+\tau_1)^2\left(\frac{1}{2}\right)\left\{\left[\frac{(R+a+\tau_1)^2+l^2-(R+a+\tau_2)^2}{2(R+a+\tau_1)l}\right]^2 - \left[\frac{(R+a+\tau_1)^2+l^2-(R+a+\tau_3)^2}{2(R+a+\tau_1)l}\right]^2\right\} - (\varepsilon_1+\varepsilon_2)(R+a+\tau_2)^2\left(\frac{1}{2}\right)\left\{1 - (1+\varepsilon_1)\left[\frac{(R+a+\tau_2)^2+l^2-(R+a+\tau_1)^2}{2(R+a+\tau_2)l}\right]^2 + \varepsilon_1\left[\frac{l}{2(R+a+\tau_2)}\right]^2\right\}$	$2R\le l\le 2R+2a+\tau_1+\tau_2$
4	$\varepsilon_2(1+\varepsilon_1)(R+a+\tau_1)^2\left(\frac{1}{2}\right)\left\{1-\left[\frac{(R+a+\tau_1)^2+l^2-(R+a+\tau_3)^2}{2(R+a+\tau_1)l}\right]^2\right\}$	$2R+2a+\tau_1+\tau_2 \le l \le 2R+2a+\tau_1+\tau_3$
5	$\varepsilon_1(-\varepsilon_1-\varepsilon_2)(R+a+\tau_2)^2\left(-\frac{1}{2}\right)\left\{1-\left[\frac{l}{2(R+a+\tau_2)}\right]^2\right\}$	$2R+2a+\tau_1+\tau_2\le l\le 2(R+a+\tau_2)$
6	$\varepsilon_2(-\varepsilon_1-\varepsilon_2)(R+a+\tau_2)^2\left(\frac{1}{2}\right)\left\{\left[\frac{l}{2(R+a+\tau_2)}\right]^2 - \left[\frac{(R+a+\tau_2)^2+l^2-(R+a+\tau_3)^2}{2(R+a+\tau_2)l}\right]^2\right\}$	$2R\le l\le 2(R+a+\tau_2)$

7	$\varepsilon_2(-\varepsilon_1-\varepsilon_2)(R+a+\tau_2)^2\left(\frac{1}{2}\right)\left\{1-\left[\frac{(R+a+\tau_2)^2+l^2-(R+a+\tau_3)^2}{2(R+a+\tau_2)l}\right]^2\right\}$	$2(R+a+\tau_2)\le l\le 2R+2a+\tau_2+\tau_3$
8	$\varepsilon_2(R+a+\tau_3)^2\left(\frac{1}{2}\right)\left\{1-(1+\varepsilon_1)\left[\frac{(R+a+\tau_3)^2+l^2-(R+a+\tau_1)^2}{2(R+a+\tau_3)l}\right]^2+\varepsilon_1\left[\frac{(R+a+\tau_3)^2+l^2-(R+a+\tau_2)^2}{2(R+a+\tau_3)l}\right]^2\right\}$	$2R\le l\le 2R+2a+\tau_1+\tau_3$
9	$\varepsilon_1\varepsilon_2(R+a+\tau_3)^2\left(-\frac{1}{2}\right)\left\{1-\left[\frac{(R+a+\tau_3)^2+l^2-(R+a+\tau_2)^2}{2(R+a+\tau_3)l}\right]^2\right\}$	$2R+2a+\tau_1+\tau_3 \le l\le 2R+2a+\tau_2+\tau_3$
10	$\varepsilon_1\varepsilon_2(R+a+\tau_3)^2\left(\frac{1}{2}\right)\left\{\left[\frac{(R+a+\tau_3)^2+l^2-(R+a+\tau_2)^2}{2(R+a+\tau_3)l}\right]^2-\left[\frac{l}{2(R+a+\tau_3)}\right]^2\right\}$	$2R\le l\le 2R+2a+\tau_2+\tau_3$
11	$\varepsilon_1\varepsilon_2(R+a+\tau_3)^2\left(\frac{1}{2}\right)\left\{1-\left[\frac{l}{2(R+a+\tau_3)}\right]^2\right\}$	$2R+2a+\tau_2+\tau_3\le l\le 2(R+a+\tau_3)$

The Matlab program for the square well model is listed in Appendix A3. In addition, a comparison of the profile predicted with this approximate model and the more rigorous model is presented in section 6.3.2.

4. Atomic Force Microscopy (AFM) Technique

4.1. Introduction

The AFM was invented by Binnig *et al.*[82] in 1986. In the beginning, its purpose was primarily to image the topography of conducting and insulating surfaces with atomic resolution. The schematic of an AFM used in this proposal is shown in figure 4.1.

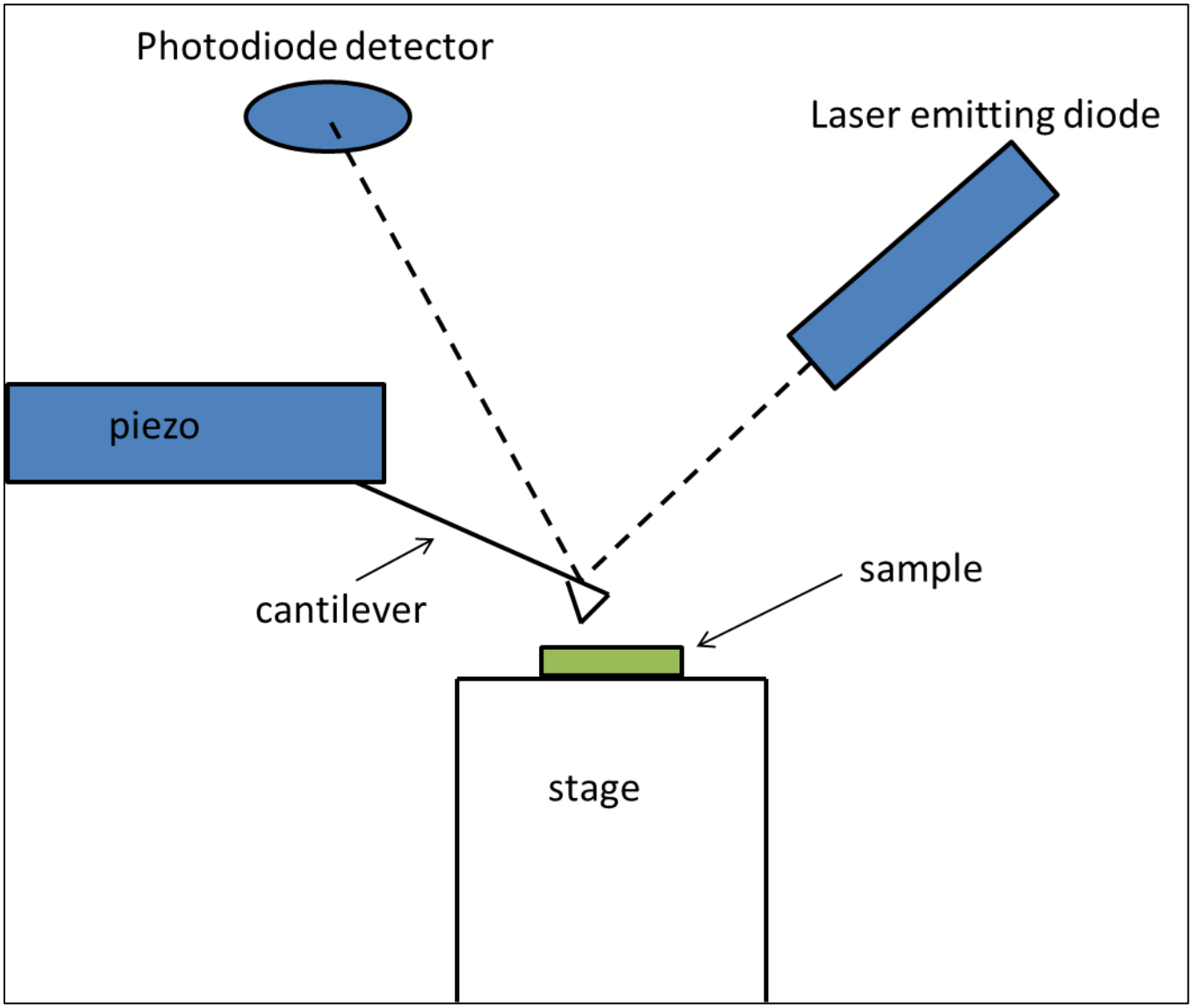

Figure 4.1. Schematic of AFM used in the work done in this proposal.

One way to scan a sample is based on the cantilever deflection as a function of tip position. As the piezo drives a cantilever both laterally and vertically, the cantilever deflects because of the interaction between the tip and the sample surface. The cantilever deflection is collected by the photodiode detector. Another way to acquire a surface image is to monitor the changes in height position of the piezo, which is

controlled by a feedback loop and programmed to maintain a constant force between tip and sample.

Another application of AFM is force measurement. It was first driven by the need to reduce tip-sample interaction so that fragile materials can be imagined. The first force measurement on a scale of colloidal systems in an aqueous environment was reported by Butt[83]. Ducker *et al*.[84, 85] first conducted direct force measurements between a microsphere and a plate in an aqueous solution. This was performed by attaching a micro-scale particle onto the tip of a cantilever so that the force exerted on the cantilever primarily results from the microsphere-plate interaction. This method was also used in this proposal and details will be given in subsequent sections.

4.2. Particle Mounting Procedure

In this project, glue is used to attach microspheres onto the tips of cantilevers. The schematic of particle mounting apparatus is shown in figure 4.2.

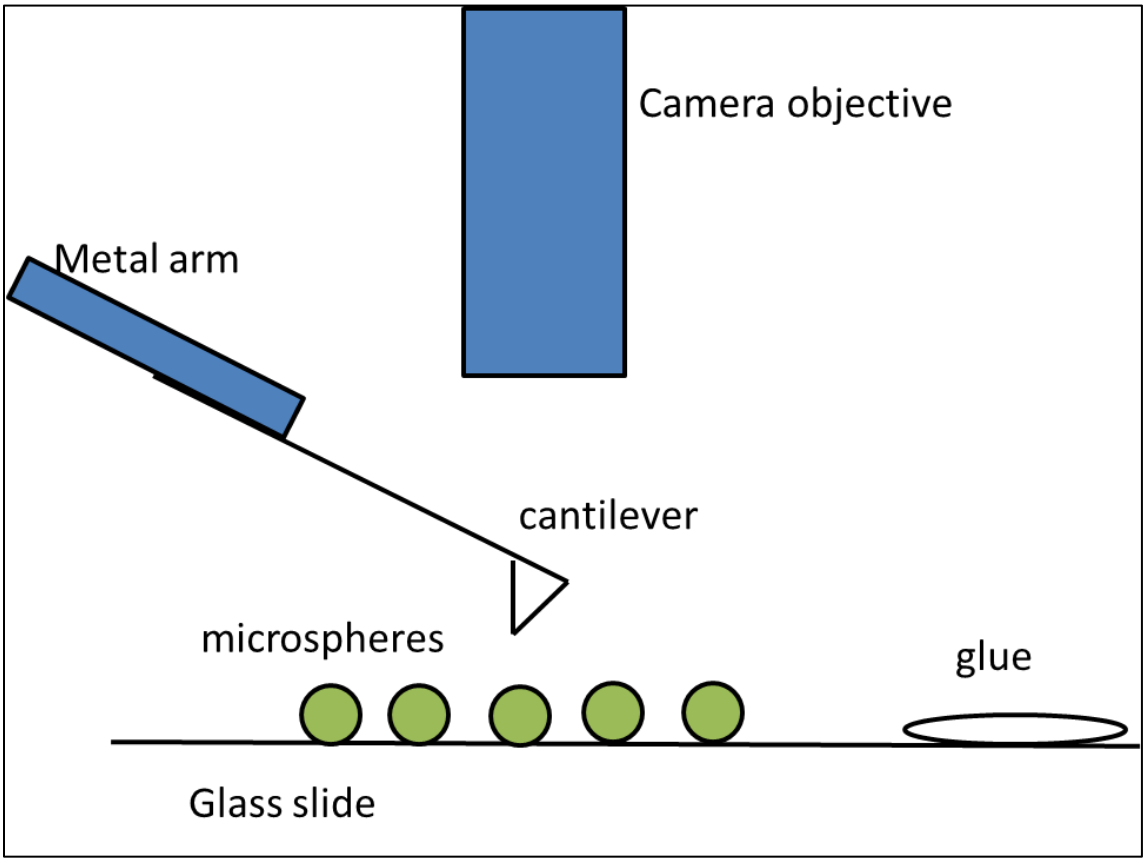

Figure 4.2. A schematic of the particle mounting apparatus.

As shown in the schematic, a cantilever is installed on a metal arm, for which the position can be adjusted by twisting the connecting knobs. The cantilever first contacts with the glue placed on a glass slide. The microspheres on the same slide can be picked up by adhesion of the glue that remains on the cantilever tip. The whole process is observed under a camera that has a 10X optical objective. Figure 4.3 shows a SEM picture of a cantilever mounted with a microsphere.

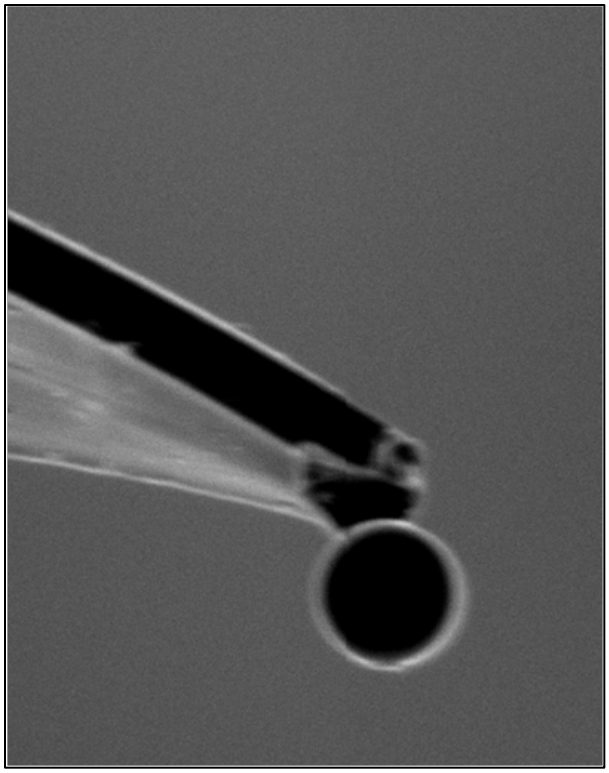

Figure 4.3. SEM picture of a cantilever with a microsphere on the tip.

It should be mentioned that there must not be too much glue on the cantilever tip. One reason is that it can cover part of the sphere so that the measured force between spheres and plates would be weakened. Another reason is that the extra glue can also cover the back of the cantilever tip and reflection of the laser beam can possibly be affected.

Two types of glues, heat-cured epoxy and UV-cured glue, were used in the work described in this dissertation, depending on the experimental requirements. When epoxy was being used, a heat plate was placed under the glass slide such that the temperature could be adjusted by tuning the applied electric voltage. When UV-cured glue was being used, the cantilever with the freshly attached sphere needed to be placed under the UV lamp for 40 minutes. This step ensured that the UV-cured glue did not dissolve in the aqueous solution.

4.3. Spring Constants of Cantilevers

The method used to determine spring constants of cantilevers was developed by Hutter and Bechhoefer [86].In the experiments performed in this proposal, the cantilevers used were relatively weak such that the spring constants were up to only 0.06 N/m. These cantilevers can be approximated as simple harmonic oscillators with one degree of freedom. A harmonic oscillator will fluctuate in response to thermal noise in equilibrium, which can be described as

$$H=\frac{p^2}{2m}+\frac{1}{2}m\omega_0{}^2q^2 \qquad [4.1]$$

where H is the Hamiltonian, q is the displacement of the oscillator, p represents the momentum, m is the oscillating mass and ω_0 is the resonant angular frequency of the system. The average value of each quadratic term in the Hamiltonian is given by $kT/2$. In particular,

$$\langle \tfrac{1}{2} m\omega_0^2 q^2 \rangle = \tfrac{1}{2} kT \qquad [4.2]$$

Since $\omega_0 = k_{spring}/m$, the spring constant can be obtained by a measurement of the mean-square spring displacement as

$$k_{spring} = kT/\langle q^2 \rangle \qquad [4.3]$$

Equation [4.3] implies that the spring constant can be estimated by measuring the rms fluctuations of a freely moving cantilever with a sampling frequency much higher than the resonant frequency. Now the question remains as how to isolate the contribution due to thermal oscillations from the system. One way to do that is based on two unique features of thermal fluctuations that background noises do not acquire. One is that in the absence of additional noise sources and in the limit of small damping, the power spectral density of the fluctuations in the spring displacement has a Lorentzian line shape. The other is that none of the other noise sources is likely to have a resonance at the resonant frequency of the cantilever. With these assumptions, the background noises can be easily subtracted from the system after thermal fluctuations are identified.

The area below the remaining peak is then a measure of the power of the cantilever fluctuations. Since the integral of the power spectrum equals the mean square of the fluctuations in the time-series data, the estimation of the spring constant becomes

$$k_{spring} = kT/P \qquad [4.4]$$

where P is the area of the power spectrum of the thermal fluctuations alone.

4.4. Data Analysis and Averaging

An averaging program was used to eliminate the noise in the data in order to obtain smooth curves. In this program, all the curves that were to be averaged (50 were typically used) were combined and then discretized into bins of widths ranging between 0.3 nm – 2 nm (smaller bin widths were used for the steeper regions of the force curves). The measured forces within each bin were then averaged.

The method of analyzing the raw data, along with more details about using AFM for force measurements, can be found in the review paper by Butt *et al*.[87].

5. Manipulating Microparticle Interactions Using Highly-Charged Nanoparticles

The work described in this chapter has been previously published as Ji, S., Herman, D., Walz, J.Y., *Colloids Surf. A* **396,** 51 (2011).

5.1. Introduction

Our goal in this work was to conduct a comprehensive experimental study in a relatively model system to determine how nanoparticles alter forces between microparticles as a function of the nature of the microparticle-nanoparticle interaction, and specifically to probe the issue of strong nanoparticle adsorption. Our experimental system consists of silica microparticles or surfaces in aqueous dispersions containing polystyrene nanoparticles. Because the surface potential of the silica surfaces depends sensitively on pH while that of the polystyrene does not, this system allowed accurately controlling the nature of the microparticle-nanoparticle interaction.

Two different types of experiments were performed. First, direct measurement of the force profile between a silica microparticle and silica plate in the presence of highly-charged nanoparticles was obtained using the technique of colloidal probe atomic force microscopy. Such measurements allow precise determination of the characteristic decay length of the force produced by the nanoparticles and thus provide some clues as to the nature of the force. While the nature of these experiments are clearly similar to those performed by Hong and Willing[71] and also McKee and Walz[72], our focus here was to evaluate how the nature of the nanoparticle-microparticle interaction alters the microparticle-plate force profile. In addition to measuring the force profile in the presence of the nanoparticles, we also investigated how the force profile changes when the nanoparticles were subsequently flushed from the system, as reversibility of the force profiles upon adding and removing the nanoparticles would support the idea that the nanoparticles are weakly held near the surface.

Second, simple adsorption studies were performed to determine whether the polystyrene irreversibly adsorbs to the silica at the conditions of interest. The tests consisted of using scanning electron microscopy to image the surfaces of slides that had been exposed to a solution of nanoparticles, gently washed and air-dried using scanning electron microscopy.

Part of the motivation of this study was to determine whether the changes in the observed force profile are consistent with the concept of a nanoparticle halo, described in greater detail in Chapter 2.3. Specifically, because nanoparticle halos involve particles trapped in relatively weak energy wells, the resulting impact of the halos on the force between the microparticle and plate should disappear upon flushing the nanoparticles from the system.

5.2. Materials

The water used in the experiments was deionized and filtered by a Barnstead EASYpure II system (Thermo Scientific, catalog #D7401). The water had a resistivity of 18.2 MΩ-cm. The force measurements were conducted with an AFM (Asylum Research, model MFP-3D). The cantilevers had mean spring constants of 0.02 N/m (Asylum Research, model TR400PSA, catalog #950831).

The AFM measurements were made between a 5 μm diameter silica sphere (Polysciences, Inc., catalog #24332-15) and a silica slide with dimension of 10 x10 x1.0

mm (MTI Corporation, Richmond, CA, catalog #SOZ101010S2). The raw data from the AFM (cantilever deflection vs. position of piezo was converted to force vs. separation using the method of Ducker *et al*.[84], The slides were polished z-cut single crystal with a manufacturer-reported rms roughness of <1 nm over 1 μm^2. Elemental analysis on the slides performed using X-ray spectroscopy (Bruker AXS, MiKroanalysis Gmbh, Berlin, Germany) showed the presence of only silicon and oxygen. The nanoparticles used in the measurements were polystyrene sulfate latex (Invitrogen Corporation, catalog #S37200) with a manufacturer reported diameter of 20 nm.

5.3. Methods

5.3.1. Particle Size and Zeta Potential Measurements

The size and zeta potentials of the polystyrene nanoparticles were measured with a Malvern Zetasizer Nano-ZS (Malvern Instruments, Ltd, Worcestershire, UK). For size distribution measurements, a disposable sizing cuvette was used, while a disposable zeta cell was used for zeta potential measurements. Both containers were rinsed with ethanol and deionized water and dried with nitrogen gas prior to use. Prior to running an AFM experiment, each suspension was sonicated for approximately 15 minutes to completely disperse the solutions.

The average diameter of the latex nanoparticles particles was found to be 22 nm, which is consistent with the manufacturer-reported diameter of 20 nm. The zeta potential of the nanoparticles was measured at pH values ranging from 2.0 to 9.0

Because of complications arising from the size of the silica particles and the size and shape of the silica slides, it was not possible to obtain zeta potential measurements on these exact materials. Instead, measurements were performed on smaller silica spheres (that did not gravity settle so rapidly) and larger silica slides. Fused silica microscope slides (Corning 7980 fused quartz silica) were purchased from TGP (Technical Glass Products, Inc., Painesville, OH), while 1 μm diameter silica microspheres were purchased from Polysciences, Inc. (Warrington, PA). The zeta potential of the silica slides was determined from streaming potential measurements using a SurPASS Electrokinetic Analyzer (Anton Paar GmbH, Graz, Austria). The SurPASS tubing was rinsed, using the extended rinse program instructions, with very dilute isopropanol (<1% by volume in water) and then with deionized water; rinse cycles were approximately 5 min for each. The fused silica microscope slides were cleaned with pure ethanol, rinsed in deionized water, and cleaned for 30 min in a UV/Ozone ProCleaner (BioForce Nanosciences, Inc., Ames, IA). Once clean, the slides were mounted in the SurPASS clamping cell. A 5 min rinse cycle was then run using the chosen electrolyte, which had been adjusted to the highest pH for which that was to be measured using 0.2 M NaOH. After rinsing, the measurement program was run, and the zeta potential was determined at pH intervals from high to low pH, being titrated using 0.2 M HCl.

The zeta potential of the microspheres was measured in folded capillary cells across a range of pH values. The Malvern MPT-2 Multi Purpose titrator was used, with 0.25 M HCl, 0.25 M NaOH, and 0.01 M HCl as titrants.

5.3.2. Force Profile Measurements

The nanoparticle suspensions were made by adding a specific amount of nanoparticle stock solution into deionized water. The solutions were prepared in 20 ml scintillation vials (Wheaton Science Products Inc., catalog #986540). Prior to use, the vials were rinsed by ethanol and deionized water. Dialysis of the suspension was performed by adding ion exchange resin (Bio-Rad, catalog #143-7425) to each vial and allowing each vial to stand for four hours with intermittent mixing.

Once dialysis was complete, the suspensions were decanted from the dialysis vials (the resin would easily sediment) and placed into clean vials. The pH of the suspension was then adjusted to the desired value using 1.0 M HCl (Mallinckrodt Standard). Force profile measurements were obtained at pH 2.7, 3.0, 4.0 and 6.0. A simple electrolyte (KCl) was added to the pH 4.0 and 6.0 solutions to keep the ionic strength of all solutions approximately the same. The size distribution and zeta potential of the nanoparticles was then measured as described above.

A UV-curable adhesive (Norland Products, model Norland Optical Adhesive 123L) was used to attach the 5 μm silica particle to the tip of an AFM cantilever (Asylum Research, moel TR400PSA). An Asylum Cypher AFM was then used to measure the spring constant of the cantilever/particle system using the method of Hutter and Bechhoefer[86], which involved determining the resonant frequency of the assembly (the spring constants for the cantilevers used here were approximately 0.02 N/m).

The roughness on the sphere was determined by mounting the cantilever into the Cypher AFM and then passing the sphere over a TGT01 ultrasharp silicon grading plate (NT-MDT, Santa Clara, CA). Typically, an rms roughness of 2 nm was measured.

The force measurements were performed in the Asylum fluid cell. A silica slide was attached on the glass disc of the fluid cell using epoxy glue. Each part except the cantilever holder and the clamp was immersed in ethanol and sonicated for one hour. Those parts were then rinsed by deionized water and dried with N_2. A piece of Kimwipe® was used to rub the top of the cantilever holder gently with chloroform and then ethanol. The cantilever with the attached sphere was placed under a UV lamp for 40 minutes.

The fluid cell was assembled and installed on the AFM before each experiment. The fluid cell allowed performing experiments with nanoparticle solutions at varying concentrations using the same cantilever, particle and slide. Solution exchange was accomplished by injecting 15 ml of the new solution slowly into the fluid cell through the connected Teflon® tubing, which forced out the old solution.

Force profiles were obtained by moving the particle toward and away from the surface with a scan rate of 200 nm/s and a scan range of 1 μm. This scan rate ensured that hydrodynamic forces acting on the sphere and cantilever were minimal. The data collection rate was set to 2000 Hz.

5.3.3. Nanoparticle Adsorption Measurements

The procedure used to test for adsorption of the nanoparticles onto the silica surfaces was to image surfaces (using scanning electron microscopy) that had been immersed in a nanoparticles solution, rinsed and dried. The silica slides were first cleaned by sonication in ethanol. Initially, the slides were next cleaned via UV/ozone, however this step was discontinued after tests showed no difference in behavior

between surfaces with and without the UV/ozone cleaning. An appropriate volume of nanoparticle solution at 0.1% vol. concentration was prepared, briefly sonicated, and then titrated to the desired pH using 0.2 M HCl (Mallinckrodt Standard).

A beaker of deionized water was then titrated, using 0.2 M HCl, to the same pH as the nanoparticle solution. The cleaned and dried silica slides were briefly soaked in the pH-adjusted water before being placed in a beaker containing the nanoparticle solution for 30 min. After the adsorption time, the silica was removed from the latex particles and gently rinsed in the beaker of pH-adjusted water in order to remove any excess (non-adsorbed) nanoparticles from the slide. By using the same pH in both solutions, the surface charge should remain the same and the adsorbed particles (if they were present) would remain on the slide. The silica was then allowed to air dry, and then spuuter-coated a 1-2 nm layer of gold for SEM imaging.

5.4. Results

5.4.1. Zeta Potentials

Shown in Figure 5.1 are the zeta potentials measured on the polystyrene nanoparticles. While there is considerable scatter in the results, (*e.g.*, from Brownian movement of the nanoparticles), it is clear that the particles maintain a strong negative charge, with zeta potentials ranging from -60 to -70 mV over the entire pH range.

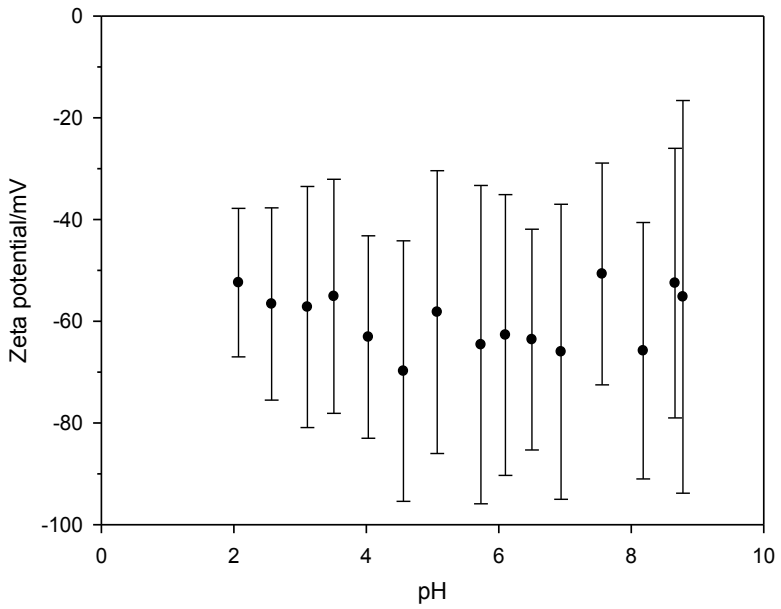

Figure 5.1. Zeta potential of polystyrene nanoparticles versus solution pH. The error bars represent standard deviation.

Figure 5.2 presents the zeta potential measured obtained on the 1 μm silica slides and silica plates. Again, it should be mentioned that while these were not the same slides and particles used in the force measurement, they were pure silica and thus should be quite similar. Also shown for comparison are the published results of Scales *et al*.[88], which were obtained on silica slides in a parallel plate configuration.

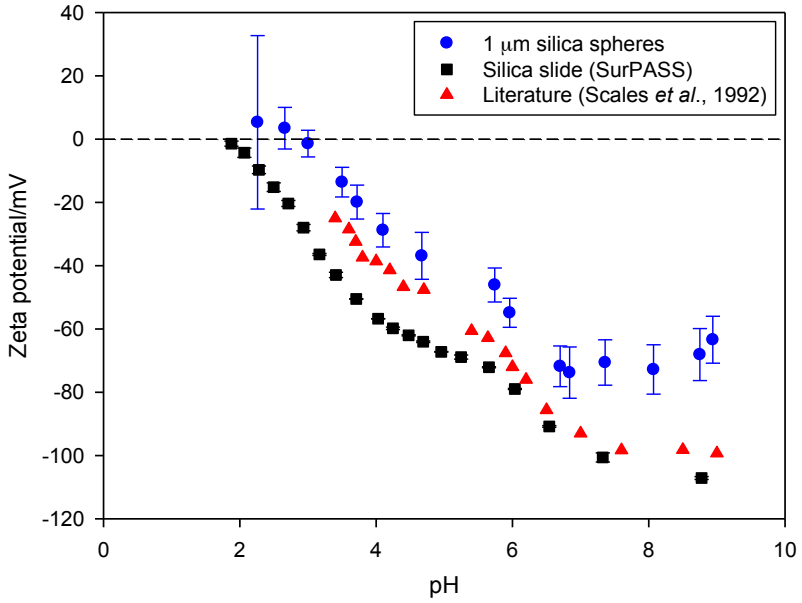

Figure 5.2. The measured zeta potential of 1 μm silica spheres and a silica plate versus solution pH. Also shown are the literature values reported by Scales *et al*.[88] for silica slides in a parallel plate configuration. The error bars represent standard deviation.

While there are clear differences in the magnitude of the zeta potential measured in the various experiments, the overall trends are clearly consistent. The isolectric point varies between pH 2 and 3, depending on the geometry and type of measurement performed.

Table 5.1 summarizes the zeta potentials of the latex and silica nanoparticles at the four different pH values used in the force experiments. For the polystyrene nanoparticles, the average zeta potential measured over the entire range of pH values shown in Figure 5.1 (approximately -60 mV) is listed. For the silica microparticle and silica plate, the listed value is the average of the results in Figure 5.2 at each pH. These values were also used in the predicted nanoparticle-microparticle pair potentials described and presented in the Discussion section below.

Table 5.1. Approximate zeta potentials of nanoparticles, microparticle and plate at the experimental conditions used in the experiments.

pH	Solution Ionic Strength/mM	$\zeta_{nanoparticle}$/mV	$\zeta_{microparticle,plate}$/mV
2.7	2.0	-60	-6
3.0	1.0	-60	-22
4.0	1.1	-60	-42
6.0	1.0	-60	-65

5.4.2. Force Profiles in Presence of Nanoparticles

The effect of the polystyrene nanoparticles on the force profile (force-vs.-distance) between the silica microparticle and plate is presented in Figure 5.3. The measured forces have been normalized by $2\pi R$, where R is the radius of the microparticle, as this is equivalent to the energy per unit area between two parallel plates assuming the Derjaguin approximation is valid for the microparticle/plate interaction. Forces were measured at bulk pH values of 2.7, 3.0, 4.0 and 6.0, and at each pH, nanoparticle concentrations of 0, 0.1, 0.6, and 1.0% vol. were used. As mentioned above, salt (KCl) was added to the pH 4 and 6 solutions to keep the ionic strength of each test solution approximately the same (the ionic strengths are listed in Table 5.1).

It should be mentioned that the results at a given pH involved a separate experiment with a unique silica microparticle, freshy-cleaned silica slide, and fresh nanoparticle solution. Thus while the trends in the forces obtained in these different experiments can be compared (*e.g.*, the variation of the force profile with nanoparticle concentration), these different conditions can affect the absolute magnitude of the forces.

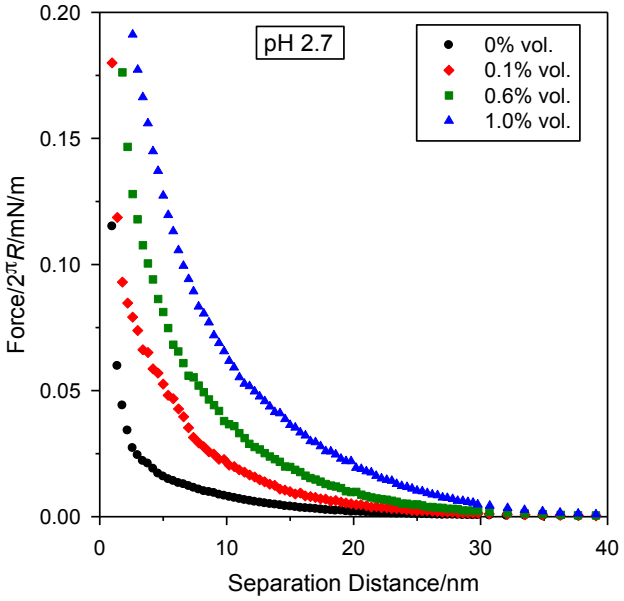
pH 2.7
0% vol.
0.1% vol.
0.6% vol.
1.0% vol.
Force/2πR/mN/m
Separation Distance/nm
0.00
0.05
0.10
0.15
0.20
0
10
20
30
40

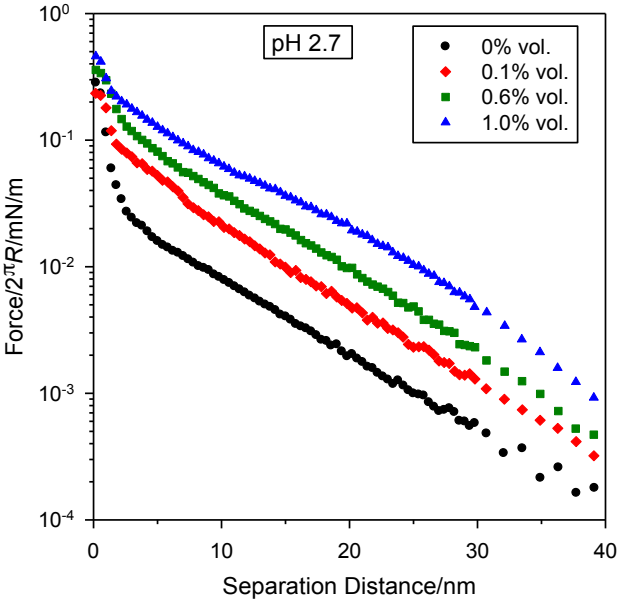
pH 2.7
0% vol.
0.1% vol.
0.6% vol.
1.0% vol.
Force/2πR/mN/m
Separation Distance/nm
10^0
10^-1
10^-2
10^-3
10^-4
0
10
20
30
40

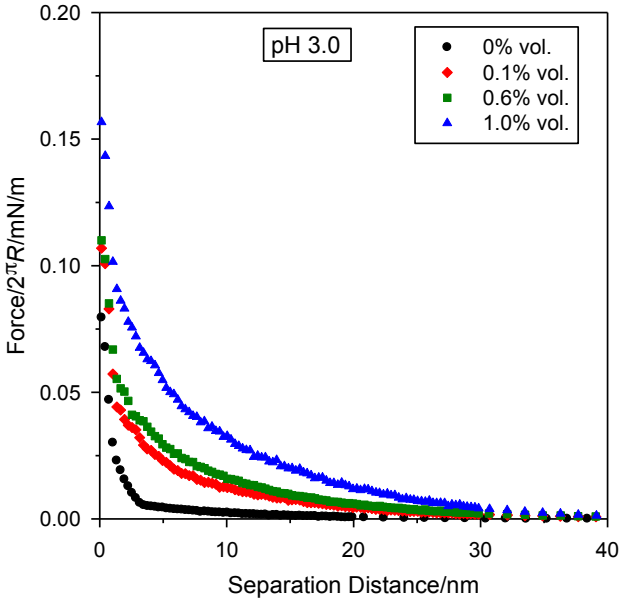
pH 3.0
0% vol.
0.1% vol.
0.6% vol.
1.0% vol.
Force/2πR/mN/m
Separation Distance/nm
0.00
0.05
0.10
0.15
0.20
0
10
20
30
40

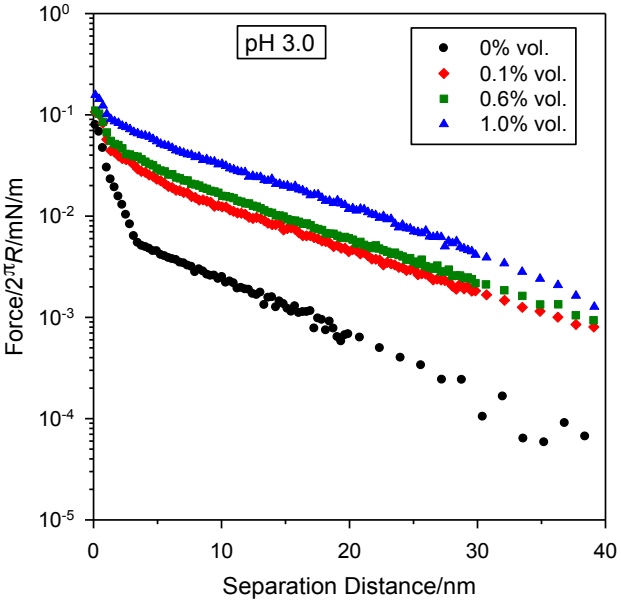
pH 3.0
0% vol.
0.1% vol.
0.6% vol.
1.0% vol.
Force/2πR/mN/m
Separation Distance/nm
10^0
10^-1
10^-2
10^-3
10^-4
10^-5
0
10
20
30
40

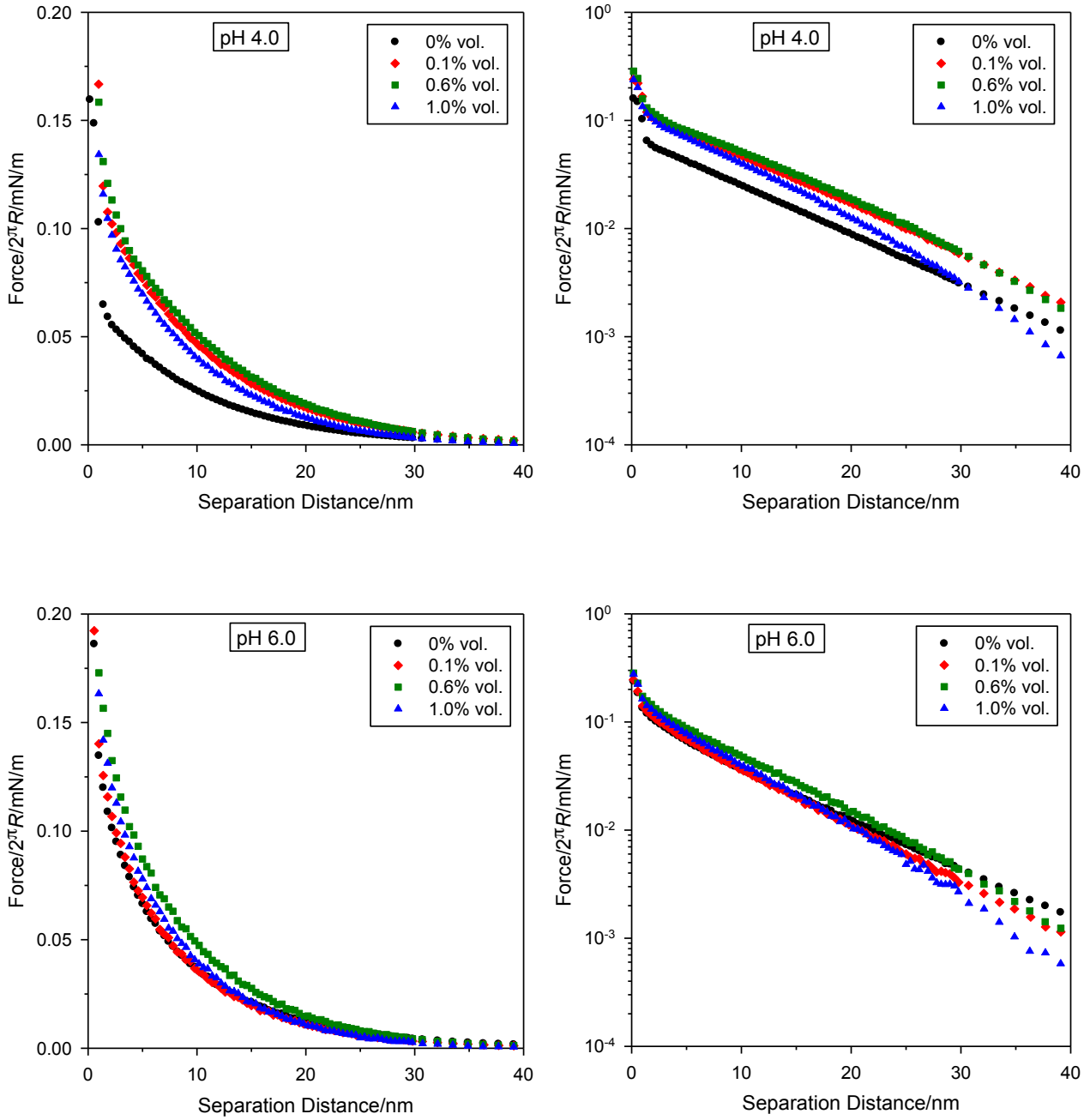

Figure 5.3. Measured force profiles (force-vs.-distance) at varying solution pH. The graphs in the right-hand column are semi-log plots of the results.

There are several clear trends in these results. At pH 2.7 and 3.0, the repulsive force increases consistently with increasing nanoparticle concentration. Even at 0.1% vol., the force is substantially increased above that with no nanoparticles (at least a factor of two, and in some cases much more). Second, as can be seen in the right-hand column, in which the log of force vs. separation distance is plotted, the force

generally follows an exponential decay with distance over most of the range plotted. At very small separations (*i.e.*, < 5 nm), a sharp deviation from this exponential decay is clearly seen in several of the graphs. We hypothesize that this decay arises from a short range repulsive interaction between the silica particles, such as from steric or hydration forces. Similar behavior was seen in the experiments of McKee and Walz[72] using glass particles and substrates.

At pH 4.0, the same general trend is seen with the exception of the results at the highest nanoparticle concentration of 1.0% vol. Specifically, the force for this concentration is actually below that of the 0.1 and 0.6% vol. solutions and clear deviations from an exponential decay are seen. The cause of this different behavior is the onset of attractive depletion forces at these higher nanoparticle concentrations. These can be seen more clearly in the results presented below in Figure 5.4, which plots expanded views of the force profiles at larger separations. As seen, at each pH, a slight attractive force (negative) can be seen in the force profile for the 1.0% vol. solution. In fact, for some of the systems (*e.g.*, pH 3.0), clear structural forces can also be seen, evidenced by oscillations in the force profile. The magnitude of this depletion force will increase with decreasing separation distance all the way down to contact, reducing the magnitude of the net repulsion between the microparticle and plate, causing the profile to deviate from an exponential decay.

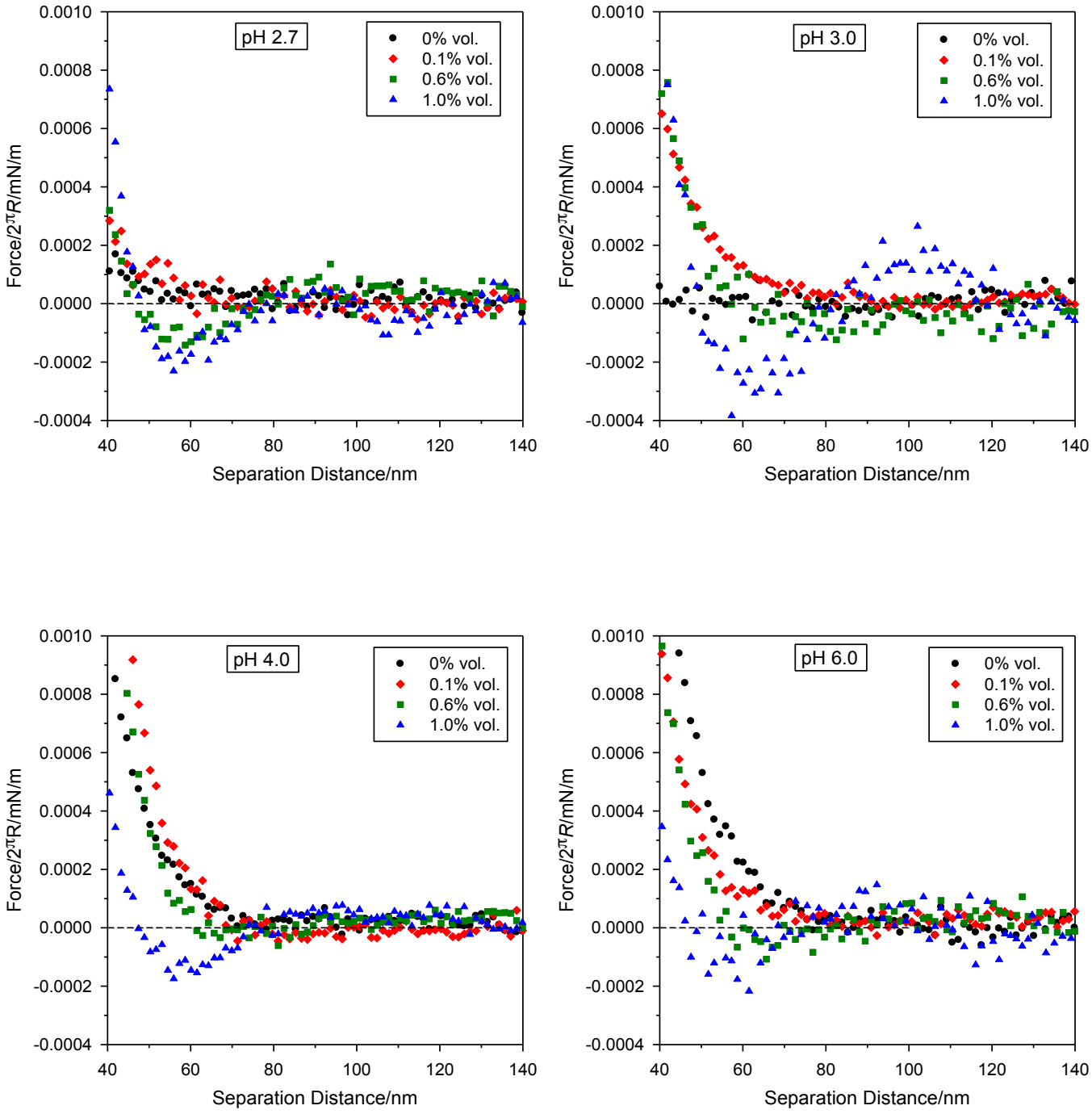

Figure 5.4. Expanded scale plots of the measured force profiles showing the depletion force developing at the higher nanoparticle concentrations.

At pH 6.0, where the polystyrene nanoparticles and the silica microparticle and plate are highly negatively-charged, the addition of the nanoparticles has a much smaller impact on the force, especially at separation distances below 30 nm (Figure 5.3).

Specifically, the force profile measured at 0.1% vol. is almost identical to that with no added nanoparticles. Again, the force at 1% volume is less than that for 0.6% vol., and at larger separations (*i.e*., 30 - 60 nm, Figure 5.3), the repulsive force at this concentration is actually below that at all of the other nanoparticle concentrations, indicating the increased magnitude of the depletion force in this system. (The depletion interaction increases as the electrostatic repulsion between the nanoparticle and microparticle/plate increases, which is the case at pH 4.0 in figure 5.3.

From the semi-log plots given in the right-hand column of Figure 5.3, the approximate decay lengths of the repulsive force profiles could be determined (*i.e,*. the decay length is the reciprocal of the slope of the semi-log plots). These decay lengths, which were only determined for the cases where the plot was linear, are given in Table 5.2. Also listed in Table 5.2 are the theoretical Debye lengths for each system, which were calculated using the ionic strengths given in the table (the calculated ionic strength for each solution included ions from any acid or based added to adjust the pH plus any added KCl). As seen, the measured decay lengths show relatively good agreement with the expected Debye lengths, with deviations of less than 10% for most of the systems.

Table 5.2. Comparison of the experimentally-measured decay length in each experimental system with the solution Debye length.

pH	Ionic Strength/mM	Nanoparticle Conc./% vol.	Theoretical Debye Length/nm	Measured Decay Length/nm	% Difference
2.7	2.0	0	6.75	7.14	5.8
		0.1		7.14	5.8
		0.6		7.09	5.0
		1.0		7.11	5.3
3.0	1.0	0	9.54	8.33	-12.7
		0.1		10.15	6.4
		0.6		10.12	6.1
		1.0		10.29	7.9
4.0	1.1	0	9.09	9.59	5.5
		0.1		9.59	5.5

		0.6		9.21	1.3
		1.0		--*	--
6.0	1.0	0	9.54	9.32	-2.3
		0.1		8.45	-11.4
		0.6		8.47	-11.2
		1.0		--*	--

*Due to significant depletion force, the semi-log plot of the force at these conditions was not linear, so a decay length was not determined.

5.4.3. Reversibility Measurements

The second type of force measurements that were performed investigated the reversibility of the effects of the added nanoparticles on the microparticle-plate force profile. The experiments consisted of measuring the force profile at a given pH and ionic strength without added nanoparticles, flushing into the flow cell a 0.1% vol. nanoparticle solution, measuring the force profile, flushing into the flow cell a solution containing no added nanoparticles, and finally measuring the force profile again. It should be stressed that the pH and ionic strength of all solutions was kept the same so that any changes observed in the force profiles were a result of the presence of the nanoparticles.

The results of these experiments in solution of pH 2.7, 3.0, 4.0 and 6.0 are shown below in Figure 5.5. It is clear that at each pH, the magnitude of the repulsive force increases upon addition of the nanoparticles and remains higher upon flushing the nanoparticles back out of the flow cell.

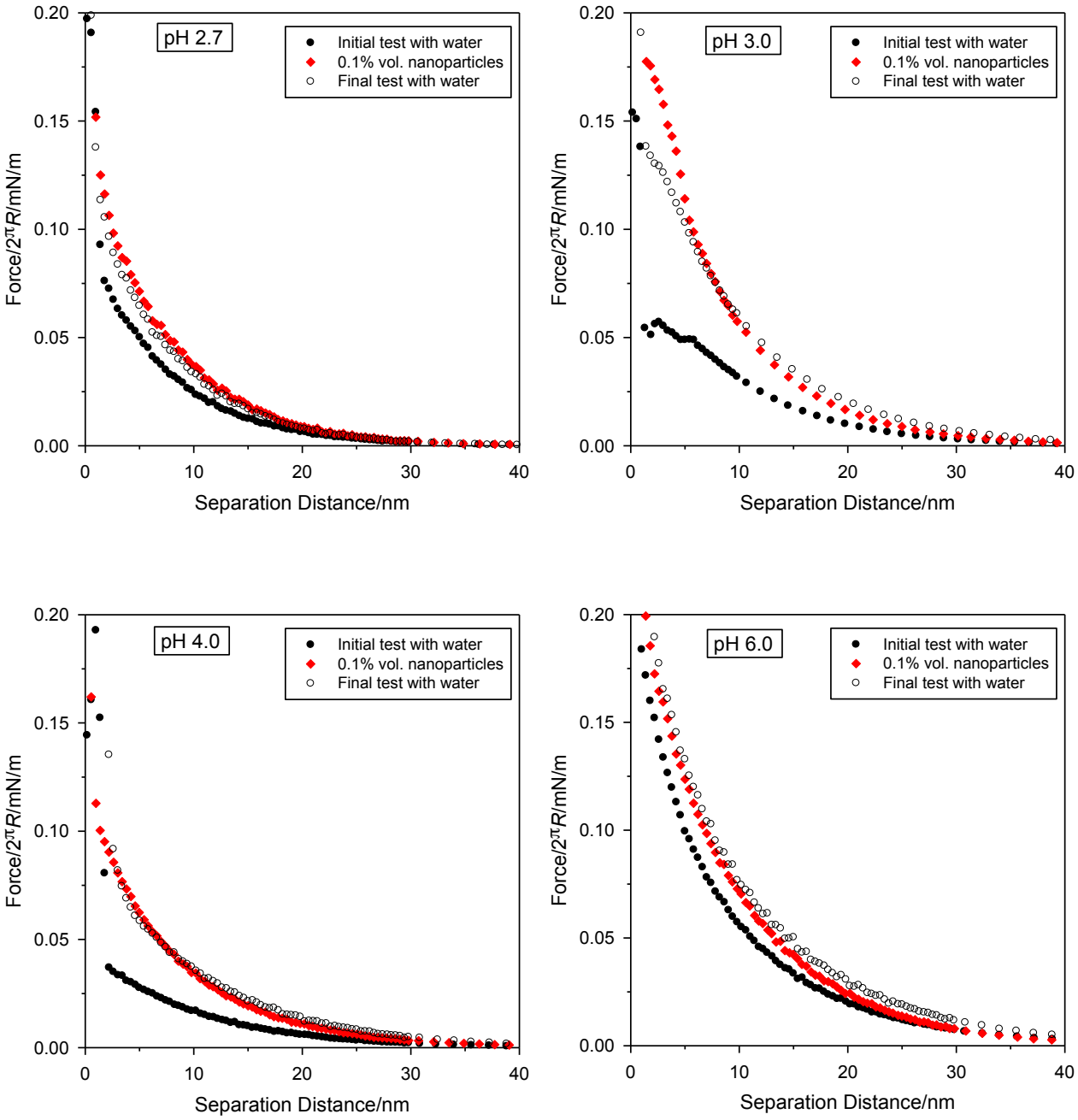

Figure 5.5. Results of experiments to test the reversibility of the effect of the nanoparticles on the microparticle-nanoparticle force profile.

5.5. Discussion

The results from the experiments presented above can be summarized as follows.

1. In solutions of pH 2.7, 3.0 and 4.0, the initial addition of the nanoparticles (0.1% vol.) causes an increase in the repulsive force. This force decays exponentially with a decay length that is in good agreement with the bulk Debye length. At pH 6.0, little change in the force profile is seen upon the initial addition of nanoparticles.
2. At all pH values, significant depletion forces are clearly seen at larger separation distances as the nanoparticle concentration is increased to 0.6 and 1.0% vol. Evidence of oscillatory structural forces is also present in some systems. These depletion forces are strong enough to cause significant deviations from exponential behavior in the pH 4.0 and 6.0 solutions at 1.0% vol. nanoparticles.
3. At each pH studied, the increased electrostatic force caused by the addition of 0.1% vol. nanoparticles did not disappear upon flushing the nanoparticles out of the system.

These results clearly suggest that the nanoparticles strongly adsorb to the surfaces of the silica microparticle and/or plate. The result of this adsorption is an increase in the magnitude of the electrostatic repulsion between the particle and plate, arising from an increased surface charge density. The fact that this increased repulsion does not disappear upon flushing the nanoparticles out of the sample cell further confirms that the nanoparticles are being held in relatively deep energy wells, likely arising from strong van der Waals forces. The longer-range depletion and structural forces seen at the higher nanonparticle concentrations are thus arising between the nanoparticle-coated silica microparticle and plate.

Additional evidence of this adsorption can be seen in the SEM micrographs shown in Figure 6. As described above, these were taken on silica slides that had been immersed in a 0.1% vol. nanoparticle solution at the pH values indicated for a period of 30 minutes, gently rinsed with a nanoparticle-free solution at the same pH, and then air dried.

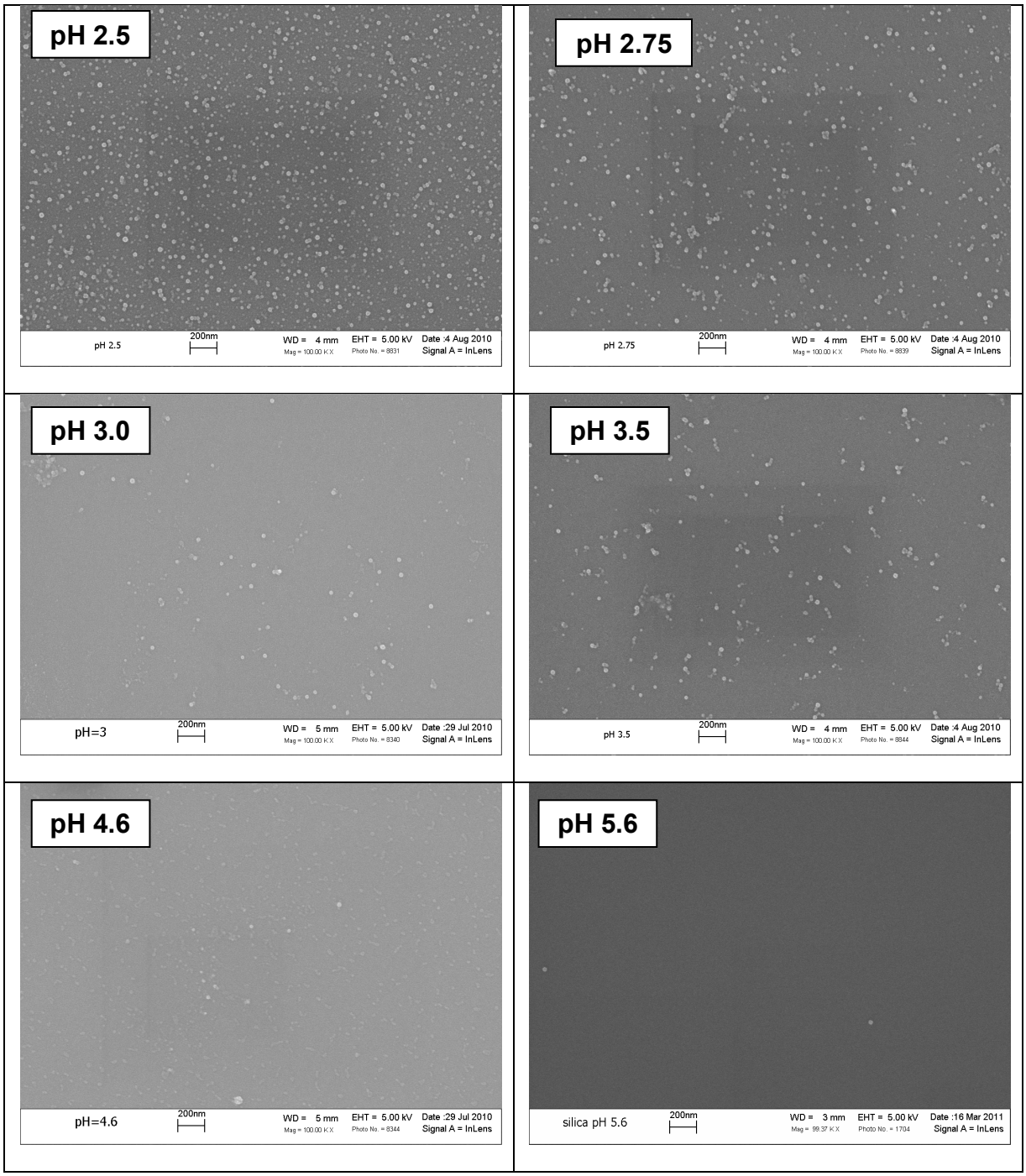

Figure 5.6. Scanning electron micrographs obtained on silica slides that had been immersed in a 0.1% vol. nanoparticle solution for 30 min, gently rinsed in a nanoparticle-free solution at the indicated pH, and then air dried. The white dots seen in the images are the polystyrene nanoparticles.

From these micrographs, rough approximations of the density of adsorbed nanoparticles were made. These estimates were obtained by manually counting the number of nanoparticles in a given area at several locations on the slide and averaging the results. The results as a function of pH are shown in Figure 5.6.

As seen, very little deposition occurs above a critical pH value of approximately 3.0, and the number of adsorbed nanoparticles increases rapidly as the pH value decreases below this value. As shown in Table 5.1, the zeta potential on the silica surfaces was measured to be approximately -22 mV.

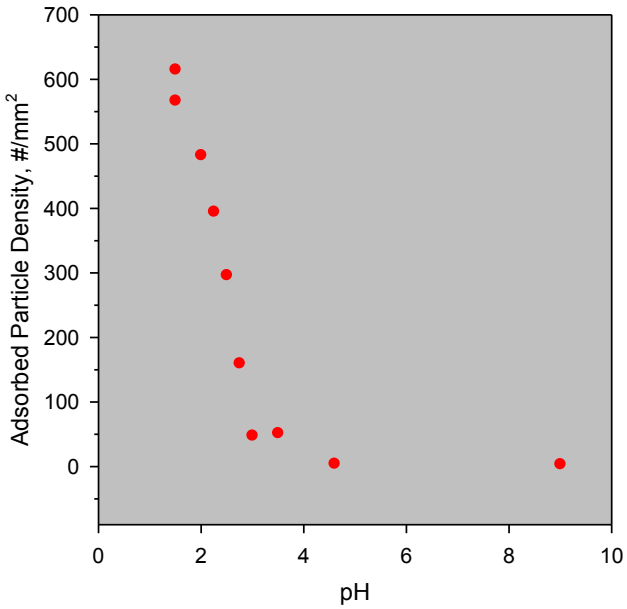

Figure 5.7. Approximate surface density of adsorbed nanoparticles as a function of pH obtained from the SEM images.

One obvious question that arises in analyzing these results is whether the adsorption of the nanoparticles should be expected at these conditions. To answer these, we present below in Figure 5.7 an estimate of the nanoparticle-microparticle pair potential at each condition listed in Table 5.1. (Because of the size of the microparticles, the nanoparticle-plate pair potential would look essentially the same as those showin in Figure 5.7.) The pair potential was calculated as the sum of the electrostatic and van der Waals potential energy.

The van der Waals energy between the two spheres was calculated using

$$E_{VDW}(h)=-\frac{A_0}{6(1+14h/\lambda)}\left[\frac{2a_1a_2}{R^2-(a_1+a_2)^2}+\frac{2a_1a_2}{R^2-(a_1-a_2)^2}+\ln\frac{R^2-(a_1+a_2)^2}{R^2-(a_1-a_2)^2}\right] \quad [5.1]$$

where R is the center-to-center distance between a micro- and nanosphere ($R=a_1+a_2+h$), A_0 is the Hamaker constant characterizing the interacting materials and medium, and λ is the retardation wavelength. The value of A_0 and λ were obtained by calculating the van der Waals interaction between two planar half-spaces using Lifshitz theory and fitting the results to the Hamaker expression for van der Waals interaction for this geometry. Dielectric spectra data for water, polystyrene and silica was taken from Berstrom *et al*.and Parsegian and Weiss . Using this approach, the Hamaker constant and retardation wavelengths were found to be $0.99\text{x}10^{-20}$ J and 105 nm, respectively.

Calculating the electrostatic interaction is more problematic, as there are no analytical solutions covering this system. Specifically, the energy barrier controlling deposition will likely occur at a separation distance roughly equal to one Debye length, meaning significant overlap of the double-layers, and the radius of the nanoparticle here is approximately equal to the Debye length. The results presented in Figure 5.7 were estimated using the linear superposition model (LSA) of Bell *et al.*, given as

$$E_{electric}(h)=4\pi\varepsilon\varepsilon_0\left(\frac{kT}{e}\right)^2 Y_1 Y_2 \frac{a_1 a_2}{(h+a_1+a_2)} exp(-\kappa h) \qquad [5.2]$$

Here Y_1 and Y_2 are the effective surface potentials of the two particles of radii a_1 and a_2, $\varepsilon\varepsilon_0$ is the dielectric permittivity of the medium, kT is thermal energy, e is the charge of a proton, and κ is the inverse Debye length. The electrostatic surface potentials for the microparticle and plate used to calculate Y_1 and Y_2 are those listed in Table 5.1. Because this equation assumes linear superposition of potentials, it is strictly valid only at gap widths larger than several Debye lengths. At smaller separations, this equation overestimates the interaction, however the error is not unreasonable. Specifically, according to Bell *et al.*, at a gap width of one Debye length and absolute surface potentials less than 100 mV, Eq. [5.2] overestimates the interaction energy by about 10%, which is more than sufficient for our purposes.

It should also be mentioned that we are assuming here that the surfaces approach under the boundary condition of constant surface potential. This assumption will yield a lower (less repulsive) estimate of the total interaction than the constant charge density condition and is thus a 'worst-case' condition for estimate nanoparticle deposition.

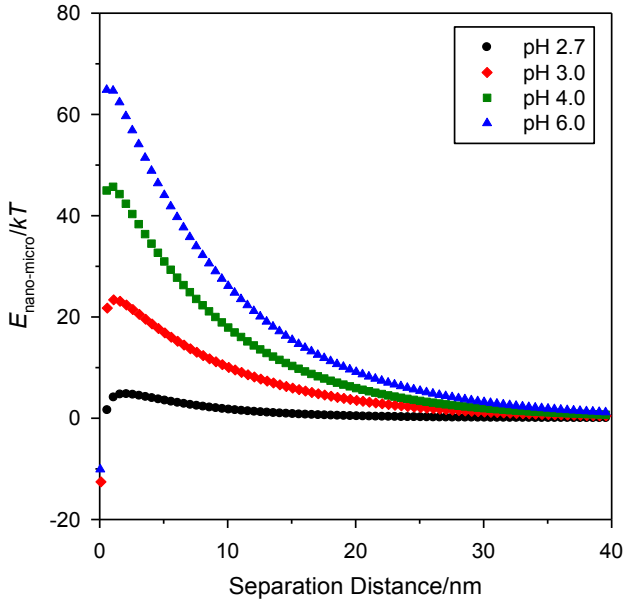

Figure 5.8. The predicted pair potential between the nanoparticle and microparticle at the conditions listed in Table 5.1.

As seen in Figure 5.7, a relatively modest energy barrier (< 5 *kT*) is predicted at pH 2.7, so it is not surprising that significant nanoparticle adsorption is observed here. Likewise, barrier heights of over 45 and 60 *kT* are predicted at pH 4.0 and 6.0, respectively, which again is consistent with the observation of very little nanoparticle deposition in the SEM micrographs of Figure 5.6.

Perhaps the most interesting case is pH 3.0, where the predicted barrier height is approximately 23 *kT*. As seen in Figure 5.6, this is essentially at the boundary where significant adsorption is seen. Thus within the accuracy of the LSA approximation, these results suggest that barrier heights of approximately 20 *kT* are required to prevent significant deposition. It should be stressed, however, that small amounts of deposition can still occur even when the barrier height is much larger than this, which is likely the result of either roughness or chemical heterogeneity.

It is worth noting that even though little nanoparticle adsorption occurred at pH 4.0, the force profile measured in a 0.1% vol. nanoparticle solution (Figure 5.3) at this pH was still significantly more repulsive than with no nanoparticles. Specifically, using the results shown in Figure 5.6, the approximate number density of particles at pH 4.0 was 28 particles/μm^2 (average of the values of 52 nanoparticles/μm^2 at pH 3.5 and 4 nanoparticles/μm^2 at pH 4.6). Assuming a cross-sectional area of each nanoparticle of 3.8×10^{-4} μm^2 (πa^2) gives an approximate fractional surface coverage of 1%. (By comparison at pH 2.75, the estimated adsorbed nanoparticle density was 160 particles/μm^2, giving a fractional surface coverage of nearly 6%.) These results suggest that the electrostatic repulsive force is highly sensitive to the presence of even small numbers of the nanoparticles.

To further evaluate this observation, we used the following expression for the electrostatic force between the microparticle and plate to estimate the surface potential of the silica surfaces at pH 4.0 in the 0.0 and 0.1% vol. nanoparticle solutions

$$F_{electric,micoparticle\text{-}plate}(h)=64\pi\varepsilon\varepsilon_0\left(\frac{kT}{e}\right)^2\kappa R tanh^2\left(\frac{\Psi_0}{4}\right)exp(-\kappa h) \qquad [5.3]$$

Here Ψ_0 is the dimensionless surface potential on the silica particle and plate (assumed equal) and *R* is the radius of the microparticle. This equation assumes linear superposition of potentials and is thus valid at separations greater than one Debye length. In addition, the Derjaguin approximation is used to account for the effects of curvature, however this should be a very valid assumption for the microparticle-plate interaction. According to this equation, a semi-log plot of the force versus separation distance should yield a straight line at large separations with a slope of the inverse Debye length and an intercept that depends on the silica surface potentials. (Such plots are shown in Figure 5.3.) Because both the depletion and van der Waals forces are small at these nanoparticle concentrations and separations, respectively, they were ignored in this analysis.

Using this approach, the surfaces potentials on the silica surfaces shown below in Table 5.3 were obtained. As seen, the value of -21.8 mV in the nanoparticle-free solution is in reasonable agreement with the zeta potentials reported in Figure 5.2. (For example, at pH 4.1, the measured zeta potential for a 1 μm silica particle was -28.8 mV).

Also shown in Table 5.3 are the corresponding surface charge densities on the silica plate calculated using

$$q = \frac{\varepsilon\varepsilon_0 kT}{ez}\kappa\left[2sinh\left(\frac{\Psi_0}{2}\right) + \frac{4}{\kappa a}tanh\left(\frac{\Psi_0}{4}\right)\right] \quad [5.4]$$

Here q is the surface charge density (C/m^2), Ψ_0 is the dimensionless surface potential, and a is the radius of curvature of the surface (equal to infinity for the flat silica plate).

Table 5.3. The surface potentials of the silica microparticle and plate and corresponding surface charge densities for the 0.0 and 0.1% vol. nanoparticle solutions at pH 4.0.

Nanoparticle Conc./% vol.	Surface Potential of Silica/mV	Surface Charge Density on Silica Plate/C/m^2
0.0	-21.8	-1.72x10^{-3}
0.1	-29.8	-2.42x10^{-3}

As seen, the nanoparticles increase the surface charge density on the plate by -7.2x10^{-4} C/m^2. The question, then, is what adsorption density of nanoparticles is required to provide this much additional charge.

Using Eq. [5.4], a nanoparticle zeta potential of -60 mV (Table 5.1), and a nanoparticle radius of 11 nm, each nanoparticle has a total charge, Q ($Q=4\pi a^2 q$), of -1.39x10^{-17} C (valence of approximately -87). This means that an adsorption density of 52 nanoparticles/μm^2 would be required to provide the increased surface charge that arises in the 0.1% vol. nanoparticle solution. This value is in reasonably good agreement with the adsorption densities reported above (*i.e.*, 52 nanoparticles/μm^2 at pH 3.5 and 4 nanoparticles/μm^2 at pH 4.6). These results thus confirm that relatively low coverages of adsorbed nanoparticles (*i.e.*, order 1%) can produce significant increases in the magnitude of the electrostatic repulsive force.

5.6. Conclusion

An experimental investigation was performed to determine whether highly-charged nanoparticles can alter the interaction forces between weakly-charged microparticles in an easily-reversible manner. Colloidal probe AFM studies clearly showed that except for cases where the nanoparticle-microparticle pair potential was strongly repulsive (*e.g.*, absolute zeta potential of at least 50 – 60 mV on each surface), sufficient nanoparticle deposition occurred, even at bulk nanoparticle concentration as low as 0.1% vol., that the electrostatic repulsive force between the microparticles was increased significantly. Most importantly, this increased repulsion did not disappear upon flushing the nanoparticles from the bulk solution, indicating that the nanoparticles were held in relatively deep energy wells. Confirmation of this adsorption was provided by SEM images of silica slides that had been immersed in a nanoparticle solution.

These results illustrate the difficulty associated with using nanoparticles to reversibly stabilize a colloidal dispersion. Specifically, small amounts of nanoparticles

will strongly adsorb on modestly-charged microparticles, and those adsorbed do not readily desorb upon dilution. Furthermore, the electrostatic force between the microparticles was found to be highly sensitive to the adsorption, such that surface coverages as low as 1% led to significant shifts in the repulsive interaction. These findings were consistent with estimates of the number density of adsorbed nanoparticles needed to produce the observed change in force.

Finally, some comments should be made about what these results say about the formation of a nanoparticle halo. As described in Chapter 2.3, the original definition of a halo by Lewis and coworkers[3, 60] involves nanoparticles held near the surface of the microparticles in a relatively shallow energy well (i.e., order of a few kT). As such, the adsorption of these nanoparticles would be reversible, such that the halo would disappear upon flushing the system.

The experimental results described in this chapter, however, make it clear that this was not the case in these experiments. Specifically, these results indicate that the increased repulsion measured by the microparticle and plate upon the introduction of the nanoparticles arose from strong, irreversible deposition of the microparticles into deep energy wells.

While these results of course do not preclude the possible formation of a nanoparticle halo, they do indicate that it is not a general phenomenon of all microparticle/nanoparticle systems. In the next chapter, a unique system involving three different particle sizes is described in which a particle halo is predicted to form.

6. Interaction Potentials between Two Colloidal Particles Surrounded by an Extremely Bidisperse Suspension

The work described in this chapter has been previously published as Ji, S., Walz, J.Y., *J Colloid Interface Sci* **394,** 611 (2013).

6.1. Introduction

Our experimental results described in the Chapter 5 strongly indicate that a nanoparticle halo is not a general phenomenon of microparticle/nanoparticle systems. Specifically, these results suggest that the van der Waals forces between the microparticles and nanoparticles would lead to strong, irreversible deposition of the nanoparticles, which is contrary to the original concept of a halo as given by Lewis and coworkers[3, 60].

Nonetheless, motivated by the general concept of reversible adsorption of particles, we sought to determine whether a particle halo could indeed be formed and, if so, what conditions would be required. To do this, we performed and describe in this chapter the results of a computational study on particle order in a *ternary* system consisting of a solution of particles of three very distinct sizes (i.e., micron, submicron, and nanometer). The specific goal was to determine whether the attractive depletion force between the microparticles and submicroparticles, produced by the nanoparticles, could lead to the formation of a halo of submicroparticles around the microparticles and, if so, what would be the resulting equilibrium interaction between two such microparticles.

This chapter presents the results of a computational study of such a system that shows that a halo can indeed be produced. In addition, we present the results from an approximate model for calculating the depletion interaction that utilizes a square-well description of particle pair potentials. It is shown that this simplified model is capable of capturing key features of the force profile using a set of *algebraic* equations.

6.2. Theory

6.2.1. Description of System

A schematic of the system is shown in Figure 6.1. Two micron particles of radius R, separated by distance h, are immersed in a solution of submicron particles (radius R_{sub}, bulk number density ρ_{sub}) and nanoparticles (radius a, bulk number density ρ_{nano}). All of the species are assumed to interact with each other via electrostatic and van der Waals forces (i.e., direct interactions). Depletion and structural forces (induced interactions) also arise and are calculated as described in §6.2.2 and §6.2.3.

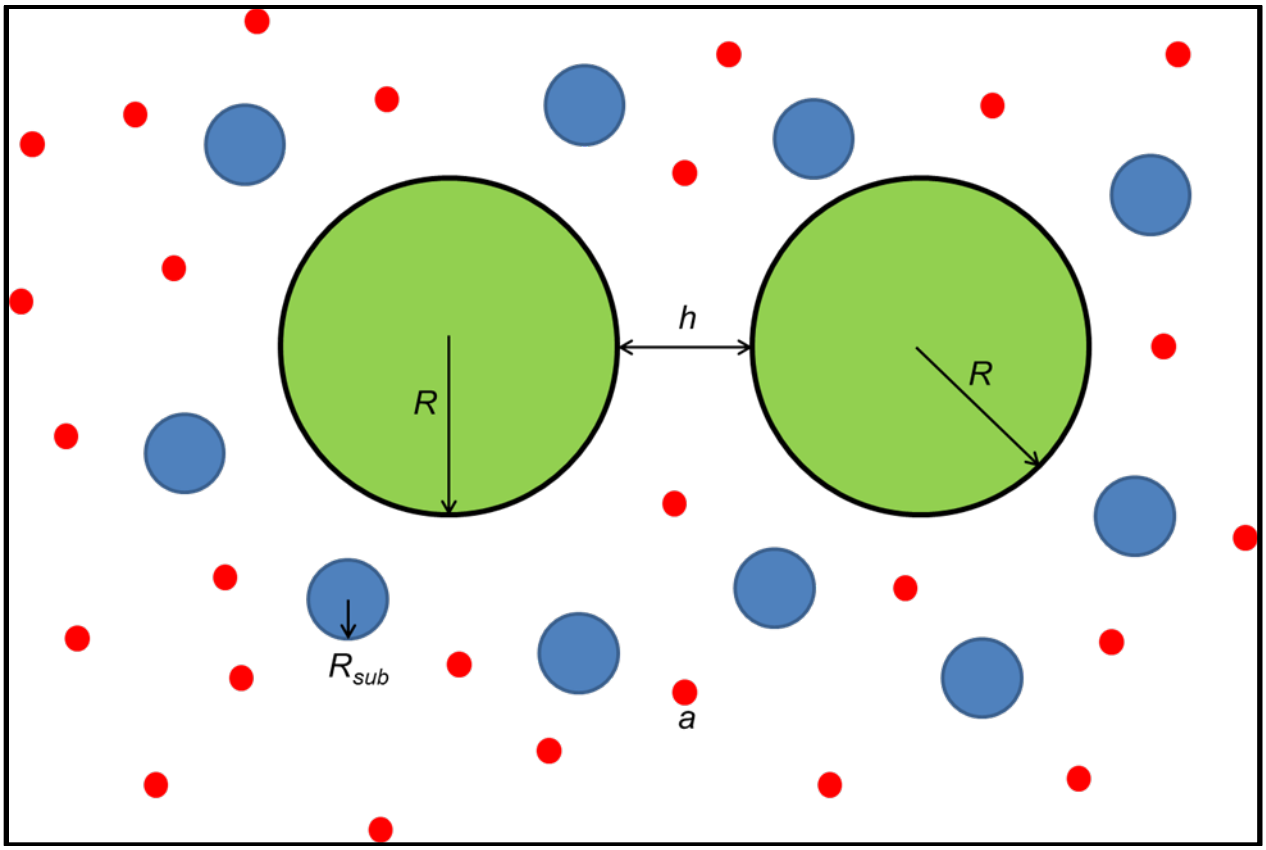

Figure 6.1. Schematic of the system used in the modeling work. Two microparticles of radius R are immersed in a solution containing submicron particles (radius R_{sub}) and nanoparticles (radius a).

6.2.2. Forces in a Binary System

The goal in this work was to calculate the net interaction between the two micron-sized particles in Figure 1, specifically the interaction that arises from the submicron and nanoparticles. The primary assumption used is that the key features of the interaction can be captured as the sum of binary particle interactions. Chapter 3.3 provides details about the approach used to calculate the depletion/structural interaction in a binary system (e.g., two large particles interacting in a solution of smaller particles of uniform size). Essentially, the modeling approach is to sum the forces on the microparticles by an equilibrium configuration of smaller particles, which was originally described by Walz and Sharma[8]. Chapters 3.1 and 3.2 present the equations used to calculate the electrostatic and van der Waals interactions between the particles.

6.2.3. Application to Ternary System

The primary assumption used in calculating the depletion and structural interaction between the two microparticles in this system is that the effect of the nanoparticles is to modify the pair potential between two submicroparticles and between a microparticle and a submicroparticle. Using the binary system equations from Chapter 3.3, the microparticle-microparticle interaction in the ternary system depicted in Figure 1 could then be calculated as follows:

1. The depletion/structural interaction between a microparticle and submicroparticle due to the nanoparticles was calculated. This allowed expressing the total interaction profile between a microparticle and submicroparticle as:

$$E_{micro\text{-}submicro} = (E_{elec} + E_{vdw} + E_{depl})_{micro\text{-}submicro} \quad [6.1]$$

   where the electrostatic and van der Waals energies are calculated as described in §6.2.4.

2. In a similar fashion, the depletion/structural interaction between two submicroparticles due to the nanoparticles was calculated, giving:

$$E_{submicro\text{-}submicro} = (E_{elec} + E_{vdw} + E_{depl})_{submicro\text{-}submicro} \quad [6.2]$$

3. Using Eqs. [3.15] and [3.18] and the results from steps (1) and (2) above, the depletion/structural interaction between two microparticles due to the submicroparticles was calculated. For this calculation, the microparticle-submicroparticle pair potentials in Eqs. [3.15] and [3.18] included not only direct electrostatic and van der Waals interactions but also depletion/structural interactions induced by the nanoparticles.

4. The depletion/structural interaction between the two microparticles due to just the nanoparticles was calculated (i.e., ignoring the presence of the submicroparticles).

5. Finally, the total interaction between the two microparticles was calculated as the sum of the direct electrostatic and van der Waals interactions between the two microparticles plus the induced depletion/structural interactions arising from both the submicroparticles and the nanoparticles. Thus

$$E_{micro\text{-}micro} = (E_{elec} + E_{vdw})_{micro\text{-}micro} + \left(E_{depl:submicro} + E_{depl:nano}\right)_{micro\text{-}micro} \quad [6.3]$$

   where $E_{depl:submicro}$ and $E_{depl:nano}$ are the depletion interactions between the two microparticles produced by the submicroparticles and the nanoparticles, respectively.

In this calculation scheme, the possible effect of a halo arises in the pair potential between the microparticle and submicroparticle ($E_{micro\text{-}submicro}$). Specifically, since this pair potential can now contain a long-range secondary energy well due to attractive depletion forces, the equilibrium density profile of submicron particles around a microparticle can be substantially greater at the location of this energy well. This is shown more specifically in Figure 6.7 in the Results and Discussion section.

6.2.4. System Properties

Our system consists of two large microparticles (radius, R, of 10 μm) immersed in a solution of submicroparticles (radius, R_{sub}, of 0.1 μm) and nanoparticles (radius, a, of 6 nm). To connect our results to a possible real system, we assume that the microparticles are silica and the submicro- and nanoparticles are polystyrene.

The solution pH is assumed to be close to the isolectric point of silica (≈2.4), such that the silica microparticles are weakly charged while the polystyrene submicro- and nanoparticles are strongly charged. The Debye length of the solution was assumed to be 10 nm (i.e., ionic strength of approximately 1 mM). The specific sizes, electric surface potentials, and concentrations used in the calculations are given in Table 6.1.

Table 6.1. Parameters for the microparticles, submicroparticles and nanoparticles used in the calculations.

	Microparticles (silica)	Submicroparticles (polystyrene)	Nanoparticles (polystyrene)
Radius	10 μm	100 nm	6 nm
Surface potential*/mV	-25	-70	-70
Volume conc.	-	5%	1%

*Surface potential assumed equal to the zeta potentials reported by Scales *et al*.[88].

The Hamaker constants and retardation wavelengths needed to calculate the van der Waals interaction (using Eq. [3.5]) for each of the possible pair interactions are listed in Table 6.2. These values were obtained as fits to results from Lifshitz calculations. Dielectric spectra data for each material (silica, polystyrene and water) was taken from Bergstrom *et al*.[89] and Parsegian and Weiss[90].

Table 6.2. Hamaker constants and retardation wavelengths for each of the possible pair interactions.

	Silica-silica (microparticle-microparticle)	Silica-polystyrene (microparticle-submicroparticle and microparticle-nanoparticle)	Polystyrene-polystyrene (submicroparticle-submicroparticle and nanoparticle-nanoparticle)
Hamaker constant/J	7.6×10^{-21}	9.9×10^{-21}	1.36×10^{-20}
Retardation wavelength/nm	85	105	130

6.3. Results and Discussion

6.3.1. Predicted pair potentials

Shown in Figure 6.2 is the pair potential between the two microparticles in the absence of any other added particles, calculated using the properties shown in Tables 6.1 and 6.2. The energy profile displays a slight secondary well of approximately 1 kT, arising from the van der Waals attraction, followed by an exponentially-decaying electrostatic repulsion at smaller separations.

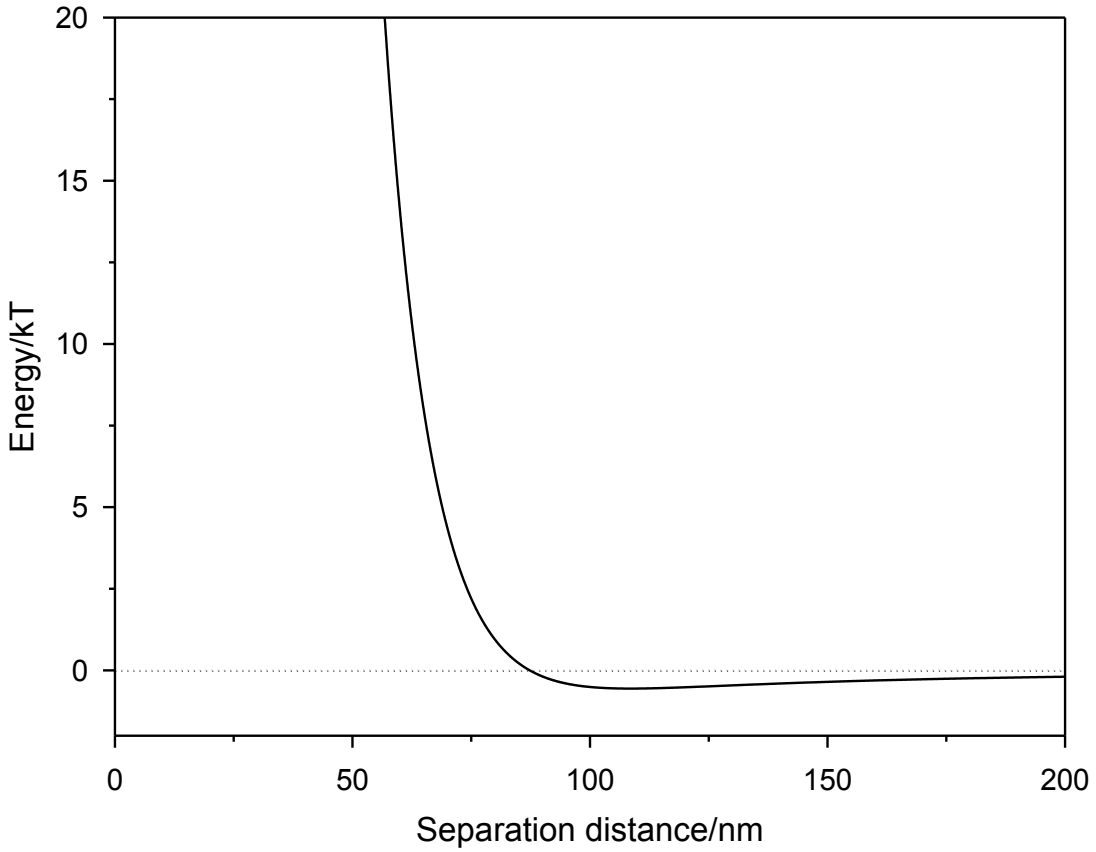

Figure 6.2. Predicted microparticle-microparticle interaction in absence of any added particles.

Figure 6.3 shows how this microparticle-microparticle pair potential changes when the 6 nm nanoparticles are added (1% vol.). As seen, a large repulsive barrier (over 100 kT) is predicted at approximately 70 nm, along with a deep secondary energy well (over 200 kT) at approximately 25 nm. The energy barrier results from ordering of the nanoparticles around the microparticles (i.e., structural forces), while the energy well is a result of an attractive depletion force arising from the exclusion of the nanoparticles from the gap region.

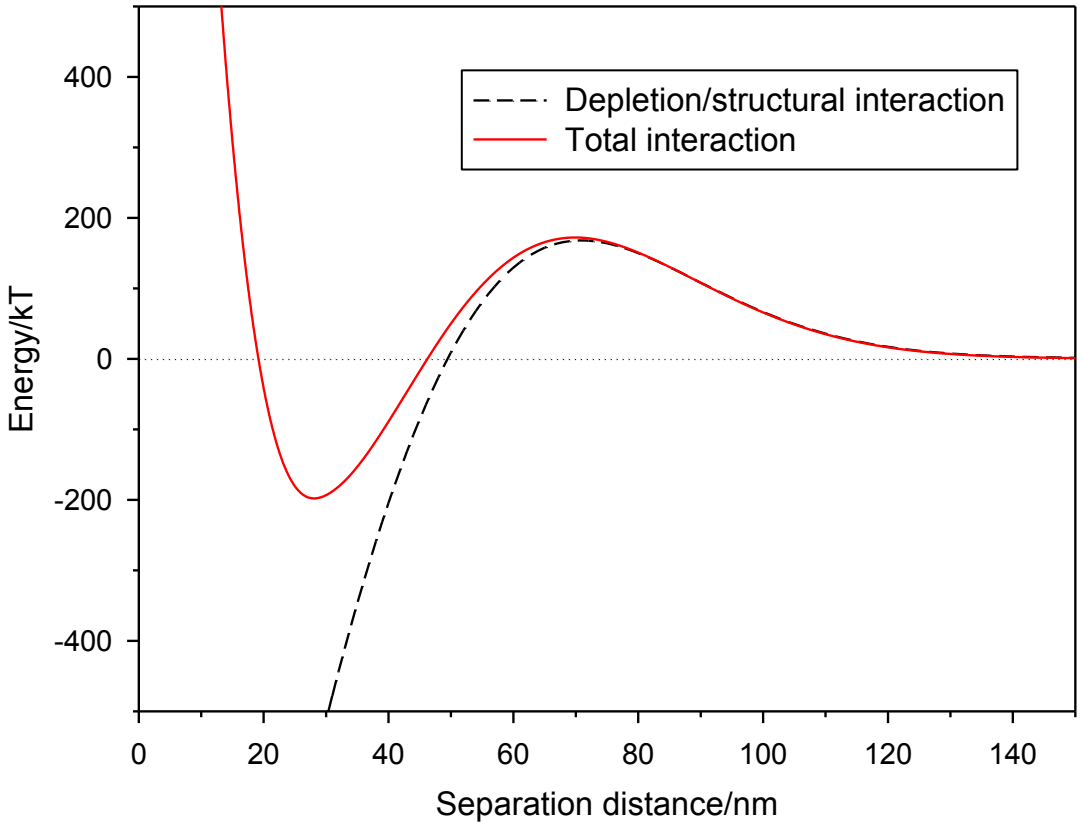

Figure 6.3. The depletion/structural and total interaction energy profiles between two microparticles due to the presence of only nanoparticles at 1% vol. The total interaction includes electrostatic and van der Waals interactions between the microparticles.

By comparsion, Figure 6.4 shows the effect of adding only the 100 nm submicroparticles (5% vol.). While the same qualitative features are observed as when adding only the nanoparticles, the magnitude of the energy barrier and secondary well are substantially smaller because of the much lower bulk number density. In addition, the larger size of the submicroparticles compared to the nanoparticles increases the separation distance at which these features are predicted to form (e.g., nearly 300 nm for the energy barrier in the submicroparticle system versus roughly 70 nm with the nanoparticles).

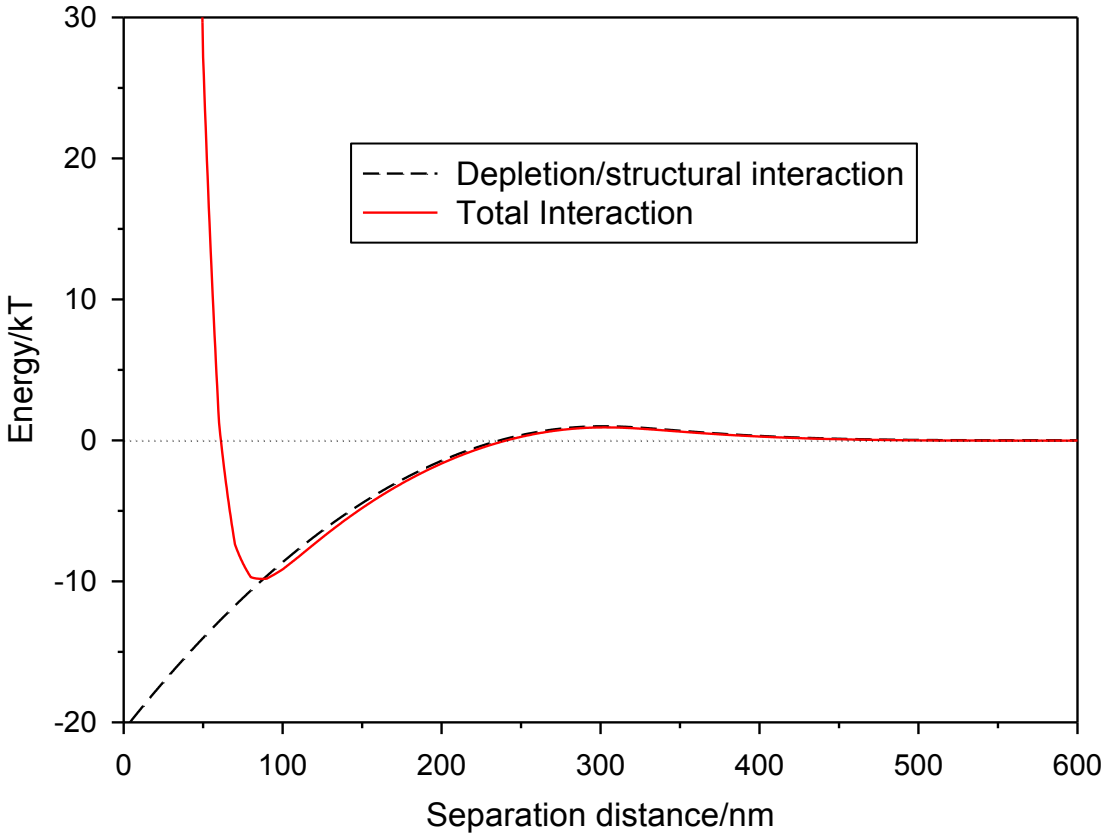

Figure 6.4. The depletion/structural and total interaction energy profiles between two microparticles due to the presence of only submicroparticles (5% vol.).

Figure 6.5 shows the total microparticle-microparticle pair potential when both the nanoparticles *and* submicroparticles are added to the system. While this energy profile shows some of the same qualitative features of the curves shown in Figures 6.3 and 6.4, there are a number of key differences that should be noted.

First, the long range repulsive barrier (~300 nm) is now over an order-of-magnitude larger compared to the case when only submicroparticles are present (Figure 6.4). In addition, a relatively large energy well (~20 kT) is now predicted at approximately 250 nm. At closer separations (<150 nm), the features of the profile are similar to those predicted in the nanoparticle only case (Figure 6.3), though the magnitudes of the energy barrier and well are slightly different.

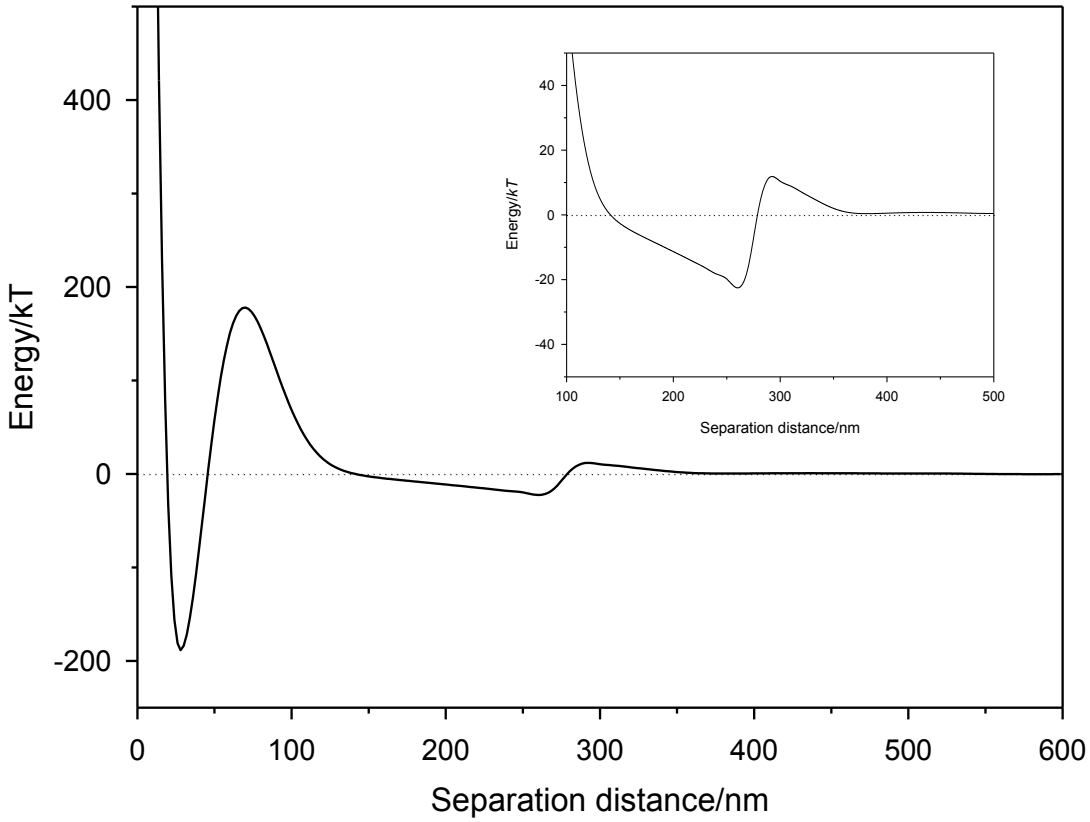

Figure 6.5. The total energy profile between two microparticles in the presence of both submicroparticles and nanoparticles. The inset is an expanded view of the potential at large separations.

The changes in the long-range nature of this profile are a result of the effects of the nanoparticles on the microparticle-submicroparticle and submicroparticle-submicroparticle pair potentials. Here, the very long-range repulsion (separation of approximately 300 nm) arises from the interaction of the submicroparticles forming the halo as the microparticles approach. As the separation decreases, the microparticles become excluded from the gap region, resulting in a lower concentration in this 'inner' region relative to the 'outer' region (away from the gap), and a long-range depletion attraction arises (separation of approximately 250 nm).

Shown in Figure 6.6 is the microparticle-submicroparticle interaction profile with and without the presence of nanoparticles (the submicroparticle-submicroparticle profiles look qualitatively similar). Without added nanoparticles, the profile consists strictly of an exponentially-decaying electrostatic repulsion. With the nanoparticles present, however, both a long-range repulsive barrier and a shorter-range energy well are predicted, resulting from structural and depletion forces, respectively.

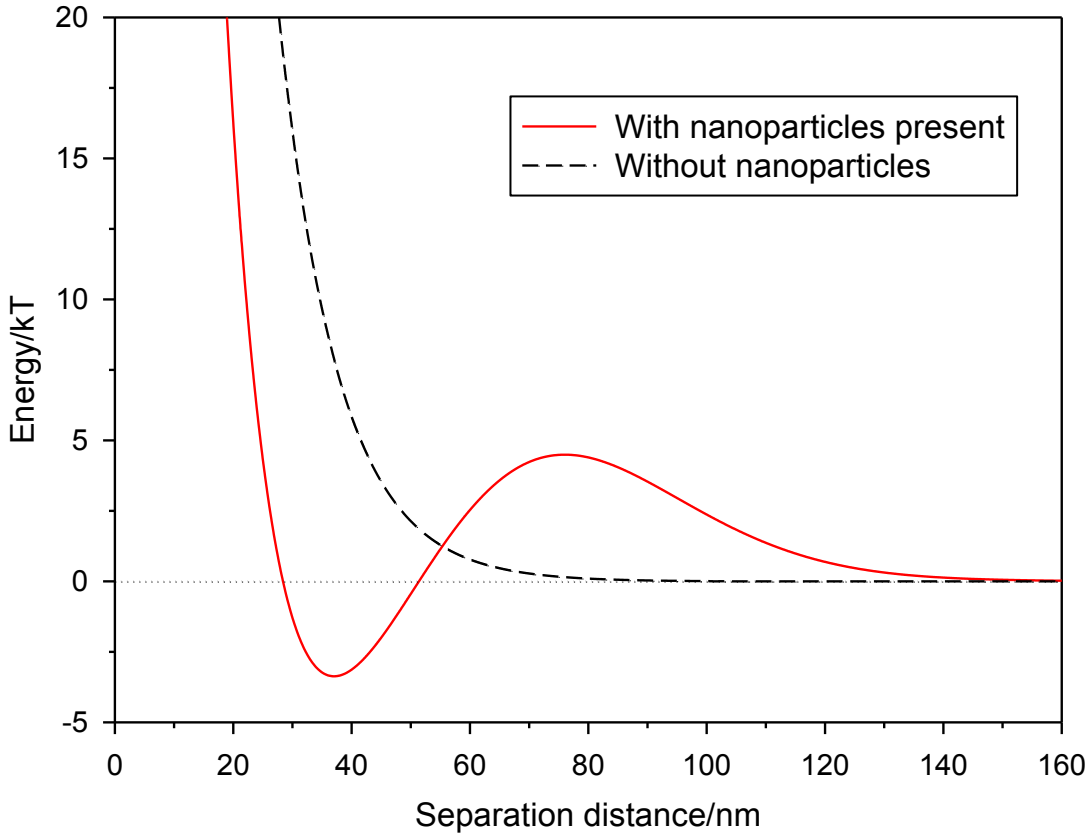

Figure 6.6. The pair between between a microparticle and a submicroparticle without (dashed line) and with (solid line) the presence of added nanoparticles.

These changes in the microparticle-submicroparticle and submicroparticle-submicroparticle energy profiles cause significant changes in the density distribution of the submicroparticles around the microparticles. This can be seen clearly in Figure 6.7, which plots the local submicroparticle density relative to the bulk as a function of position from the microparticle surface. These calculations were performed for an isolated microparticle and thus are independent of radial direction.

As seen, without the presence of added nanoparticles, the relative density profile is essentially zero out to a distance of nearly 50 nm, increases to approximately 1.2 times the bulk value at a distance of roughly 100 nm, and then asymptotically returns to the bulk value. This submicroparticle concentration above the bulk value arises from the repulsion between the submicroparticles themselves, which is captured by the 2nd virial coefficient in Eq. [3.44], and results in the slight repulsive energy observed in the microparticle-microparticle interaction profile at large separations (Figure 6.4).

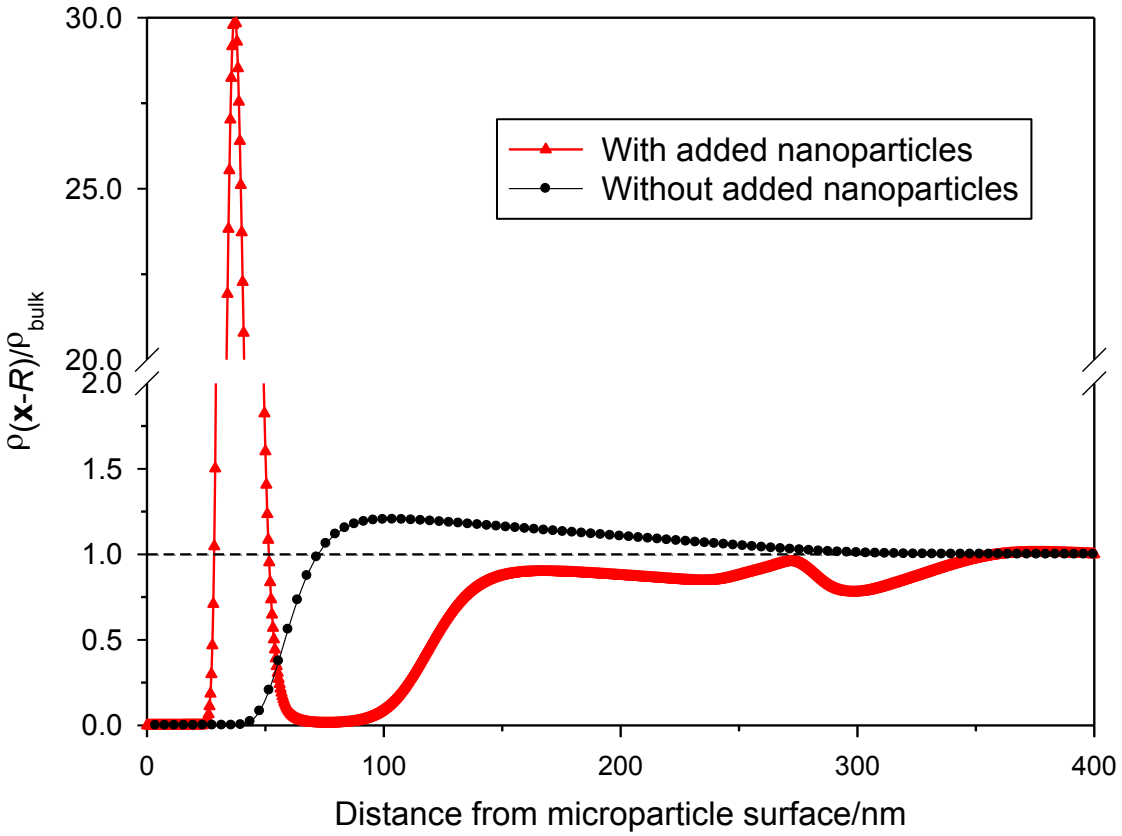

Figure 6.7. Local number density of submicroparticles (relative to the bulk value) as a function of radial distance from the surface of an isolated microparticle.

By comparison, when then nanoparticles are added, the number density profile changes markedly. Perhaps the most notable feature is the large increase in concentration predicted at a separation distance of approximately 40 nm. This, of course, results from the secondary energy well predicted in Figure 6 at this distance, and implies that a ring or halo of these submicroparticles will form around the microparticle. At larger distances (between roughly 60 and 100 nm), the submicroparticle concentration drops to near-zero, due to the microparticle-submicroparticle repulsion predicted in Figure 6. At larger distances, the density profile remains slightly below the bulk value and then returns to the bulk density at approximately 350 nm. These unique features at large distances are not readily intuitive from the energy profiles shown in Figure 6 but arise from the inclusion of the higher-order concentration effects through the 2nd virial coefficient. In addition, it should be mentioned that because only a second-order virial expansion was used in predicting the density profiles, the relative number densities shown in Figure 6.7 are only approximate, especially at the large peak at approximately 40 nm.

As two such microparticles approach, the interaction of these unique density profiles (a halo of submicroparticles bracketed by regions essentially void of nanoparticles) leads to the interesting energy profile predicted at large separations in Figure 6.5.

6.3.2. Approximate model

One of the drawbacks associated with calculating the depletion interaction using the equations in Chapter 3.3 is the time and difficulty associated with numerically calculating the three dimensional integrals. This primarily arises from the extreme and rapidly changing values that result from the exponential terms in the equations.

In many cases, an approximate but much faster model for predicting the depletion interaction would be extremely helpful. Toward this goal, we described in section 3.4 a model applicable for a binary system (e.g., two large particles interacting in a solution of small particles) in which the pair potential between the large and small particles is approximated using a simple square well expression of the form

$$E_{large\text{-}small} = \begin{cases} \infty & \text{if } d \le \tau_1 \\ -kT\,ln(1+\varepsilon_1) & \text{if } \tau_1 < d \le \tau_2 \\ -kT\,ln(1-\varepsilon_2) & \text{if } \tau_2 < d \le \tau_3 \\ 0 & \text{if } d > \tau_3 \end{cases} \qquad [6.4]$$

Here ε_1 and ε_2 are energy parameters, τ_1, τ_2 and τ_3 are distance parameters, and d is surface-to-surface separation between large and small particles. This interaction is shown graphically in Figure 3.2. As seen, this functional form is general enough to allow long range attraction and repulsion in addition to a hard-wall repulsion at contact.

The resulting depletion interaction between two large particles is obtained by inserting this potential into Eqs. [3.43] and [3.44] and integrating (the integrals can now all be performed analytically). It should be noted that higher-order interactions between the small particles themselves are ignored in this approach (i.e., no 2nd virial coefficients in Eq. [3.44]), meaning that the model is limited to relatively low concentrations of small particles. The resulting algebraic expressions are given in Chapter 3.4.

An illustration of the usefulness of this approximate square-well model is given in Figures 6.8 and 6.9. Shown in Figure 6.8 is the actual and approximate pair potential between a large and small particle. (In this case, the actual potential is the microparticle-submicroparticle interaction shown in Figure 6.6 for the case when nanoparticles are present in the system.) The parameters for the square well model, ε_1, ε_2, τ_1, τ_2 and τ_3, used to approximate the rigorous potential, were, 29, 0.99, 33 nm, 41 nm, and 108 nm, respectively.

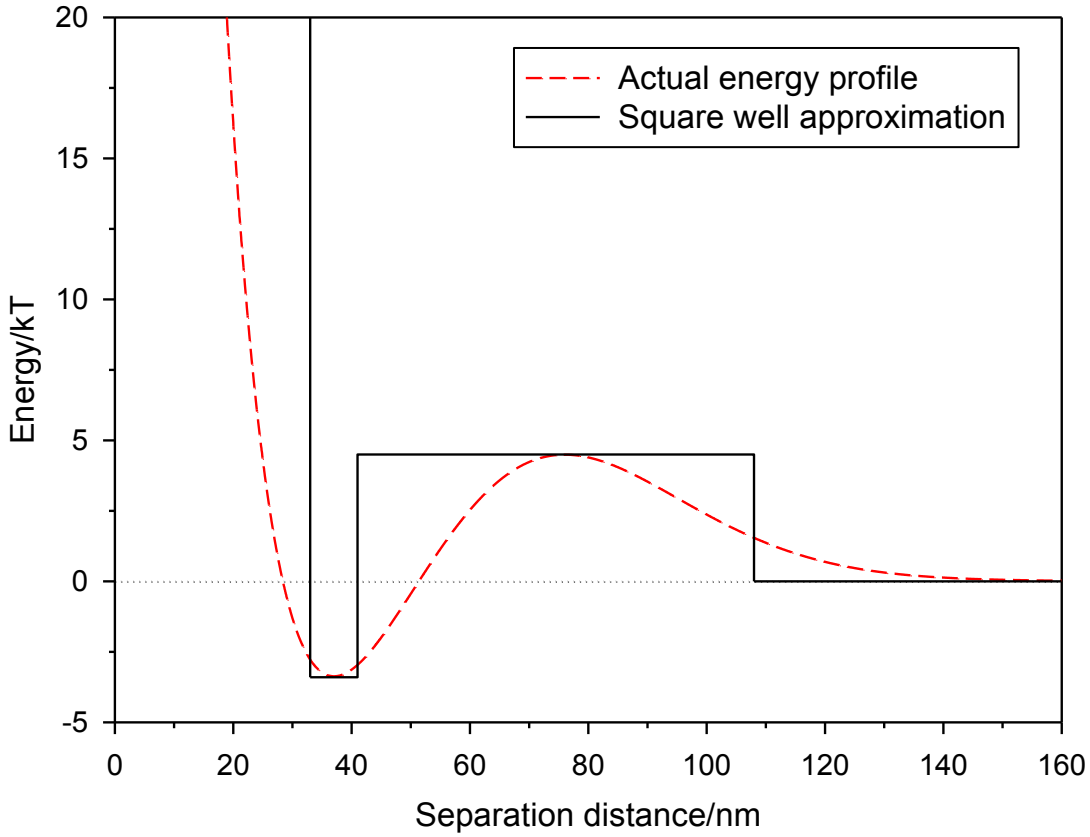

Figure 6.8. Illustration of the use of the square well potential of Eq. [6.4] to represent the true interaction between a large and small particle (actual energy profile taken from Figure 6.6).

Figure 6.9 compares the force profiles predicted using both the rigorous integration approach and the approximate square well model. As seen, the unique features of the force profile agree quantitatively with those predicted rigorously.

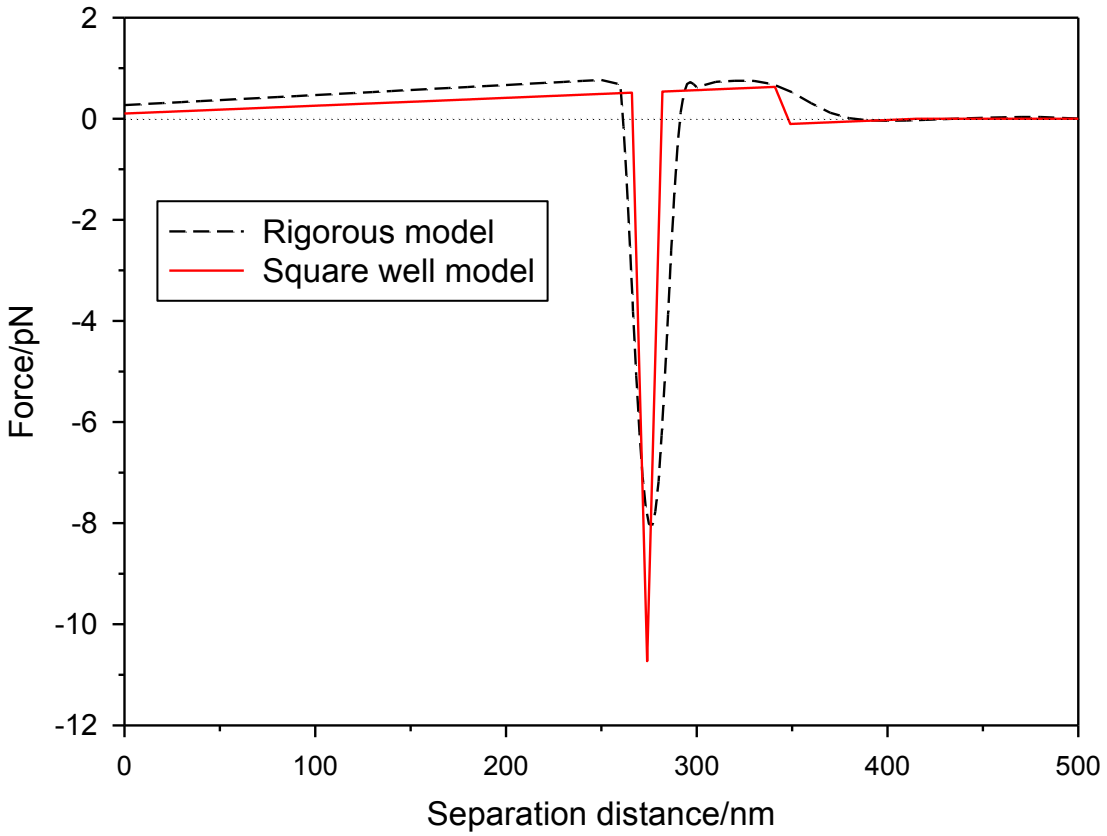

Figure 6.9. Comparison of the force profile between two microparticles predicted rigorously using Eqs. [3.43] and [3.44] and that predicted using the square well model described in Chapter 3.4. The microparticle-submicroparticle pair potentials used in the calculations are given in Figure 6.8.

6.4. Conclusions

We have shown that attractive depletion interactions, arising from the presence of nanoparticles, can be used to produce a halo of submicroparticles around larger microparticles. Specifically, the nanoparticles produce a secondary energy well in the microparticle-submicroparticle pair potential that leads to a local increase in the concentration of submicroparticles displaced a finite distance from the microparticle surface. The effect produces unique features in the microparticle-microparticle pair potential that cannot be predicted from the profiles in binary-only systems (i.e., microparticles with only submicroparticles or microparticles with only nanoparticles). Perhaps most interesting of these features are a very long range repulsive barrier and energy well that are clearly of sufficient magnitude to alter the stability of a dispersion of such microparticles.

In addition, a simple approximate model was presented for calculating the depletion interaction between two larger particles in a dispersion of smaller particles. The model is based on a square well description of the pair potential between the large and small particles. Using the algebraic expressions, this model was shown to be

capable of accurately capturing the important features of the microparticle-microparticle force profile.

7. Synergistic Effects of Nanoparticles and Polymers on Depletion and Structural Interactions

The work described in this chapter has been previously published as Ji, S., Walz, J.Y., *Langmuir* **29,** 49 (2013).

7.1. Introduction

This chapter describes an investigation into the synergistic effects produced by mixtures of polymers and nanoparticles, specifically negatively-charged silica nanoparticles and poly(acrylic) acid (PAA) polymer. Because of adsorption of the PAA onto the nanoparticles, we hypothesize that mixing these two materials together could create a depletion force that is much larger than found in either nanparticle-only or PAA-only systems. Colloid probe atomic force microscopy (CP-AFM) was used to measure the force profile between a large (30 μm) particle and silica plate in suspensions containing only nanoparticles, only polymers, or polymers and nanoparticles. The measured force profiles were then compared to predictions made using the force-balance model of Walz and Sharma,[8] in which the effective size of the depletant was an adjustable parameter. Using these fitted sizes, a possible structure of the polymer/nanoparticle complex is proposed.

7.2. Theory

The synergistic effect can be understood by considering the Asakura-Oosawa expression for the depletion interaction between two hard microspheres in a suspension of hard nanospheres. In this system, the force between two microspheres of radius R separated by gap width h is given by

$$F(h) = \begin{cases} -\rho_\infty kT\pi \left[a^2 + 2aR - Rh - \frac{h^2}{4}\right] & \text{for } 0 \le h < 2a \\ 0 & \text{for } h \ge 2a \end{cases} \qquad [1]$$

where ρ_∞ is the bulk number density of nanospheres of radius a. Consider, for example, the force between two microspheres of radius 5 μm in a suspension containing two different sizes of spherical nanoparticles, a_1 = 5 nm and a_2 = 10 nm, where the bulk number density of each nanoparticle type is $1 \times 10^{20}/m^3$. If the two nanoparticles do not interact, then the depletion force between the microparticles will, to first approximation, equal the sum of the forces calculated separately for each nanoparticle size using Eq. 1. This result is shown as the dashed red line in Figure 7.1. Note that the break in the line at a separation distance of 10 nm is the point where the smaller nanoparticles become excluded from the gap region between the microparticles.

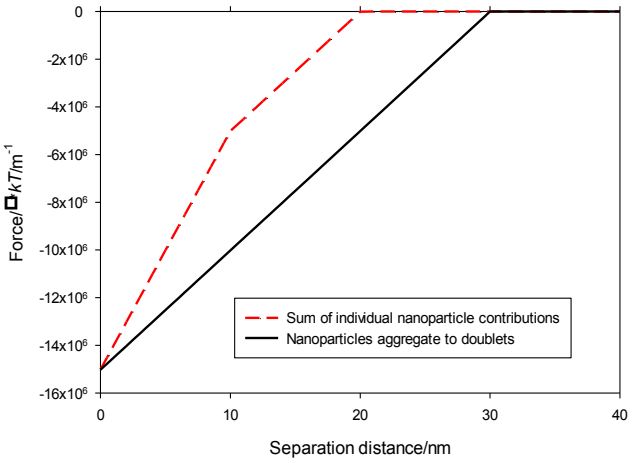

Figure 7.1. Shown here is the depletion force between two 5 μm spherical particles in a suspension of spherical nanoparticles of 5 nm and 10 nm radii (both at equal number densities). The dashed red curve is the force obtained by summing the forces produced by each type of nanoparticle independently, while the solid black curve is the force that results if each smaller nanoparticle forms a doublet with a larger nanoparticle.

By comparison, consider the result that would arise if each smaller nanoparticle were to form a doublet with a larger nanoparticle. It has been shown that the depletion force created by nonspherical depletants can be calculated as that produced by spherical depletants with an effective size equal to that obtained by rotating the depletant over all orientations (i.e., the excluded volume).[91] For this particular case, this would be a sphere of radius $a_1 + a_2$ equal to 15 nm. The resulting depletion force for this case is shown as the solid black line in Figure 7.1. Note that while the forces for the two cases are nearly identical at contact, the force for the aggregating case is significantly larger at larger separations.

7.3. Materials and Methods

7.3.1. Materials

A Barnstead EASYpure II system (Thermo Scientific, Asheville, NC, catalog #D7401) was used to deionize and purify the water used in the experiments, which had a resistivity of 18.2 MΩ-cm. The force measurements were obtained using an Asylum Research MFP-3D atomic force microscope. The cantilevers (Bruker, Santa Barbara, CA, model ORC8-10) had nominal spring constants of 0.05 N/m. Exact values for the spring constant of each cantilever used were obtained using the method of Hutter and Bechhoefer.[86]

The force measurements were conducted between a 30 μm diameter silica microparticle (Microsphere-Nanosphere, Cold Spring, NY, USA) and a silica plate (MTI Corporation, Richmond, CA, USA). The microparticles had a measured rms roughness of less than 1 nm over 1 μm^2. The same roughness was measured on the silica plates, which were polished z-cut single crystals with dimensions of 10 mm × 10 mm × 1.0 mm. LUDOX TMA silica nanospheres (Sigma-Aldrich, St. Louis, MO, catalog #420859, reported diameter of 22 nm) were used as the nanoparticles in the experiments. (Note that single crystal here refers to the fact that the slides were polished in such a way that only a single crystalline face was exposed.)

Poly(acrylic) acid (PAA) polymer (Sigma-Aldrich, St. Louis, MO, catalog #523925) with a manufacturer-reported molecular weight of 100,000 g/mol was used as the polyelectrolyte. The properties of the PAA were obtained by PSS-USA, Inc. (Amherst, MA) using gel permeation chromatography coupled with a static light scattering apparatus. The measurements were performed in a solution containing 3 g/l of polymer and 12 g/l of Na_2HPO_4. The measured number average and weight average molecular weights were 24,500 g/mol and 87,300 g/mol, respectively.

7.3.2. Methods

7.3.2.1. Force Measurements

Two groups of suspensions were used in the CP-AFM force measurements, all of which has a pH of 7.0. The concentrations of the silica nanoparticles and the PAA polymer as well as the ionic strengths in the experiments, are given in Table 7.1.

Table 7.1. The nanoparticle and polymer concentrations used in the force measurements.

Group 1 (Ionic strength: 0.2 mM)			Group 2 (Ionic strength: 1 mM)		
#	Silica nanoparticle concentration (volume fraction)	PAA polymer concentration (weight fraction)	#	Silica nanoparticle concentration (volume fraction)	PAA polymer concentration (weight fraction)
1	0.2%	0 ppm	1	1.5%	0 ppm
2	0.2%	30 ppm	2	1.5%	30 ppm
3	0	30 ppm	3	0	30 ppm

In order to prepare the nanoparticle suspensions, a specific amount of the stock suspension (15.8 vol%) was first diluted with deionized water in 20 ml scintillation vials (Wheaton Science Products Inc., Millville, NJ, Catalog #986540). Ion exchange resins (Bio-Rad, Hercules, CA, catalog #1437425) were then added into the suspensions and left with intermittent mixing for 18 hours. The suspensions were then removed and placed into clean vials. Polymer solutions of known concentration (e.g., 5000 ppm) were prepared, from which a specific volume was taken and added to the nanoparticle suspension such that the resulting PAA concentration was 30 ppm. The pH and ionic strength of each suspension were then adjusted using 0.1 M NaOH and 0.1 M NaCl.

An Asylum fluid cell was used to conduct the force measurements in liquid. An epoxy adhesive was applied to attach a microparticle to the tip of a cantilever and also to attach a silica plate to the glass disc of the fluid cell. Before the fluid cell was assembled, all of its parts were sonicated in ethanol, rinsed with deionized water and

then dried with nitrogen gas. The cantilever was cleaned by 40 minutes of exposure to UV light.

The sample fluid in the fluid cell was exchanged between each force measurement, which allowed measuring forces between the same microparticle and silica plate with various test suspensions. This was accomplished by injecting 2 ml of new sample fluid into one side of the cell while the old fluid was displaced from the other side. Fluid exchange was performed between each measurement.

When a force measurement was being performed, the microparticle was driven towards the plate at a speed of 80 nm/s, which ensured that hydrodynamic forces acting on the microparticle and cantilever were negligible. (Because our focus in this work was the long range depletion and structural forces, we utilized only the approach curves, as no additional information about these forces was provided in the withdrawal curves.) The data collection rate was 1000 Hz. Noise in the data was eliminated using an averaging program in order to obtain smooth curves. In this program 50 curves were combined and discretized into bins with widths ranging from 0.3 nm to 2 nm depending on the steepness of the curve. The forces in each bin were then averaged.

7.3.2.2. Size and Zeta Potential Determination

The sizes and zeta potentials of the nanoparticles were measured with a Malvern Zetasizer Nano-ZS (Malvern Instruments, Ltd., Worchestershire, UK). To measure the size, a sizing cuvette was used, while a zeta cell was used for the zeta potential measurements. Prior to the measurements, both the cuvette and cell were first rinsed with ethanol and then deionized water.

A Micro-Electrophoresis Apparatus Mk II (Rank Brothers, Ltd., Cambridge, England) was used to measure the zeta potential of the large silica particles used as the AFM probe. Because of sedimentation issues with the actual 30 μm silica particles used in the force measurements, the zeta potential of 1 μm silica particles (Polysciences, Warrington, PA, catalog #24326) was measured instead. To conduct the measurements, the speed of the particle's horizontal movement under a known electric field was measured, from which the electrophoretic mobility and zeta potential could be calculated. The zeta potential of the silica plate was assumed to be equal to that of the silica microparticles.

7.3.2.3. Adsorption Measurement

A QCM-D instrument (Q-Sense, Linthicum, MD, Model E1) with a silica crystal sensor was used to investigate the adsorption of the PAA polymers on the silica surfaces. To clean the experimental equipment, a silica sensor crystal was first sonicated in a 2% sodium dodecyl sulfate (SDS) solution for 10 minutes. The crystal was then rinsed with ethanol and water and dried with nitrogen gas. After that it was left under UV exposure for 30 minutes. The flow module was cleaned by sonication in deionized water for 30 minutes then dried with nitrogen gas.

The silica sensor crystal was installed in the assembled flow module before each experiment. Water and the PAA solution (30 ppm) were then flowed into the module consecutively. Both solutions had pH and ionic strength values of 7.0 and 0.2 mM, respectively. The data collection did not start until 5 minutes after the solution was flowed into the system so that the system could reach equilibrium.

In order to measure the adsorption of the PAA on the silica surfaces, the resonance frequency of the vibrating silica sensor crystal was collected with and without the PAA in the solution. The change of the resonance frequency was then converted to the mass change of the sensor crystal using the Sauerbrey equation,[92] $\Delta m = -C\Delta f$. Here Δf represents the frequency change and C is equal to 17.7 ng/cm^2. (The constant C in the Sauerbrey equation is related to the resonance frequency, surface area, and density of the sensor crystal.)

7.4. Results

7.4.1. Size and Zeta Potential Measurements

The measured sizes and zeta potentials of the microparticles (1 μm diameter measured at 0.1 vol%) and nanoparticles (measured at 0.2 vol%) are listed in Table 7.2. The PAA concentration used in the measurements, 30 ppm, is the same as that used in the force experiments. The pH and ionic strength of the samples were adjusted to be 7.0 and 0.2 mM, respectively.

Table 7.2. The results of the size and zeta potential measurements on the silica nanoparticles.

Property	Without the presence of PAA	With the presence of PAA
$\zeta_{microparticle}$/mV	-50	-65
$\zeta_{nanoparticle}$/mV	-65	-80
Nanoparticle diameter/nm	22	54

According to the table, the magnitudes of the zeta potentials for both the nanoparticles and microparticles increase after being mixed with the PAA polymer. In addition, the diameter of the nanoparticles increases from 22 nm to 54 nm upon addition of the PAA. These results suggest adsorption of the PAA onto the silica with an adsorbed layer thickness of 16 nm.

Note that these size and zeta potential measurements were not performed with the 1.5 vol% nanoparticle system plus 30 ppm polymer, as in these systems there was significantly less than one polymer chain per nanoparticle and the results would not be meaningful.

QCMD measurements were performed to confirm the adsorption of the PAA polymer onto silica. In this measurement, a 30 ppm PAA polymer solution with pH and ionic strength equal to 7.0 and 0.2 mM, respectively, was flowed over a single crystal silica plate with a flow rate of 0.1 ml/min. The measurement was taken after the polymer solution flowed for 5 minutes when the adsorption reached equilibrium. The mass of the silica sensor crystal became greater with the presence of the PAA polymers. The area density of the adsorbing PAA polymer on the silica sensor crystal was measured to be 15.9 ng/cm^2, which gave a number density of 3.9×10^{11} chains/cm^2 based on the measured number average molecular weight (24,500 g/mol).

We should mention that the exact mechanism driving the PAA adsorption is currently not known. Because both the PAA and silica slides are negatively charged, the driving force for adsorption must overcome the general electrostatic repulsion between them. Liufu *et al.*[93] studied the adsorption of PAA onto TiO_2, another metal oxide, and suggested hydrogen bonding and specific chemical interactions as important to adsorption in this system, however it is not clear the significant of such interactions in our PAA-SiO_2 system.

7.4.2. Force Profiles

Figure 7.2 shows the results of the CP-AFM force measurements conducted in systems containing either silica nanoparticles only (0.2 vol%), PAA polymer only (30 ppm), or a mixture of nanoparticles and PAA (0.2 vol% and 30 ppm). The ionic strength in all samples was 0.2 mM. In the mixed nanoparticle/polymer system, the ratio of the number density of polymer chains to nanoparticles was approximately 2.1. As seen, at small separation distances the force curves are dominated by a strong repulsion. The inset of Figure 7.2 shows a semi-log plot of force versus separation distance. Calculating the inverse slope of the linear portion of these curves yields a decay length of approximately 20 nm for all systems, which is in good agreement with the calculated Debye length of 21.3 nm. This indicates that at these separations, the force is dominated by an electrostatic repulsion. At larger distances, a distinct nonlinearity is observed in the semi-log plot of the force profile measured in the nanoparticle/PAA suspension, suggesting the presence of other forces.

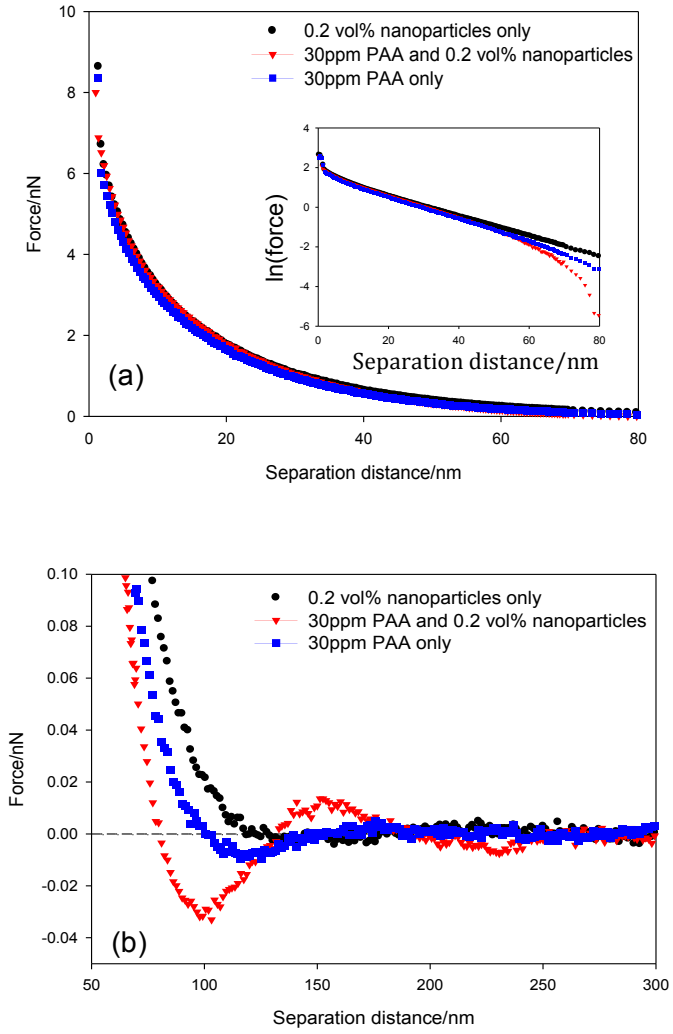

Figure 7.2. The measured force profiles between a 30 μm silica microparticle and a silica plate and the pH and ionic strengths of the samples were equal to 7.0 and 0.2 mM respectively. Figure 2b is an expanded view of Figure 2a at larger separations. The inset of Figure 2a shows the logarithm of force vs. separation distance profiles.

Figure 7.2b shows an expanded view of the force profile at large separation distances. With only nanoparticles present, a very small depletion attraction is seen. With only the polymer present, a slightly larger depletion attraction is found with a maximum attraction at approximately 110 nm. With both the nanoparticles and polymer, however, the magnitude of the maximum attraction is increased by more than a factor of four, while a significant longer range repulsive barrier is also measured with a maximum at approximately 150 nm. This repulsive component, frequently termed the structural force, arises from ordering of the depletants around the microparticle and plate due to strong repulsions between them. This force has been studied extensively by numerous researchers.[7, 17, 21-23, 68]

It is clear by simply looking at the curves that there is a significant synergistic effect of having both of the nanoparticles and PAA together, as the magnitude of the depletion attraction and structural repulsion are much larger than the sum of the forces observed with only nanoparticles or only polymer. This finding suggests that the nanoparticles and PAA are associating into larger complexes, consistent with the size measurement results presented in Table 7.2.

Figure 7.3 shows the CP-AFM results in the systems that contained either nanoparticles only (1.5 vol%), PAA polymer only (30 ppm) or a mixture of nanoparticles and PAA polymer (1.5 vol% and 30 ppm). The pH and ionic strength of the samples were adjusted to be 7.0 and 1.0 mM, respectively. Because of the much higher nanoparticle concentration, the ratio of the number density of polymer chains to nanoparticles is only 0.28. Like the force profiles shown in Figure 7.2, the interactions at short distances are dominated by an electrostatic repulsion and are similar in all systems.

Figure 7.3b shows an expanded view of the force profile in these systems at larger separations. While no clear depletion attraction is seen with the polymer only system, depletion and structural forces are evident in the system of nanoparticles only and the mixed nanoparticle/polymer system. This lack of a depletion force in the polymer only system, specifically when compared to Figure 7.2b where depletion forces at the same polymer concentration were clearly evident, arises from the fact that the ionic strength in Figure 7.3b is five times higher than that in Figure 7.2b.

As with the 0.2 vol% nanoparticle system, it is clear that the depletion and structural forces in the mixed nanoparticle/polymer system cannot be obtained by simply summing the forces from the single depletant system. However the magnitude of the maximum attraction in the nanoparticle/polymer system in Figure3b is only approximately 50% greater than in the nanoparticle only system, compared to an increase of a factor of four in the 0.2 vol% nanoparticle system (Figure 7.2b). In other words, the synergistic effect, while still clear, is significantly smaller in this latter system. The likely explanation for this phenomenon is that with the higher nanoparticle concentration, there is significantly less than one polymer chain per nanoparticle (specifically 1 polymer chain to every 3.6 nanoparticles), meaning that only a small number of nanoparticle/polymer complexes can be formed.

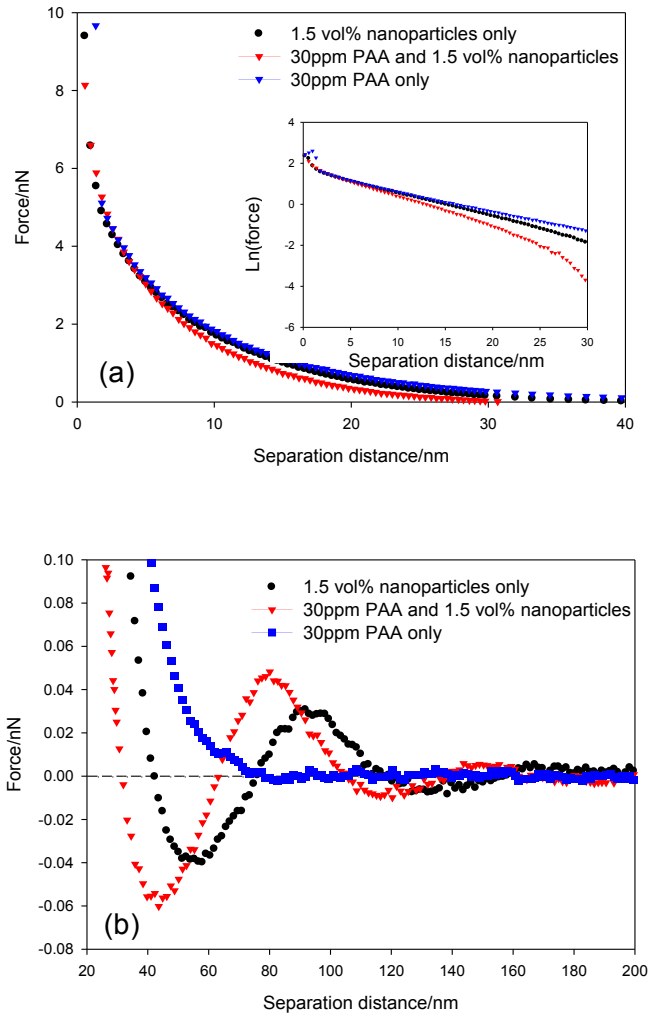

Figure 7.3. The measured force profiles between a 30 μm silica microparticle and a silica plate and he pH and ionic strengths of the samples were equal to 7.0 and 1.0 mM respectively. Figure 3b is an expanded view of Figure 3a at larger separations. The inset of Figure 3a shows the logarithm of force vs. separation distance profiles.

7.5. Discussion

7.5.1. Determination of the Sizes of the Nanoparticles and Polymer

The results presented in the Results section can be summarized as follows:

1. The PAA polymer adsorbs to the silica microparticle and plate, increasing the magnitude of the zeta potential. Based on the size measurements, the adsorbed layer thickness is 16 nm.
2. Force measurements with a low concentration of the nanoparticles (0.2 vol%) indicate a small depletion force with both nanoparticles only and 30 ppm polymer only. With both nanoparticles and polymer present (ratio of bulk number density of polymer chains to nanoparticles equal to 2.1), the

magnitude of the maximum attractive force increases by a factor of 4 and a significant, longer-range repulsive force is measured.

3. Force measurements with high concentration of the nanoparticles (1.5 vol%) and ionic strength of 1 mM showed a small depletion and a structural repulsion with only nanoparticles. No depletion forces were observed with only 30 ppm PAA at this ionic strength. In the mixed system, with a ratio of bulk number density of polymer chains to nanoparticles of 0.28, stronger depletion and structural forces were observed, however, the maximum attraction force increased by only 50% compared to the case of nanoparticles only.
4. In each sample group, the short-range component of the force profile was dominated by a strong electrostatic repulsion that was approximately equal in all systems (i.e., nanoparticles only, polymer only, and mixed nanoparticle/polymer systems).

To analyze these force curves further, we compared the measured results at low ionic strengths (Group 1 in Table 7.1) to predictions made using the force balance model of Walz and Sharma,[8] which calculates the depletion interaction between two charged spherical microparticles in a suspension of charged spherical nanoparticles. The pair potential between the nanoparticles and microparticles is assumed to consist of a screened electrostatic repulsion plus a van der Waals attraction, and the density distribution of nanoparticles around the microparticles is calculated using a 2^{nd} order virial expansion of the single particle distribution function. More details can be found in the paper of Walz and Sharma[8] as well as the subsequent work done by Walz and co-workers.[10, 12, 26, 91]

The model requires knowing both the bulk number density of the depletant material as well as its size. Because the size of the bulk PAA chains was not known, this value was used as a fitting parameter. The fitting criterion used was to match the value of the maximum attraction force predicted by the model to that measured. (Using the maximum attractive force avoid problems with inaccurate determination of the separation distance in the CP-AFM measurements.) To be consistent, and to provide a test of the model's validity, this same fitting procedure was used for all of the experimental systems, even when the size of the depletants had been measured independently. It should be mentioned that the decay lengths used for the electrostatic interactions in the model were determined from the short-range component of the force profiles (i.e., where electrostatic repulsion dominates), while the zeta potentials were based on the dynamic light scattering measurements. In addition, for all model results, we have assumed that the electrostatic surface potentials are equal to the measured zeta potentials.

Shown in Figure 7.4 are the results for the fitting procedure for the nanoparticle only system (0.2 vol%). For the model calculations we have assumed a decay length of 20.0 nm, $\zeta_{microparticle}$ and ζ_{plate} equal to -50 mV, $\zeta_{nanoparticle}$ equal to -65 mV, and a nanoparticle number density of $3.58 \times 10^{20}/m^3$. The nanoparticle diameter that provided the best fit to the maximum attractive force measured, is 22 nm, which is equal to that reported by the manufacturer and also to that measured experimentally, which supports the validity of the model.

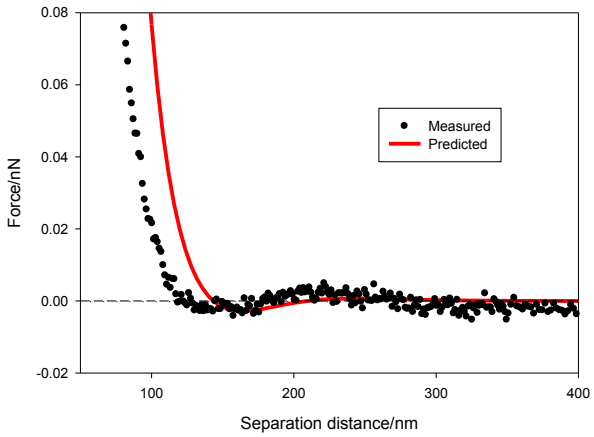

Figure 7.4. The comparison between the measured and predicted forces in the system containing only 0.2 vol% silica nanopartciles. The pH and conductivity are equal to 7.0 and 0.2 mM, respectively.

Nonetheless, it is clear from Figure 7.4 that while the shape of the measured curve is well described by the model, there is nonetheless an offset of approximately 20 nm in the separation distance. Our hypothesis is that this offset arises from one of two possible sources. First, any deposition of nanoparticles on to the surface of the silica plate or probe particle could result in an error in the measured force. (Separation distance in these experiments is measured relative to the point of hard contact between the probe particle and plate, which would clearly be affected any adsorbed nanoparticles.) While we note that the size of the offset in this case is approximately equal to the diameter of the nanoparticles, this could be something of a coincidence, since the offset would depend on the precise location of adsorbed nanoparticles relative to the point of closest approach between the large particle and plate.

The second possibility has to do with the very weak cantilevers used in the experiments. Specifically, determining the point of hard contact in these experiments is performed by pushing the probe particle toward the plate and looking for the point of constant compliance between the deflection of the cantilever and the movement of the AFM scanner. For systems in which there is a very strong repulsive force near contact, determining this point with weak cantilevers can be difficult. (This issue is discussed in greater detail by Luderitz *et al.*[94] and Piech.[95])

Shown in Figure 7.5 is a comparison of the force curves when the measured result from Figure 7.4 is shifted by 20 nm outward. As seen, agreement between the curves is now very good. It should be noted that a small, long-range repulsion can be also present in the measured curve. This repulsion is not completely captured by the model, presumably because only a 2nd-order density expansion is used.

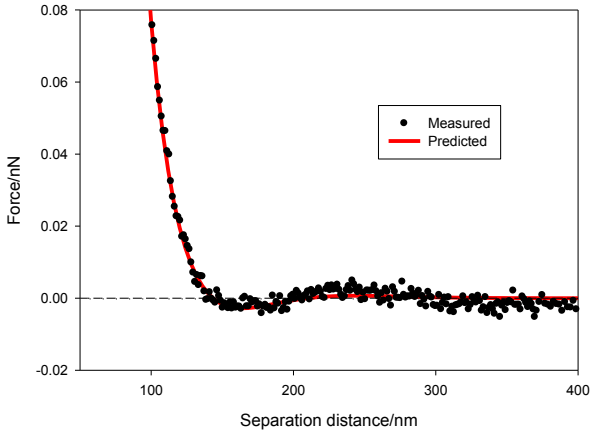

Figure 7.5. The comparison between the corrected measured and predicted forces in the system containing only 0.2 vol% silica nanoparticles. The measured curve has been shifted outward by 20 nm.

The same fitting procedure was used to determine the size (effective diameter) of the PAA polymer chains in the solution with an ionic strength of 0.2 mM. Figure 7.6 shows a comparison of the measured versus predicted forces. Note that the measured curve in the figure has again been shifted outward by 20 nm. For the model calculations we have assumed a decay length of 19.3 nm, $\zeta_{microparticle}$ and ζ_{plate} equal to -65 mV, $\zeta_{depletant}$ equal to -80 mV, and a polymer number density of $3.58 \times 10^{20}/m^3$. The number density of the PAA polymer is calculated from its weight percentage (30 ppm) and number average molecular weight. One assumption that was made here was that the zeta potential of the PAA polymer is equal to that measured in the nanoparticle/polymer system given in Table 7.2 (i.e., -80 mV). In addition, van der Waals interactions between the polymer chains and between the polymer chains and the interacting surfaces were ignored in the model calculations in this system.

The effective size (diameter) of the polymer chain that provided the best fit to the maximum attractive force was 17 nm. This is in very good agreement with the measured polymer layer thickness (16 nm) reported in Table 7.2.

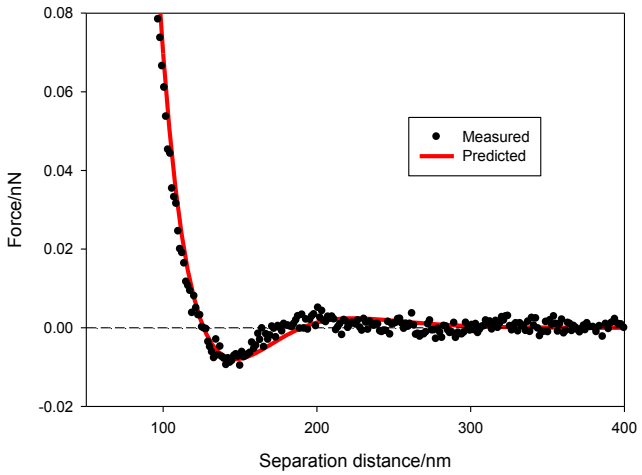

Figure 7.6. The comparison between the corrected measured and predicted forces in the system of 30 ppm PAA. The pH and conductivity are equal to 7.0 and 0.2 mM, respectively.

7.5.2. Determination of the Depletant Size in the Mixed Nanoparticle/Polymer System

Shown in Figure 7.7 are the results of the fitting procedure for the mixed nanoparticle/polymer system. The specific parameters used in the model calculations are a decay length of 20.0 nm, $\zeta_{microparticle}$ and ζ_{plate} equal to -65 mV, $\zeta_{depletant}$ equal to -80 mV, and a depletant number density of $3.58 \times 10^{20}/m^3$. Again, all parameters with the exception of the effective depletant size were known and fixed using independent measurements. The measured curve has been shifted here by 30 nm to match the model prediction. The fact that this is larger than the 20 nm shift needed in Figures 5 and 6 could result from a small amount of deposition of the larger nanoparticle/polymer complexes onto the microparticle and/or plate, or from the somewhat subjective nature of determining the point of hard contact between the microparticle and plate.

The diameter of the depletant found to provide the best match to the magnitude of the maximum attractive force was 56 nm, which is in excellent agreement with the DLS-measured size of 54 nm. It is also clear that while the depletant also provides a good approximation to the magnitude of the long-range repulsive barrier, the position of this barrier is poorly predicted. Very similar disagreements were also observed by Piech in CP-AFM experiments using only silica nanoparticles at increasing concentrations. This deviation arises from the fact that only a 2nd order density expansion is used in the Walz and Sharma model and thus higher-order interactions between nanoparticles, which become increasingly important at higher volume fractions and which are the cause of this repulsive barrier, are only approximately captured. For example, assuming a depletant diameter of 56 nm and a number density of $3.58 \times 10^{20}/m^3$ yields a depletant concentration of over 3 vol%, which is beyond the limits of accuracy for the model suggested by Piech.[95] However, Piech also found that even at these higher depletant concentrations, the magnitude of the maximum attractive force was still predicted relatively accurately.

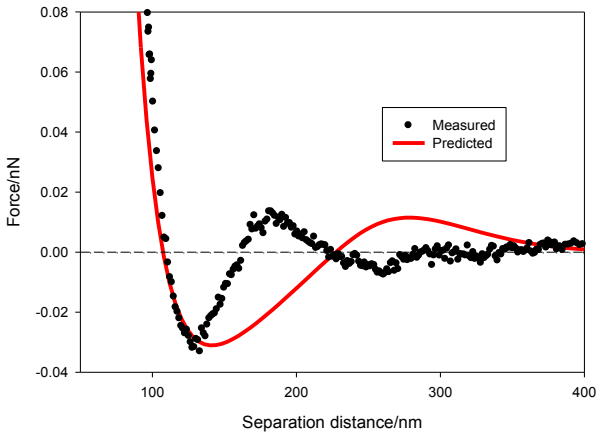

Figure 7.7. The comparison between the corrected measured and predicted forces in the system of 30 ppm PAA and 0.2 vol% silica nanoparticles. The pH and conductivity are equal to 7.0 and 0.2 mM respectively.

As further proof of the validity of this fitting approach, an experiment with only nanoparticles was performed at a nanoparticle concentration of 2 vol%, such that longer-range oscillations, similar to those seen in Figure 7.7, were evident. The results are shown in Figure 7.8, where the symbols are the measured results and the solid line is the model prediction made using a decay length of 8.0 nm, $\zeta_{microparticle}$ and ζ_{plate} equal to -50 mV, $\zeta_{nanoparticle}$ equal to -65 mV, and a nanoparticle number density of $3.58 \times 10^{21}/m^3$. The zeta potentials for the microparticle, nanoparticles and plate are the same as those used for the fitting at the lower nanoparticle concentration (Figure 7.5), while the Debye length of 8 nm was obtained from the slope of a semi-log plot of the force versus separation distance at small separations where electrostatic forces dominate. Note that because of the higher concentration of nanoparticles, the ionic strength of this solution is larger than that in Figure 7.5, hence the shorter decay length.

The nanoparticle diameter found to provide the best match to the maximum attractive force was 22 nm, which was the value found to provide the closest match to the magnitude of the maximum attractive force. This value is the same as that fit at the lower nanoparticle concentration (Figure 7.5) and also to that measured independently (Table 7.2). Thus while the model is unable to accurately match the long-range oscillations in the measured profile, it is able to accurately determine the size of the nanoparticle depletant.

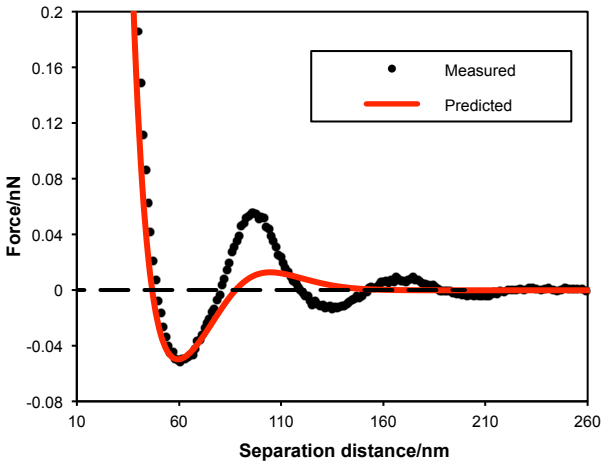

Figure 7.8. The comparison between the corrected measured and predicted forces in a suspension containing 2.0 vol% silica nanoparticles. The fitted size of the depletant was 22 nm, which is equal to the size reported by the manufacturer and also measure independently by light scattering. The measured curve has been shifted outward by 18 nm. The pH and ionic strength were equal to 7.0 and 1.0 mM, respectively.

In order the match the separation distances, the measured results in Figure 7.8 have been shifted outward by 18 nm, which is similar to the 20 nm shift needed with the lower nanoparticle concentration (Figure 7.5). Again, this shift is only used to plot the measured and predicted results and does not affect the fitting of the nanoparticle size.

Finally, it should be noted that this fitting procedure was not used with the system containing 1.5 vol% nanoparticles and 30 ppm polymer because of the low ratio of polymer chains-to-nanoparticles in the bulk. Specifically, for these concentrations there was only one polymer chain to every 3.6 nanoparticles. This means that a substantial number of the nanoparticles would not have any adsorbed polymer, thus fitting an effective depletant size would not be physically meaningful. Nonetheless, the fact that the measured curve in the nanoparticle/polymer mixture is significantly larger than the sum of the curves obtained in the polymer only and nanoparticle only systems indicates that a synergistic interaction of the two species is clearly occurring.

7.5.3. Possible Structure of the Nanoparticle/Polymer Complex

To develop a possible structure for the nanoparticle/polymer complex in the mixed system, we consider the following experimental findings:

1. Size and zeta potential measurements clearly indicate that the PAA chains adsorb to the silica nanoparticles.

2. The fitted size of the polymer chain in the polymer only solution was 17 nm while that of the depletant in the nanoparticle/polymer solution was 56 nm. This fitted size in the mixed system is approximately equal to the nanoparticle diameter (22 nm) plus twice the fitted polymer size.
3. The number density of polymer chains in the mixed system is approximately twice that of the nanoparticles.

If we assume that the majority of the polymer adsorbs and that it adsorbs somewhat uniformly, then one suggested structure is a nanoparticle with two polymer chains adsorbed radially opposite from each other. This picture is clearly the simplest one that is also consistent with the observed experimental results.

Note that one requirement of this possible structure is that the polymer chains do not change their conformation upon adsorption. This would only be true if the adsorption were quite weak, which could certainly be the case here since both the polymer chains and silica nanoparticles carry a net negative charge. It should also be emphasized that because the extended chain length of the polymer (85 nm) is nearly four times larger than the nanoparticle diameter (22 nm), any significant flattening or uncoiling of the polymer upon adsorption would result in chain-chain interactions. Without more information of the properties of the adsorbed layer, we can only speculate about its structure.

It should finally be mentioned that one other assumption made here is that the amount of polymer adsorbing to the microparticle and flat plate is much smaller than that adsorbing to the nanoparticles. Our justification for this assumption is that the total surface area presented by the nanoparticles in the AFM cell is four orders of magnitude larger than that presented by the microparticle and plate.

7.6. Conclusions

An experimental study was performed to evaluate the synergistic effects of a mixture of charged nanoparticles and like-charged ionic polymer on the depletion force between a charged microparticle and charged plate. At ratios of polymer chains-to-nanoparticles of both 2.1 and 0.28, the depletion and structural forces measured in the mixed nanoparticle/polymer system were substantially greater (i.e., as much as a factor of four) than the sum of the forces measured in the nanoparticle only or polymer only systems.

The effective size of the depletant was obtained by fitting the measured force profiles to the force-balance model of Walz and Sharma[8], with the depletant size as the only fitting variable. Comparison of the fitted sizes to available independent size measurements (i.e., for the nanoparticles and nanoparticle/polymer complexes) showed excellent agreement. In particular, the fitted size of the depletant in the mixed nanoparticle/polymer system with a bulk polymer chain-to-nanoparticle number density of 2.1, was 56 nm, which is equal to the nanoparticle diameter (22 nm) plus two polymer diameters (17 nm). While this might suggest a structure in which each nanoparticle has, on average, two polymer chains adsorbed radially opposite from each other, more information about the adsorbed layer would be required before a more accurate structure could be proposed.

These results indicate clearly that predicting the depletion force in mixed systems, such as the one used here, can be far more complicated than simply adding the results of the individual depletants. Specifically, complexation of the components can lead to substantially larger depletion and structural forces. These increased forces can potentially be large enough to alter the stability of a dispersion of microparticles.

8. Depletion Flocculation Induced by Synergistic Effects of Nanoparticles and Polymers

The work described in this chapter has been previously published as Ji, S., Walz, J.Y., *J. Phys. Chem. B,* **117,** 51 (2013).

8.1. Introduction

The work presented in this chapter is a follow-up to the force measurement work of Ji and Walz[96] and is aimed specifically at understanding how these synergistic effects can manifest themselves in altering the stability of a dispersion of colloidal particles. Two types of experiments were performed. First, visual flocculation tests were performed in which various concentrations of silica nanoparticles and PAA were added to an otherwise stable dispersion of micron-sized polystyrene latex particles. The stability results were then reconciled with direct measurement of the force between a single microparticle and plate, obtained using CP-AFM, with mixtures of the same PAA and nanoparticle concentrations as those used in the flocculation tests. These results clearly demonstrate the role that synergistic interactions between polymer and nanoparticles can have on colloidal stability.

8.2. Materials and Methods

8.2.1. Materials

A Barnstead EASYpure II system (Thermo Scientific, Asheville, NC, catalog #D7401) was used to deionize and purify the water used in the experiments, which had a resistivity of 18.2 MΩ-cm.

The flocculation tests were performed by observing the phase behavior of negatively-charged polystyrene microparticles (Thermo Fisher Scientific, Ashsville, NC, catalog #7100-2697-100250), which had a manufacturer-reported diameter of 1.2 μm.

The force measurements were obtained using an Asylum Research MFP-3D atomic force microscope. The cantilevers (Bruker, Santa Barbara, CA, model ORC8-10) had nominal spring constants of 0.05 N/m. More precise values for the spring constant of each cantilever were obtained using the method of Hutter and Bechhoefer.[86] The force measurements were conducted using a 30 μm diameter silica microparticle (Microsphere-Nanosphere, Cold Spring, NY, USA) and a silica plate (MTI Corporation, Richmond, CA, USA). The microparticles had a measured rms roughness of less than 1 nm over 1 μm^2. The same roughness was measured on the silica plates, which were polished z-cut single crystals with dimensions of 10 mm × 10 mm × 1.0 mm.

LUDOX SM silica nanospheres (Sigma-Aldrich, St. Louis, MO, catalog #420794, reported diameter of 7 nm) were used as the nanoparticles in the experiments. PAA (Sigma-Aldrich, St. Louis, MO, catalog #523925) with a manufacturer-reported molecular weight of 100,000 g/mol was used as the polyelectrolyte. The properties of the PAA were obtained by PSS-USA, Inc. (Amherst, MA) using gel permeation chromatography coupled with a static light scattering apparatus. The measurements were performed in a solution containing 3 g/l of polymer and and 12 g/l of Na_2HPO_4.

The measured number average and weight average molecular weights obtained were 24,500 g/mol and 87,300 g/mol, respectively.

One difference between the stability and force measurement experiments performed here that should be addressed is that instead of polystyrene particles, used in the flocculation tests, the force measurements were actually performed with a silica particle interacting with a silica plate. The primary reason for this change was problems with gluing a polystyrene particle to the cantilever as well as increased roughness on larger polystyrene particles.

While these are obviously different materials with different properties, our feeling is that these force measurements nonetheless provide a good approximation to the electrostatic, depletion and structural interactions in the flocculation tests performed with polystyrene microparticles. As shown later in Table 8.2, the zeta potential of the large silica microparticles used in the CP-AFM force measurements and the polystyrene microparticles used in the flocculation tests are quite similar, especially in the presence of the PAA polymer. Since the other solutions conditions (i.e., pH and ionic strength), as well as the polymer and silica nanoparticle concentrations, were the same in both experiments, the electrostatic, depletion and structural interactions would all be similar. Furthermore, because of the strong electrostatic charge on all of the surfaces, van der Waals forces would not be expected to play a major role in controlling the stability of the dispersion (i.e., the flocculation that was observed was a result of attractive depletion forces and not van der Waals forces). As a result, the forces measured between the silica surface and plate, corrected for the sphere-sphere versus sphere-plate geometry and differences in particle size, should provide a reasonable approximation to those existing between the polystyrene particles.

A summary of the materials used in the flocculation and force measurement experiments is given in Table 8.1.

Table 8.1. Materials used in the experimental measurements.

Experiment	Materials Used
Flocculation	1.2 μm polystyrene latex particles 7 nm LUDOX silica nanoparticles PAA Polymer (M_n = 24,500)
CP-AFM Force Measurements	30 μm silica microparticle 10 mm × 10 mm × 1.0 mm silica slide 7 nm LUDOX silica nanoparticles PAA Polymer (M_n = 24,500)

8.2.2. Methods

8.2.2.1. Flocculation Tests

Before each flocculation test, mixtures of the silica nanoparticle and PAA were first prepared. In order to prepare the nanoparticle suspensions, a specific amount of the stock suspension was first diluted with deionized water in 20 ml scintillation vials (Wheaton Science Products Inc., Millville, NJ, Catalog #986540). Polymer solutions of known concentration (e.g., 5000 ppm) were prepared, from which a specific volume was taken and added to the nanoparticle suspension. The pH (8.0) and ionic strength (5.0 mM) of each suspension were then adjusted using 1.0 M NaOH and 1.0 M NaCl. The concentrations of the nanoparticle suspensions were 0, 0.2, 0.4, 0.6, 0.8 vol%. For each nanoparticle concentration, PAA concentrations ranged from 0 to 700 ppm (weight fraction).

To prepare samples for visual observation of stability, 3 ml of each PAA/nanoparticle mixture was transferred from the scintillation vial to a disposable cuvette (VWR International LLC., Atlanta, GA, Catalog #97000-588) and a specific amount of the polystyrene microparticle stock suspension was added to the mixture and well dispersed such that the resulting microparticle concentration was 0.03 vol%. The cuvettes were then placed against a black background and allowed to rest for 36 hours.

8.2.2.2. Force Measurements

CP-AFM force measurements were performed using PAA/nanoparticle mixtures of the same concentrations as those used in the flocculation tests.

An Asylum fluid cell was used to conduct the force measurements in liquid. An epoxy adhesive was used to attach a microparticle to the tip of a cantilever and also to attach a silica plate to the glass disc of the fluid cell. Before the fluid cell was assembled, all of its parts were sonicated in ethanol, rinsed with deionized water and then dried with nitrogen gas. The cantilever was cleaned by 40 minutes of exposure to UV light.

The liquid in the fluid cell was exchanged between each force measurement, which allowed measuring forces between the same microparticle and silica plate with various test fluids. This was accomplished by injecting 2 ml of new liquid into one side of the cell while the old liquid was displaced from the other side.

When a force measurement was being performed, the microparticle was driven towards the plate at a speed of 80 nm/s, which ensured that hydrodynamic forces acting on the microparticle and cantilever were negligible. The data collection rate was 1000 Hz. Noise in the data was eliminated using an averaging program in order to obtain smooth curves. In this program 50 curves were combined and discretized into bins with widths ranging from 0.3 nm to 2 nm depending on the steepness of the curve. The forces in each bin were then averaged.

8.2.2.3. Size and Zeta Potential Measurements

The sizes and zeta potentials of nanoparticles were measured with a Malvern Zetasizer Nano-ZS (Malvern Instruments, Ltd., Worchestershire, UK). Prior to the measurements, both the sizing cuvette and the zeta cell were first rinsed with ethanol and then deionized water.

A Micro-Electrophoresis Apparatus Mk II (Rank Brothers, Ltd., Cambridge, England) was used to measure the zeta potential of the large silica particles used as the CP-AFM probe particles. Because of sedimentation issues with the 30 μm silica particles used in the force measurements, the zeta potential of 1 μm silica particles (Polysciences, Warrington, PA, catalog #24326) was measured instead. To conduct the measurements, the speed of the particle's horizontal movement under a known electric field was measured, from which the electrophoretic mobility and zeta potential could be calculated. The zeta potential of the silica plate was assumed to be equal to that of the silica microparticles. The same method was used to measure the zeta potential of the polystyrene microparticles.

The size of the polystyrene microparticles was measured by depositing some of the particles onto a glass slide and imaging them with scanning electron microscopy.

8.3. Results

8.3.1. Size and Zeta Potential Measurements

The measured sizes and zeta potentials of the silica and polystyrene microparticles (measured at 0.01 vol%) and nanoparticles (measured at 0.2 vol%) are listed in Table 8.2. The pH and ionic strength of the suspensions were adjusted to be 8.0 and 5.0 mM, respectively, which are the same values used in the flocculation and force measurement experiments.

Table 8.2. The results of the size and zeta potential measurements.

Property	Without the presence of PAA	With the presence of PAA
$\zeta_{\text{silica microparticle}}$/mV	-60	-72
$\zeta_{\text{polystyrene microparticle}}$/mV	-75	-75
$\zeta_{\text{silica nanoparticle}}$/mV	-60 ± 5	-70 ± 5
Polystyrene microparticle diameter/μm	1.2	No measurement
Nanoparticle diameter/nm	8.5	8.5, 28 ± 3*

*When the ratio of polymer chains to nanoparticles was less than 3, two peaks in the size measurements were observed. At polymer-to-nanoparticle ratios greater than this, only the 28 nm peak was seen.

Based on the zeta potential measurements, the PAA adsorbs to silica, increasing the zeta potential on both the silica microparticles and nanoparticles to very similar values. This adsorption is further supported by the size measurements of the silica nanoparticles, which indicate an increase nanoparticle diameter from 8.5 nm to 28 nm in

the presence of the polymer, suggesting an adsorbed layer thickness of approximately 10 nm. Based on the fact that no change of the zeta potential of the polystyrene microparticle was observed in the presence of PAA, we conclude that very little adsorption onto these particles occurred.

8.3.2. Flocculation Tests

Shown in Figure 8.1 is a photograph of a series of vials containing 0.03 vol% latex particles (1.2 μm in diameter) at varying concentrations of PAA. Again, the pH and ionic strength of each sample was adjusted to be 8 and 5.0 mM, respectively. This and all subsequent photographs were taken 36 hours after the samples were mixed.

Samples A-F (0 – 500 ppm PAA) remained stable, as indicated by the white color of the dispersion. By comparison, both the 600 and 700 ppm PAA solutions flocculated, with the latex aggregates settling to the bottom of the vial. Without further refinement, we conclude that there is a clear critical flocculation concentration of 600 ppm PAA.

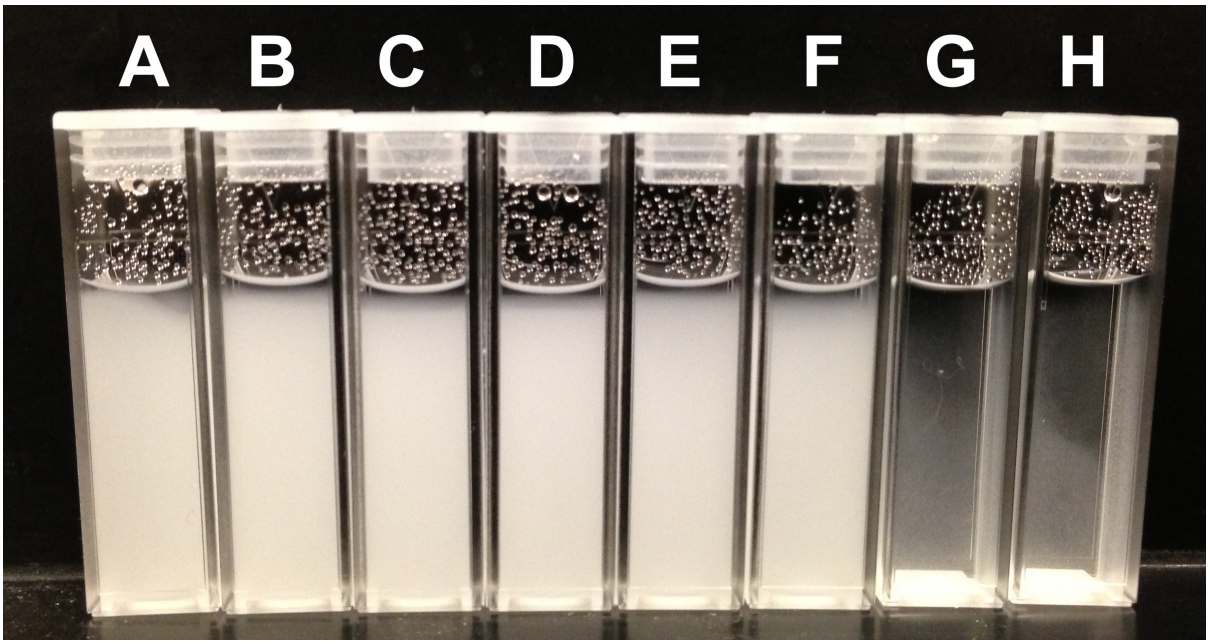

Figure 8.1. Photograph showing the stability of 1.2 μm polystyrene microparticles in the presence of only PAA. The pH and ionic strength of the suspensions were equal to 8.0 and 5.0 mM respectively. The concentrations of PAA were:

Sample	A	B	C	D	E	F	G	H
ppm (weight fraction)	0	100	200	300	400	500	600	700

By comparison, Figure 8.2 shows the results of the same experiment but now with 0.8 vol% silica nanoparticles present in each of the sample vials. Again, the pH and ionic strength of all samples was 8 and 5.0 mM, respectively. Now the critical

flocculation concentration has dropped to 300 ppm polymer, indicating that the nanoparticles have also contributed to the destabilizing the dispersion.

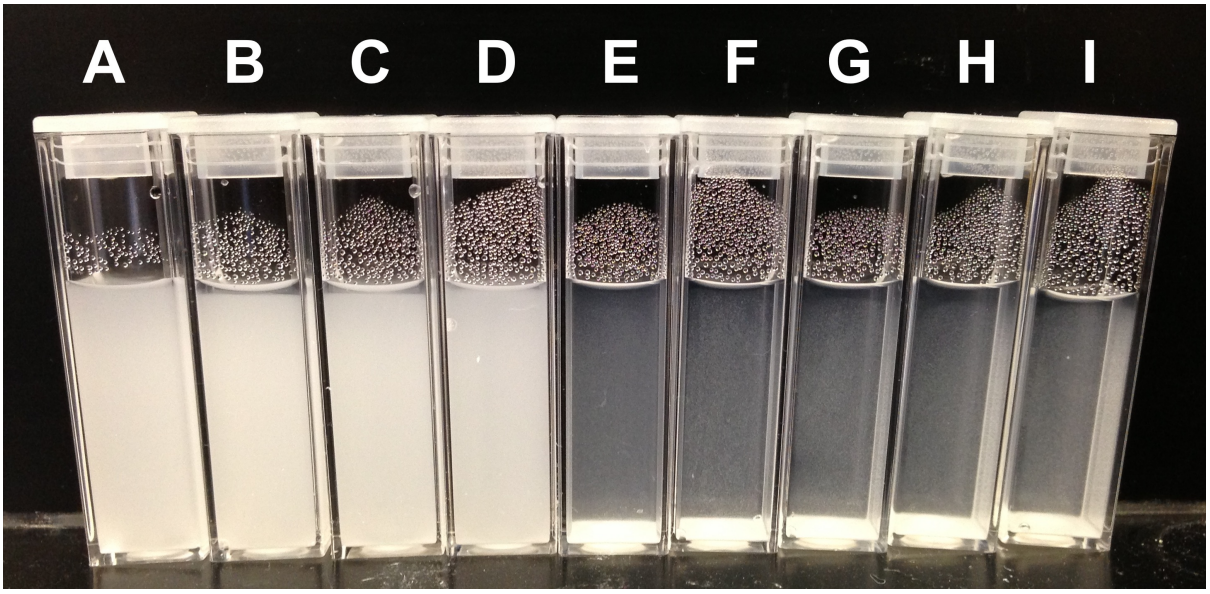

Figure 8.2. Photograph showing the stability of 1.2 μm polystyrene microparticles in the presence of 0.8 vol% silica nanoparticles and PAA of varying concentrations (The exception is that suspension A contained only microparticles). The pH and ionic strength of the suspensions were equal to 8.0 and 5.0 mM respectively. The concentrations of PAA were:

Sample	B	C	D	E	F	G	H	I
ppm (weight fraction)	0	100	200	300	400	500	600	700

Identical tests were performed with nanoparticle concentrations of 0.2, 0.4 and 0.6 vol%, again all at pH 8 and 5.0 mM ionic strength. The results are summarized in Table 8.2. As clearly seen, the critical PAA concentration needed for flocculation decreases as the silica nanoparticle concentration increases.

Table 8.3. Summary of the flocculation test results. S denotes a stable dispersion with U denotes an unstable one.

PAA concentration (weight fraction) \ Nanoparticle concentration (vol%)	0	0.2	0.4	0.6	0.8
0ppm	S	S	S	S	S
100ppm	S	S	S	S	S
200ppm	S	S	S	S	S
300ppm	S	S	S	S	U
400pm	S	S	U/S*	U	U
500ppm	S	U	U	U	U
600ppm	U	U	U	U	U
700ppm	U	U	U	U	U

*The sample containing 0.4 vol% nanoparticles and 400 ppm PAA showed some flocculation but remained partially cloudy.

8.3.3. Force Profiles

To investigate these stability tests further, CP-AFM measurements were performed to obtain the force profile between a large silica particle (30 μm diameter) and silica plate in solutions of silica nanoparticles and PAA polymer.

Figure 3 shows the measured forces in the solutions containing only PAA at varying concentrations. At small separations (Figure 3a), the force in all solutions is approximately the same. A semi-log plot of force versus separation, shown as the inset of Figure 3a, indicates that the force decays exponentially with distance, especially at the smaller PAA concentrations. Taking the slope of the linear regions in the semi-log plots yields a decay length of 3 nm, which is in good agreement with the calculated solution Debye length of 4 nm. This agreement indicates that the force at small separations is dominated by electrostatic repulsion between the large particle and plate.

Figure 3b shows an expanded view of the force profile at larger separation distances. As seen, at both 300 and 500 ppm PAA, attractive forces develop. With 700 ppm PAA, the attraction increases, plus a longer-range repulsive force is clearly evident. This repulsion is the onset of the oscillatory structural force.

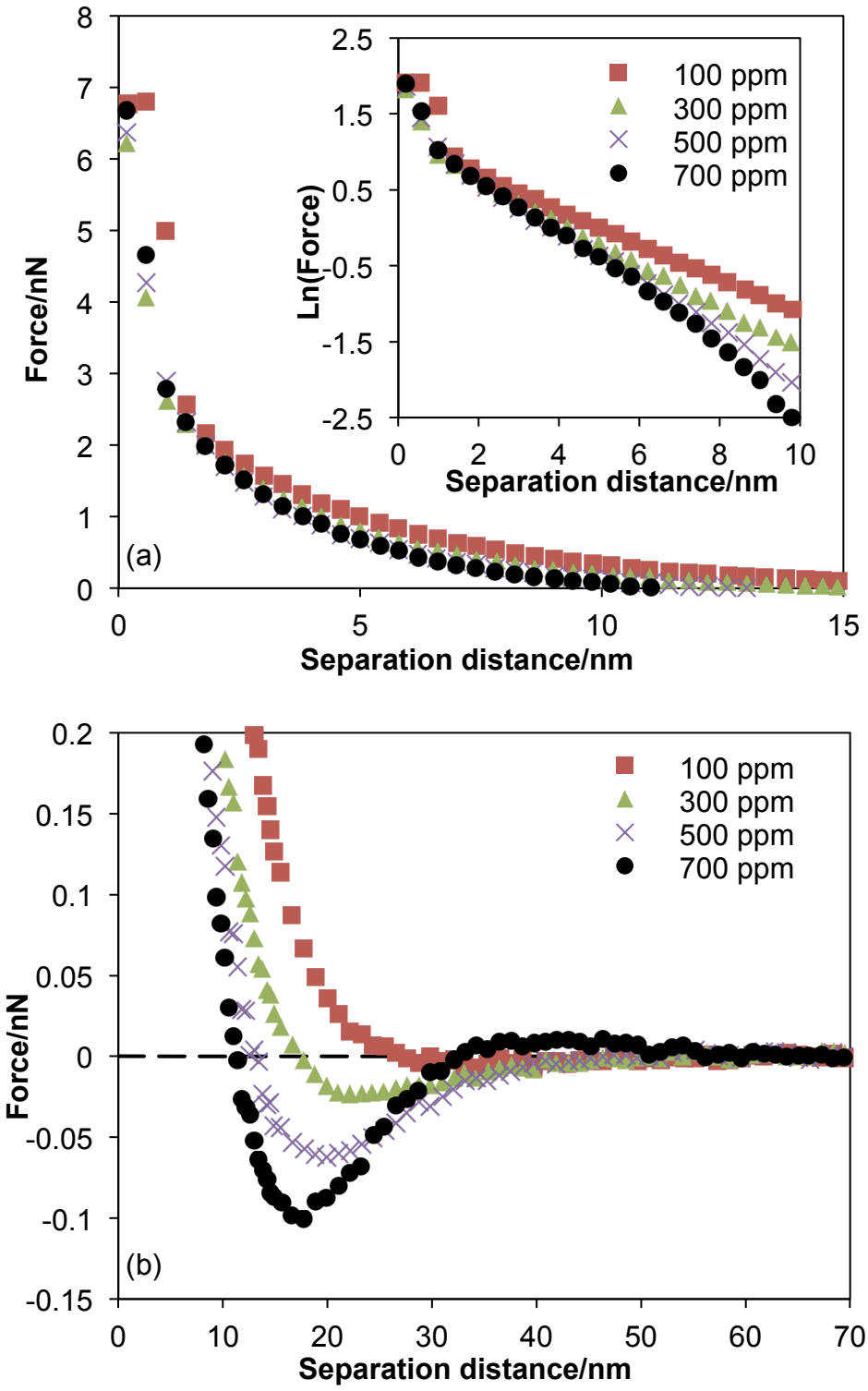

Figure 8.3. The measured force profiles between a 30 μm silica microparticle and a silica plate in solutions of only PAA. The pH and ionic strength of all solutions was 8 and 5 mM, respectively.The inset of Figure 3a shows a semi-log plot of force versus distance at small separations.

Figure 4 shows a similar set of force profiles but obtained now with 0.8 vol% silica nanoparticles in solution. At smaller separations, the profile is again dominated by electrostatic forces and the decay length obtained from the semi-log plot (inset of Figure 4a) is 3 nm, again in good agreement with the calculated Debye length.

The long-range trends shown in Figure 4b are similar to those observed without the nanoparticles (Figure 3b) except that the magnitudes are now significantly greater. For example, the magnitude of the maximum attraction measured with the 700 ppm PAA in Figure 4b (with 0.8 vol% nanoparticles) is approximately three times that observed in Figure 3b (no nanoparticles). This clearly indicates that both the PAA and nanoparticles are contributing to the depletion interaction.

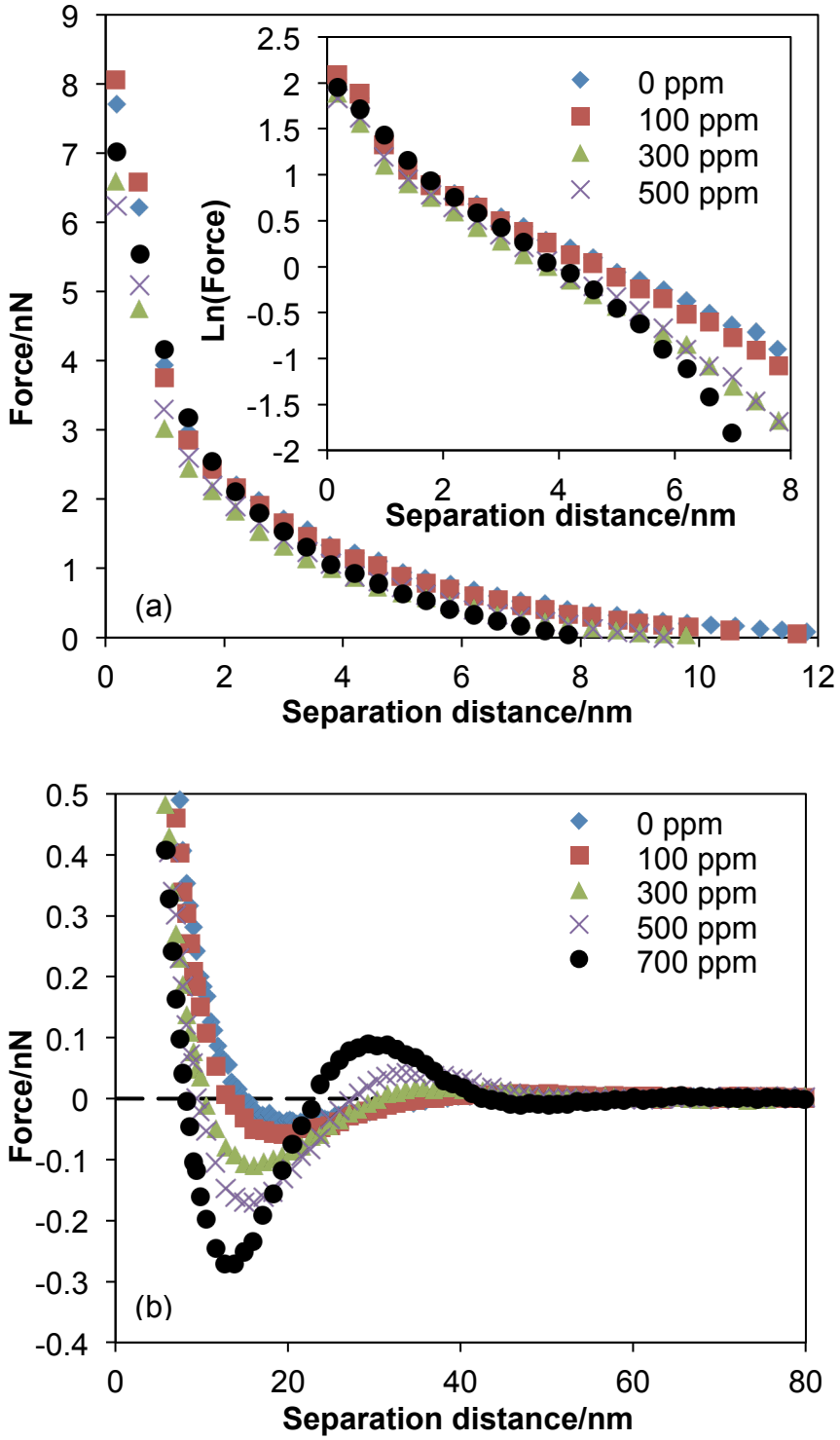

Figure 8.4. The measured force profiles between a 30 μm silica microparticles and a silica plate in suspensions of 0.8 vol% nanoparticles and varying concentrations of PAA. The pH and ionic strength of all dispersions was equal to 8 and 5.0 mM, respectively.The inset of Figure 4a is a semi-log plot of force versus separation distance at small separations.

Shown in Figure 5 are plots comparing the force profiles measured in solutions of only PAA, only nanoparticles (0.8 vol%), and PAA/nanoparticle mixtures at PAA concentrations of 100, 300, 500 and 700 ppm. It is very clear from these plots that the magnitudes of both the maximum attraction and maximum repulsion in the mixed system cannot be obtained by simply summing the equivalent values obtained with either only PAA or only nanoparticles. This result clearly supports the assertion that the two depletants in the mixed system have a synergistic effect on the depletion and structural force. Although not shown here, similar results were also observed with the 0.2, 0.4 and 0.6 vol% nanoparticle dispersions.

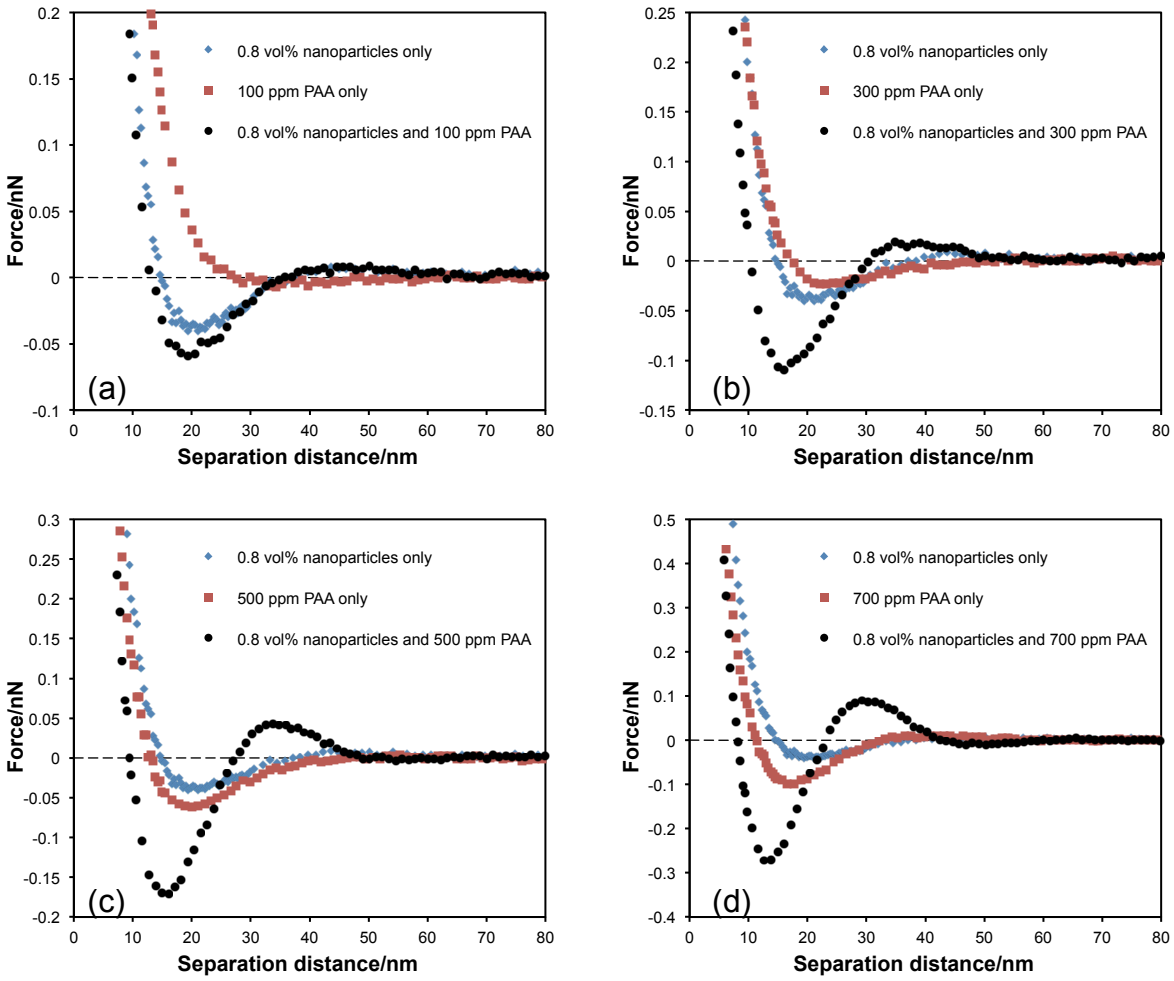

Figure 8.5. Comparison of the forces measured between a 30 μm silica microparticle and a silica plate in solutions of only nanoparticles, only PAA, and PAA/nanoparticle mixtures at varying PAA concentrations. The concentration of the nanoparticles was 0.8 vol% and the pH and ionic strength in all systems was 8 and 5.0 mM, respectively.

8.4. Discussion

The results presented above clearly show that flocculation of a dispersion of polystyrene particles occurs at PAA concentrations above a critical flocculation

concentration and that this concentration decreases as silica nanoparticles are added to the system. In addition, the measured force profiles show that the PAA and nanoparticles interact in a synergistic fashion in creating the depletion and structural forces such that the magnitude of these forces in the mixed system is larger than the sum of the forces measured separately in systems of only PAA or only nanoparticles at equivalent concentrations. In this section, we compare the observed stability behavior to the energy profiles between the polystyrene particles calculated from the measured force profiles.

To obtain the needed energy profiles, the force profiles, such as those shown in Figures 3 and 4, were first integrated to obtain the energy profiles between a 30 μm silica particle and plate. These profiles were then converted to the pair potential between two 1.2 μm diameter particles using the Derjaguin approximation,[97] which states that the energy at any separation scales with the particle radius and that the energy between two equal spheres is half that of an equivalent sphere and plate.

The resulting pair potential between two 1.2 μm particles in systems with no added nanoparticles (i.e., only PAA in solution), scaled in units of kT, is shown in Figure 6. As seen, the energy well is only 0.4 kT at 100 ppm PAA, but increases to 3.5, 4.6, 5.5 and 5.8 kT at PAA concentrations of 400, 500, 600 and 700 ppm, respectively. (The magnitude of the energy well was measured from the bottom of the well to the top of the long-range barrier, as this is the energy barrier that aggregated particles would need to overcome in order to separate.) By comparison, the long-range energy barrier never exceeds approximately 0.5 kT, meaning that it would not have a significant impact on particles aggregating in the energy well. From Table 8.2, it was found that flocculation in this system occurred at 600 ppm PAA, which would correspond to an energy well of 5.5 kT.

It should be mentioned that the energy wells shown here are secondary energy wells formed by attractive depletion forces and repulsive electrostatic forces. The much deeper primary energy wells that results from attractive van der Waals forces and short-range repulsive forces (e.g., steric forces) are not shown in these graphs. Because of strong electrostatic repulsive forces in these systems, flocculation into these primary energy wells would not be significant.

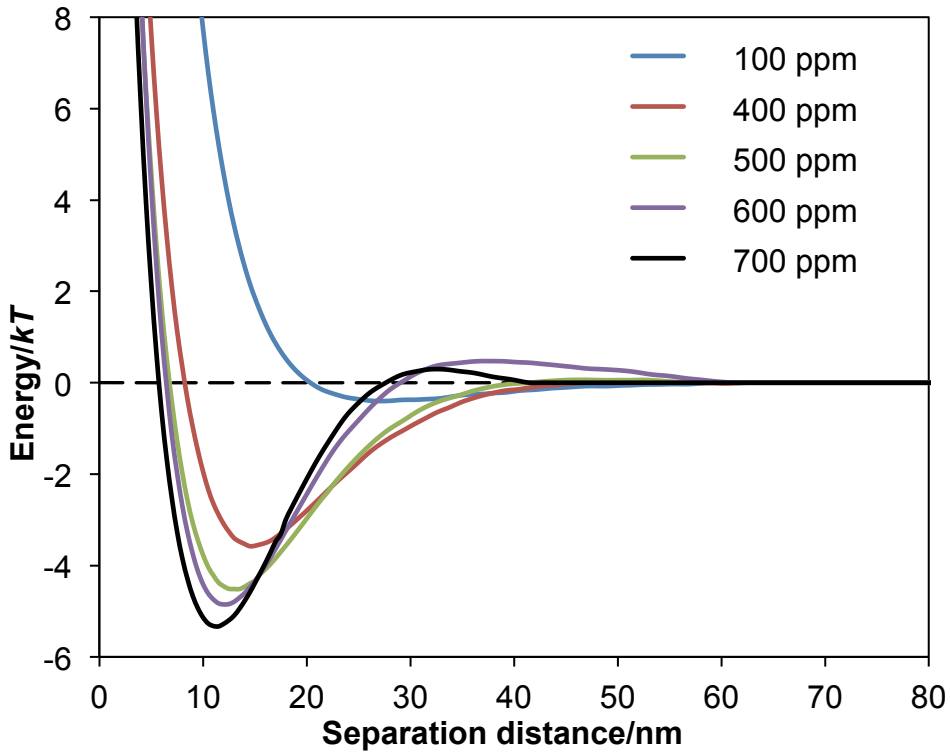

Figure 8.6. The energy profiles between two 1.2 μm polystyrene microparticles in solutions of only PAA with varying concentrations. The pHs and ionic strengths were 8.0 and 5.0 mM respectively.

By comparison, Figure 7 shows the corresponding energy wells calculated at varying PAA concentration in the presence of 0.8 vol% silica nanoparticles. Now the energy well, which is 2.4 *kT* with no added polymer, increases to 4.7, 6.1, 8.9 and 11.9 *kT* as the PAA concentration increases to 200, 300, 500 and 700 ppm. In addition, the long-range energy barrier at 700 ppm has now increased to 4.6 *kT*. However this value is still not believed to be large enough to prevent flocculation, as Feigin and Napper[98] suggest that restablization requires energy barriers of 15 – 20 *kT*.

As shown in Table 8.2, flocculation in this system was observed at 300 ppm PAA, which would correspond to an energy well of 6.1 *kT*, in good agreement with the value found in the systems with no added nanoparticles.

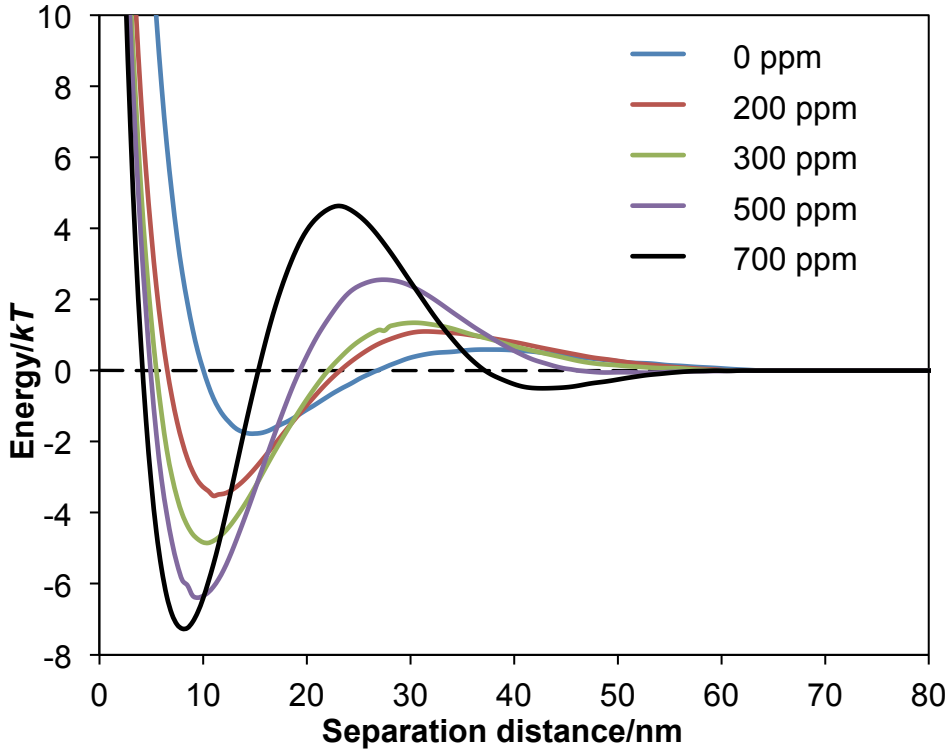

Figure 8.7. The energy profiles between 1.2 μm polyetyrene microparticles in the suspensions of 0.8 vol% silica nanoparticles and PAA of varying concentrations. The pH and ionic strength were 8.0 and 5.0 mM, respectively.

A summary of the stability results, plotted against the depth of the energy well and the height of the energy barrier, is shown in Figure 8. There is clearly a very sharp boundary between stable and unstable systems at an energy well of approximately 5 *kT*. This value is in good agreement with the values suggested by other researchers in this area. For example, Hogg and Yang[99] suggested a well depth of 1.5 – 10 *kT* as necessary to induce flocculation, while Feigin and Napper[98] suggested a value of 3 *kT*.

This graph also explains why restabilization at higher polymer/nanoparticle concentrations was not observed in our flocculation experiments. Specifically, the maximum height of the repulsive barrier achieved was only approximately 4.6 kT, which is well below the 15 – 20 *kT* value suggested by Feigin and Napper[98] as necessary for restabilization.

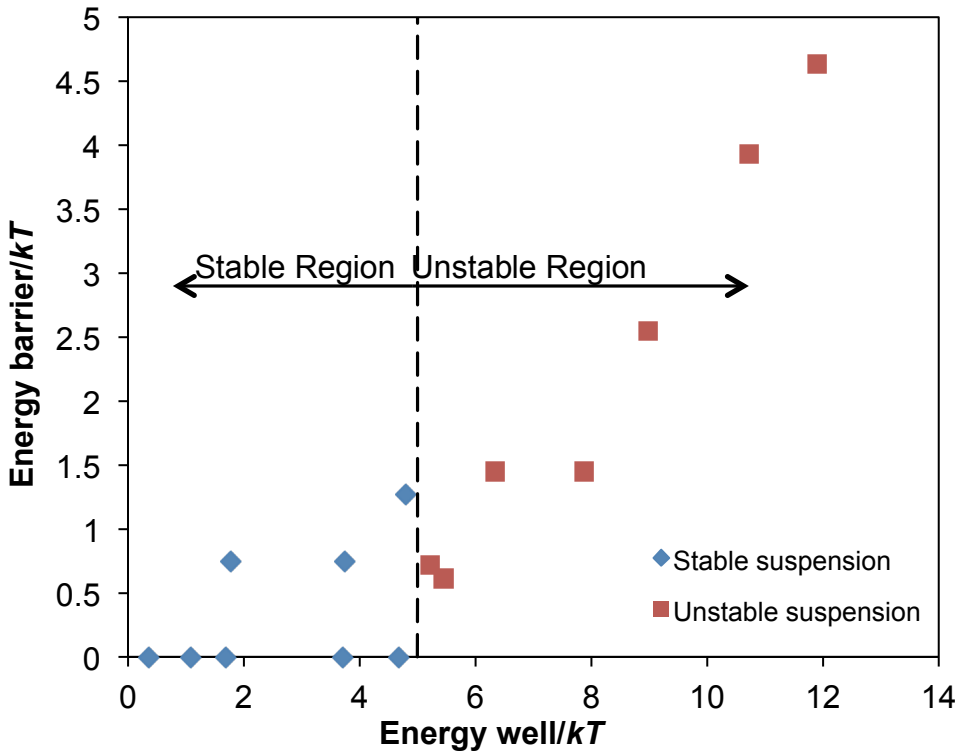

Figure 8.8. Summary of the dispersion stability and the corresponding magnitudes of depletion energy wells and structural repulsive barriers.

8.5. Conclusions

Our experiments clearly show that mixtures of poly(acrylic) acid (PAA) and silica nanoparticles can interact in a synergistic manner to destabilize an otherwise stable dispersion of charged colloidal particles. Specifically, the polymer adsorbs to the nanoparticles, creating a charged complex with higher zeta potential that is also more than three times larger than that of the bare nanoparticle. As a result, the depletion attraction and long-range structural forces that arise in mixed PAA/nanoparticle systems are significantly greater than the sum of the forces that arise in systems of only PAA or only nanoparticles at equivalent concentrations.

Flocculation experiments using 1.2 μm diameter polystyrene latex particles showed a very clear critical flocculation concentration of PAA, which was lowered as the concentration of added silica nanoparticles increased. Equilibrium pair potentials between the particles, calculated from force profiles measured between a large silica particle and plate using colloid probe atomic force microscopy, showed that flocculation occurred once the magnitude of the secondary energy well formed by the attractive depletion force exceeded 5 *kT*. This value is consistent with that reported by other researchers as that necessary for flocculation. Restabilization of the system at higher PAA/nanoparticle concentrations was not observed, which is again consistent with the fact that the long range energy barrier that arises from structural forces never exceeded 4.6 *kT* in these flocculation experiments.

These results clearly demonstrate how various solution components in a complex mixture can interact synergistically to alter system stability. As a result, predicting stability in such systems using results or predictions from single component systems may not be accurate.

9. Contributions and Suggestions for Future Work

9.1. Contributions

The work described in this dissertation focused on the synergistic effects on forces and stability that can arise when colloidal particles are in a solution that also contains at least two other dispersed species. The work produced several important contributions to the field of colloid and interface science, including:

1. It was shown experimentally that in binary systems consisting of weakly-charged microparticles and highly-charged nanoparticles, the nanoparticle halo effect that has been reported as a potential stabilizing mechanism most likely arises from simple, irreversible deposition of the nanoparticles onto the microparticle surface.
2. By comparison, a true, reversible halo effect could be formed in a ternary system consisting of highly-charged micron, submicron and nanoparticles. In this system, the nanoparticles create an attractive depletion interaction between the micron and submicron particles that is capable of trapping the submicron particles in energy wells near the surface of the microparticles.
3. In a system consisting of highly-charged nanoparticles plus a polyelectrolyte (of the same sign of charge), complexation of the nanoparticles and polyelectrolyte into a significantly larger, charged species can produce depletion and structural forces that are substantially larger than the sum of the corresponding forces measured in dispersions in which only nanoparticles or only polyelectrolyte is present.
4. The increase attractive depletion forces that are produced by the nanoparticle/polyelectrolyte complexes can cause flocculation of a dispersion of charged microparticles, even when the system remains stable when only nanoparticles or only polyelectrolyte is present.

These findings clearly indicate that predicting stability in colloidal systems containing multiple components, such as those described here, using behavior from simpler systems can be quantitatively and even qualitatively incorrect. Nonetheless, the work also suggests that the synergistic effects that arise in such systems can lead to new and novel approaches for controlling colloidal stability.

The results from this dissertation are further described in the following publications:

1. **Ji, S**.,Herman, D., Walz, J.Y., Manipulating microparticle interactions using highly charged nanoparticles, *Colloids Surf. A* **396**, 51 (2011).
2. **Ji, S.**, Walz, J.Y., Interaction potentials between two colloidal particles surrounded by an extremely bidisperse particle suspension, *J. Colloid Interface Sci.* **394**, 611 (2013).
3. **Ji, S.**, Walz, J.Y., Synergistic effects of nanoparticles and polymers on depletion and structural interactions, *Langmuir* **29,** 15159 (2013).
4. **Ji, S.**, Walz, J.Y., Depletion flocculation induced by synergistic effects of nanoparticles and polymers, *J. Phys. Chem. B* **117,** 16602 (2013).

9.2. Suggestions for Future Work

There are several interesting and useful studies that are recommended for further investigations into the topics presented here.

1. More rigorous modeling of ternary particle system
   Use of the force-balance model to calculate the depletion and structural forces in the ternary particle system described here required a number of assumptions that undoubtedly limited the accuracy of the results. Additional investigation into these types of systems should incorporate a more rigorous approach. One example would be a Monte Carlo simulation technique.

2. Comprehensive experimental measurement of forces in ternary particle system
   The force measurements presented in the Appendix represent a preliminary experimental study into the possible formation of a submicron particle halo. Unfortunately, the results were very noisy and while some evidence of a halo were observed, direct comparisons with predicted forces could not be made. It is suggested that a much more comprehensive study be conducted, specifically one in which the magnitude of the expected forces arising from the halo are much greater than the level of noise in the experimental technique. The model resulting from the previous recommendation could be used to identify such a system.

3. Effect of particle halos on dispersion stability
   In addition to direct force measurements in the ternary particle system, the effects of such particle halos on the stability of a dispersion of micron-sized particles is clearly warranted. Such measurements would demonstrate the potential use of these types of systems as novel approaches to controlling colloidal stability.

4. Additional studies into depletion/structural forces in polymer/nanoparticle mixtures
   The force-measurement and stability measurements described here with the polymer/nanoparticle system demonstrate the synergistic effects that can arise in mixed colloidal systems. Because of the common occurrence of such systems in industrial and consumer products, a wide variety of additional studies in this area could be conducted involving mixtures of nanoparticles, surfactants and polymers, each of which could be both useful as well as interesting academically.

Appendices

A1. Experimental Measurements of Ternary Systems

In this section the interactions between a microparticle and a silica plate were measured in mixtures of submicron particles and nanoparticles. The purpose was to conduct a preliminary experimental investigation demonstrating the submicroparticle halo phenomenon discussed in Chapter 6.

Table A1 shows the system conditions used in the experiment, which involved force measurements using colloidal probe atomic force microscopy. As shown by the table, all particles were silica spheres. The pHs of the solutions were equal to 8.0, while the ionic strengths of the solutions were 2.0 and 5.0 mM when the nanoparticle concentration was equal to 1 and 2 vol%, respectively. The solutions were prepared using the same preparation procedures that were described in Chapters 7 and 8.

Table A1. Experimental system.

	Microparticle	Submicroparticle	Nanoparticle
Material	Silica	Silica	Silica
Size	30 μm	80 nm	8.5 nm
Concentration	-	3 vol%	1 or 2 vol%

The results shown in Figure A1 were obtained with 3 vol% submicroparticles and 1 vol% nanoparaticles. Shown here are the force curves measured with nanoparticles only (1 vol%), submicroparticles only (3 vol%), and a mixture of both at these concentrations. The force curve obtained in the solution of only submicroparticles shows a small depletion attraction at a separation distance of 50 nm. By comparison, the force curve in the nanoparticle-only solution shows both a structural repulsion (~60 nm) and a much greater depletion attraction (~40 nm). In the nanoparticle-submicroparticle mixture, these shorter range forces are retained, while a small and long range depletion attraction is observed at around 140 nm.

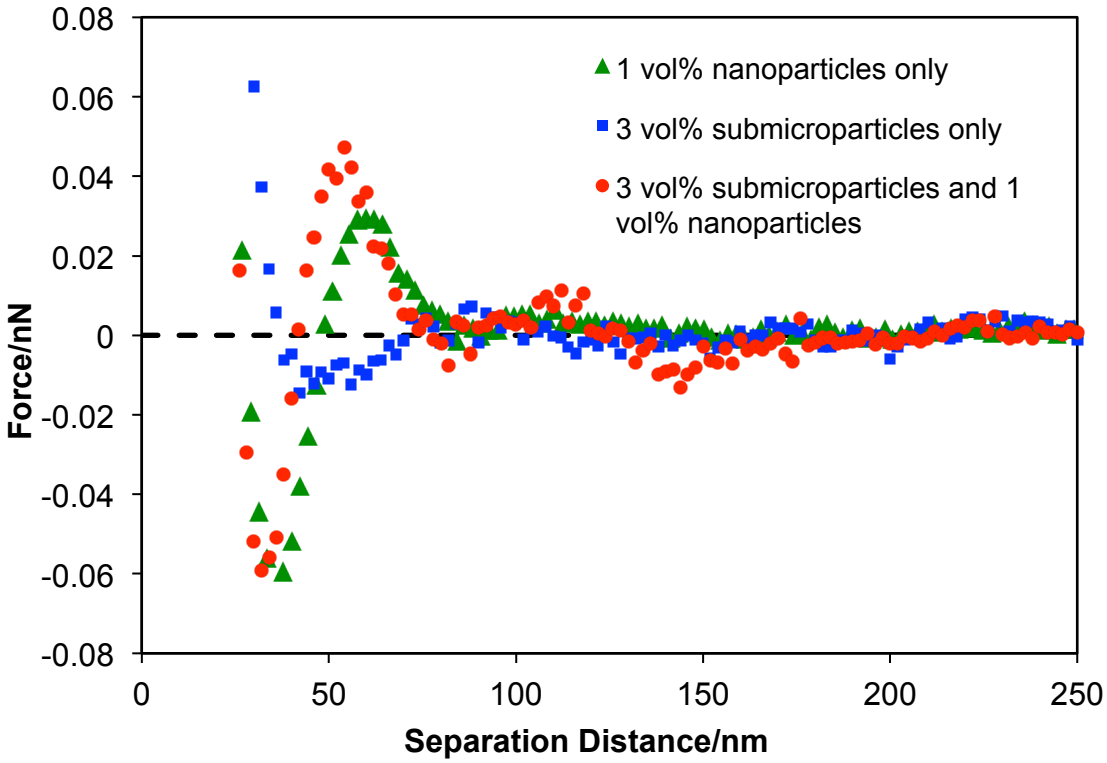

Figure A1. The measured forces with 3 vol% submicroparticles and 1 vol% nanoparticles. The solution contains nanoparticles only, submicroparticles only or the mixture of submicro- and nanoparticles. The solution pH and ionic strength are equal to 8.0 and 2.0 mM respectively.

Similar measurements were performed with a system consisting of 3 vol% submicroparticles and 2 vol% nanoparticles and the results are shown in Figure A2. Qualitatively, the results are very similar to those seen in Figure A1, namely that the short range features in the nanoparticle-only system are retained with the submicroparticle-nanoparticle mixture, while a very long range attraction appears in the mixed system at around 280 nm. While the magnitude of this depletion force is relatively small in both systems, it is still clearly larger than the level of noise in the measured force (this is especially true in Figure A2).

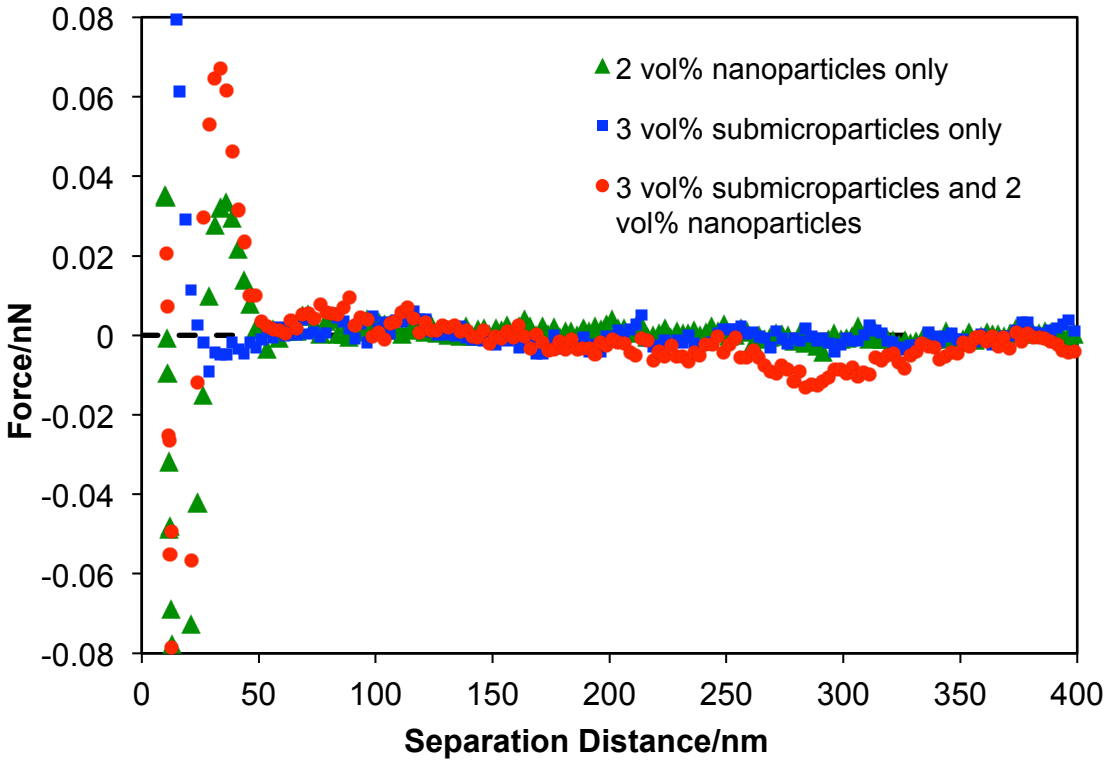

Figure A2. The measured forces with 3 vol% submicroparticles and 2 vol% nanoparticles. The solution contains nanoparticles only, submicroparticles only or the mixture of submicro- and nanoparticles. The solution pH and ionic strength are equal to 8.0 and 5.0 mM respectively.

Shown below in Figure A3 is the predicted force curve using the system described in Chapter 6. Although the modeling system is different from the experimental ones, a qualitative comparison of the data still suggests a good agreement between the predicted and experimental results, specifically the system shown in Figure A2. In both the predicted and experimental curves, an attractive depletion force of order 0.02 nN forms at a separation distance of roughly 270 nm. (In Figure A1, the attractive well is also measured, though at a much smaller separation distance. The reason for this discrepancy is not understood at this time.) These results indicate clearly that there are features in the force curves measured in the mixed system that cannot be predicted from the force curves measured in the nanoparticle-only or submicroparticle-only system. This supports the concept of a synergistic effect.

It was noticed that the noise in the experimental forces containing the submicroparticles was greater than in typical CP-AFM experiments. One possible reason for this noise is scattering of the laser beam used to measure the cantilever deflection by the submicroparticles. Because the long-range depletion force measured in these systems is relatively small, the force-to-noise ratio is lower than desired. Further experimental studies in this area should focus on a system in which the long range effects of the submicroparticle halo are expected to be larger. (Alternatively, a different experimental technique, such as total internal reflection microscopy,[27, 39, 40]

could be explored.) However, for a simple preliminary set of experiments, these results are certainly encouraging.

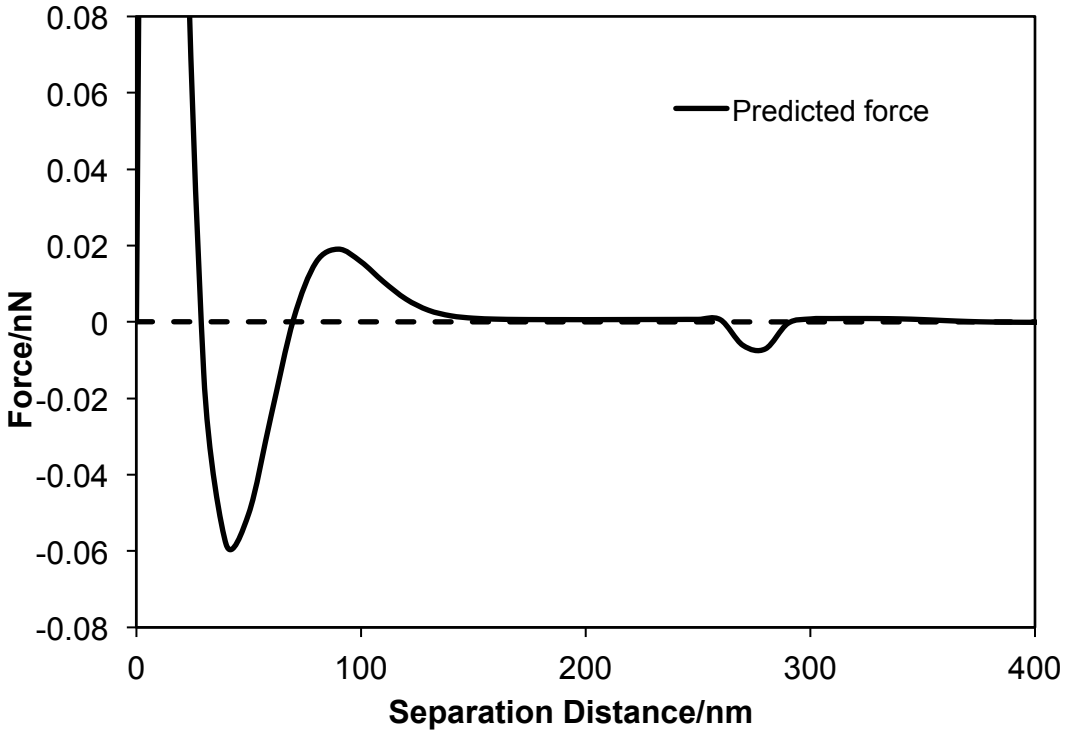

Figure A3. The predicted force calculated using the modeling system described in Chapter 6.

A2. Matlab Program for Lifshitz Theory

- Main program for obtaining the curve of Hamaker constants vs. separation.

```
global fo1 fo2 fo3 mw1 mw2 mw3 iruv1 iruv2 iruv3 mwnum1 mwnum2 mwnum3
global irnum1 irnum2 irnum3
global d1 d2 d3 tau1 tau2 tau3 w1 w2 w3 f1 f2 f3 g1 g2 g3
global kb T h1 c n material1 material2 material3 dl3 h ev unit1 unit2 unit3
rn

%1=metal (f+ir); 2=liquid (mw+ir); 3=nonconducting and nonpolar (ir only).
material1=3;
material2=3;
material3=2;

unit1=2; %1=standard unit, 2=ev unit
unit2=2;
unit3=2;

db=9.6e-9; %Debye length [=]m
pointnum=200;%number of points
hmin=0.0001e-9;%minimum distance between the surfaces [=]m
hmax=250e-9;%maximum distance between the surfaces [=]m

ev=1.601e-19; %[=]J
kb = 8.6173e-5; %boltzman constant [=]ev/K
T = 298; %[=]K
c= 3e8; %speed of light [=]m/s
h1= 6.5821e-16; %h bar [=]ev-s

%Put the spectra data in the excel file named information.
%Read data from the excel file: information.
fo1=xlsread('information.xlsx','f01');
fo2=xlsread('information.xlsx','f02');
fo3=xlsread('information.xlsx','f03');
mw1=xlsread('information.xlsx','mw1');
mw2=xlsread('information.xlsx','mw2');
mw3=xlsread('information.xlsx','mw3');
iruv1=xlsread('information.xlsx','iruv1');
iruv2=xlsread('information.xlsx','iruv2');
iruv3=xlsread('information.xlsx','iruv3');

%Measure the data size of microwave spectra and ir+UV spectra.
a=size(mw1); mwnum1=a(1);
a=size(mw2); mwnum2=a(1);
a=size(mw3); mwnum3=a(1);
a=size(iruv1); irnum1=a(1);
a=size(iruv2); irnum2=a(1);
a=size(iruv3); irnum3=a(1);

%Get material constants.
d1=mw1(:,1); d2=mw2(:,1); d3=mw3(:,1); %d=h, tau=g.
tau1=mw1(:,2); tau2=mw2(:,2); tau3=mw3(:,2);
w1=iruv1(:,1); w2=iruv2(:,1); w3=iruv3(:,1);
```

```
f1=iruv1(:,2); f2=iruv2(:,2); f3=iruv3(:,2);
g1=iruv1(:,3); g2=iruv2(:,3); g3=iruv3(:,3);

%Convert the data of standard unit to ev unit if necessary.
%According to Parsegian's book.
if (unit1==1)
    w1=w1.*h1;
    for j=1:irnum1
        f1(j)=f1(j)*w1(j)^2;
        g1(j)=g1(j)*w1(j);
    end
end

if (unit2==1)
    w2=w2.*h1;
    for j=1:irnum2
        f2(j)=f2(j)*w2(j)^2;
        g2(j)=g2(j)*w2(j);
    end
end

if (unit3==1)
    w3=w3.*h1;
    for j=1:irnum3
        f3(j)=f3(j)*w3(j)^2;
        g3(j)=g3(j)*w3(j);
    end
end

hmatrix=linspace(hmin,hmax,pointnum); %matrix of distance.
hm=zeros(1,pointnum); %set the hamaker constant in each distance to zero at
first.
inf=int32(1); %infinite used in NAG toolbox.
abs=0; %absolute error.
rel=1e-2; %relative error.

for j=1:pointnum
    h=hmatrix(j);

    for n=0:1000 %n value for the summation
%------------------------------------------------------------------------
%ksi needs to be ev unit because dielectric constant is dimensionless.
    ksin=2*pi*kb*T*n;
if (material3==1)
    irsum3=0;
   for k=1:irnum3
       irsum3=irsum3+f3(k)/(ksin^2+g3(k)*ksin+w3(k)^2);
   end
   dl3=1+fo3/(ksin)^2+irsum3;
elseif (material3==2)
    mwsum3=0;
    for k=1:mwnum3;
        mwsum3=mwsum3+d3(k)/(tau3(k)+ksin);
    end
    irsum3=0;
   for k=1:irnum3
```

```
      irsum3=irsum3+f3(k)/(ksin^2+g3(k)*ksin+w3(k)^2);
   end
    dl3=1+mwsum3+irsum3;
else
   irsum3=0;
   for k=1:irnum3
       irsum3=irsum3+f3(k)/(ksin^2+g3(k)*ksin+w3(k)^2);
   end
   dl3=1+irsum3;
end

%-------------------------------------------------------------------------
        %rn needs to be dimensionless.
        rn=2*h*(dl3^0.5)/c*2*pi*kb/h1*T*n;

        [result, abserr, w, iw, ifail] = d01am('integration', rn, inf, abs,
rel);

        if (n==0)
            %The effect of electrolyte
            intg=0.5*result*(1+2/db*h)*exp(-2/db*h);
        else
            intg=result;
        end

        hm(j)=hm(j)+intg;
    end

    hm(j)=-1*hm(j)*1.5*kb*T*ev;%convert hamaker constant from ev to J.
end

hmatrix=hmatrix*1e9;%convert unit of distance from m to nm.
plot(hmatrix,hm)
```

- Subroutine for completing integral in equation [3.6]

The file is names as “integration.m”.

```
function y=integration(x)
global n kb T h1 material1 material2 material3 fo1 f1 g1 w1 irnum1 mwnum1 d1
tau1
global irnum2 f2 g2 w2 fo2 mwnum2 d2 tau2 irnum3 f3 g3 w3 fo3 mwnum3 d3 tau3
global dl1 dl2 dl3 h c
%-------------------------------------------------------------------------
%Calculation of dielectric permitivity of material1
    ksi=2*pi*kb*T*n;
if (material1==1)

    irsum1=0;
   for j=1:irnum1
       irsum1=irsum1+f1(j)./(ksi.^2+g1(j).*ksi+w1(j).^2);
   end
   dl1=1+fo1./(ksi).^2+irsum1;
```

```
elseif (material1==2)

    mwsum1=0;
    for j=1:mwnum1;
        mwsum1=mwsum1+d1(j)./(tau1(j)+ksi);
    end
    irsum1=0;
   for j=1:irnum1
       irsum1=irsum1+f1(j)./(ksi.^2+g1(j).*ksi+w1(j).^2);
   end
    dl1=1+mwsum1+irsum1;

else

   irsum1=0;
   for j=1:irnum1
       irsum1=irsum1+f1(j)./(ksi.^2+g1(j).*ksi+w1(j).^2);
   end
   dl1=1+irsum1;

end

%Calculation of dielectric permitivity of material2
    ksi=2*pi*kb*T*n;
if (material2==1)

    irsum2=0;
   for j=1:irnum2
       irsum2=irsum2+f2(j)./(ksi.^2+g2(j).*ksi+w2(j).^2);
   end
   dl2=1+fo2./(ksi).^2+irsum2;

elseif (material2==2)

    mwsum2=0;
    for j=1:mwnum2;
        mwsum2=mwsum2+d2(j)./(tau2(j)+ksi);
    end
    irsum2=0;
   for j=1:irnum2
       irsum2=irsum2+f2(j)./(ksi.^2+g2(j).*ksi+w2(j).^2);
   end
    dl2=1+mwsum2+irsum2;

else

   irsum2=0;
   for j=1:irnum2
       irsum2=irsum2+f2(j)./(ksi.^2+g2(j).*ksi+w2(j).^2);
   end
   dl2=1+irsum2;

end
```

```
%Calculation of dielectric permitivity of material3
    ksi=2*pi*kb*T*n;
if (material3==1)

    irsum3=0;
   for j=1:irnum3
       irsum3=irsum3+f3(j)./(ksi.^2+g3(j).*ksi+w3(j).^2);
   end
   dl3=1+fo3./(ksi).^2+irsum3;

elseif (material3==2)

    mwsum3=0;
    for j=1:mwnum3;
        mwsum3=mwsum3+d3(j)./(tau3(j)+ksi);
    end
    irsum3=0;
   for j=1:irnum3
       irsum3=irsum3+f3(j)./(ksi.^2+g3(j).*ksi+w3(j).^2);
   end
    dl3=1+mwsum3+irsum3;

else

   irsum3=0;
   for j=1:irnum3
       irsum3=irsum3+f3(j)./(ksi.^2+g3(j).*ksi+w3(j).^2);
   end
   dl3=1+irsum3;

end
%-------------------------------------------------------------------------

s1=(x.^2+((2.*ksi./h1.*h./c).^2).*(dl1-dl3)).^0.5;
s2=(x.^2+((2.*ksi./h1.*h./c).^2).*(dl2-dl3)).^0.5;
s3=x;

dt13=(dl1.*s3-dl3.*s1)./(dl1.*s3+dl3.*s1);
dt23=(dl2.*s3-dl3.*s2)./(dl2.*s3+dl3.*s2);
dtb13=(s3-s1)./(s3+s1);
dtb23=(s3-s2)./(s3+s2);

y=x.*(log((1-dt13.*dt23.*exp(-1.*x)).*(1-dtb13.*dtb23.*exp(-1.*x))));
end
```

- Fitting Hamaker constants to obtain retardation wavelengths

```
lamda=105e-9;     %Manually change the value until two curves
sizehm=size(hm);
hmatrixnm=hmatrix*1e-9;
for j=1:sizehm(2)
retardation=1/(1+14*(hmatrixnm(j))/lamda);
hmapprox(j)=hm(1)*retardation;
end
```

```
plot(hmatrix,hm)
hold on
plot(hmatrix,hmapprox,'r')
```

A3. Matlab Program Used to Predict Depletion/Structural Forces in a Binary System

- Subroutine for calculation of effective surface potentials

The program was name as “surfpotential.m”.

```
function Y = surfpotential(a,phi,D)

tau = D*a;

if tau >= 25
    Y = phi*(1 - (4/3)*(phi/4)^4*(1-3/(2*tau)) +
(8/15)*(phi/4)^4*(1+25/(16*tau)));
else
    beta3 = -1/(6*(1+tau)^2)*(1/(1+tau) - exp(2*tau)*expint(2*tau) - 2*((tau-
1)/(tau+1))*exp(4*tau)*expint(4*tau));

    x3 = -((tau^2)/(6*(1+tau)^4))*(1 - 4*tau*exp(4*tau)*expint(4*tau));

    F = (@(x)(1./x).*exp(-2.*x).*expint(4.*x));
    x5 = (tau^5)/(120*(1+tau)^6)*(-1/(3*tau^3) + 1/(tau^2) + 14/tau -
10/(1+tau) - 24*exp(6*tau)*expint(6*tau) - 80/(1+tau)*exp(4*tau)*expint(4*tau)
- 80*((1-tau)/(1+tau))*exp(8*tau)*(expint(4*tau))^2 +
80*exp(6*tau)*(quadgk(F,tau,Inf)));

    z5 = 1/(240*(1+tau)^4)*(-1/(3*tau^3) + 2/(3*tau^2) + 22/(3*tau) +
10/(tau*(1+tau)) - (20*exp(2*tau)*expint(2*tau))/(1+tau) -
8*exp(4*tau)*expint(4*tau)*(11/3 + 5/(1+tau)) +
10*exp(4*tau)*(expint(2*tau)^2) + 40*((tau-
1)/(tau+1))*exp(6*tau)*expint(2*tau)*expint(4*tau));

    alpha3 = (tau^2)*((1+tau)^2)*beta3 - ((1+tau)^3)*x3;

    alpha5 = 3*((1+tau)^6)*(x3^2) - 3*(tau^2)*((1+tau)^5)*x3*beta3 -
((1+tau)^6)*x5/(2*tau) + (tau^4)*((1+tau)^4)*z5;

    Y = phi.*(1 + alpha3.*(phi.^2) + alpha5.*(phi.^4));
end
end
```

- Subroutine for calculating pair potentials (electrostatic and van der Waals interactions) between particles

The program was named as “ssenergy.m”.

```
function E = ssenergy(R,dec)
global epsl epsn k T e Y1 Y2 a1 a2 D psi1dim psi2dim model hmmn hmnn lamdamn
lamdann
```

```
if model == 1
    if dec == 1                     %large particle-nanoparticle interactions
        if R <= (a1+a2+1e-9)

            E = Inf;                %HSHW portion

        else

            %Bell, Levine, and McCartney model
            retardation=1./(1+14.*(R-a1-a2)./lamdamn);

            E = 4.*pi.*epsl.*epsn.*(k*T/(e^2)).*Y1.*Y2.*(a1.*a2./R).*exp(-
D.*(R-a1-a2))-(1.*hmmn./6.*retardation.*(2.*a1.*a2./(R.^2-
(a1+a2)^2)+2.*a1.*a2./(R.^2-(a1-a2)^2)+log((R.^2-(a1+a2)^2)./(R.^2-(a1-
a2)^2)))./(k.*T);

        end
    else                            %nanoparticle-nanoparticle interactions
        if R <= (a2+a2+1e-10)

            E = Inf;                %HSHW portion

        else

            %Bell, Levine, and McCartney model
            retardation=1./(1+14.*(R-a2-a2)./lamdann);

            E = 4.*pi.*epsl.*epsn.*(k*T/(e^2)).*Y2.*Y2.*(a2.*a2./R).*exp(-
D.*(R-a2-a2))-(1.*hmnn./6.*retardation.*(2.*a2.*a2./(R.^2-
(a2+a2)^2)+2.*a2.*a2./(R.^2-(a2-a2)^2)+log((R.^2-(a2+a2)^2)./(R.^2-(a2-
a2)^2)))./(k*T);

        end

    end
elseif model == 2
    if dec == 1             %large particle-nanoparticle interactions
        if (R-a1-a2) <= 1e-10

            E = Inf;                %HSHW portion

        else

            %modified Hogg Healy Fuersteneau model
            E = pi.*epsl.*epsn.*(k.*T./(e.^2)).*(a1.*a2./R).*(((psi1dim +
psi2dim)^2).*log(1+exp(-D.*(R-a1-a2))) + ((psi1dim - psi2dim)^2).*log(1-exp(-
D.*(R-a1-a2))));

        end
    else                            %nanoparticle-nanoparticle interactions
        if R <= (a2+a2+1e-11)

           E = Inf;                %HSHW portion
```

```
        else

            %modified Hogg Healy Fuersteneau model
            E = (4.*pi.*T.*a2.^2.*epsl.*epsn.*k.*psi2dim.^2.*log(1./exp(D.*(R
- 2.*a2)) + 1))./(R.*e.^2);

        end
    end
elseif model == 3
    if (R-a1-a2) <= 0
        E = Inf;
    else
        if (R-a1-a2) >= 2e-8
            E = 0;
        else
            E = (-2.05709e-16*(R-a1-a2) - 4.114e-24);
        end
    end
end
end
```

- Subroutine for calculating the virial coefficients.

The program was named as “virial.m”.

```
function b = virial(R, theta)
global a1 a2 x;

X = x*10^9;                          %determining the distance from any
nanoparticle to the large particle
R1 = R.*10^9;
R2 = sqrt(X.^2 + R1.^2 - 2.*X.*R1.*cos(theta));
R2 = R2./10^9;

n = length(R);
for c = 1:1:n
    if R2(c) < (a1+a2+1e-10)
        E(c) = Inf;
    else
        E(c) = ssenergy(R2(c),1);           %electrostatic energy of
interaction for a particle and a nanoparticle
    end
end

U = ssenergy(R,2);                   %electrostatic energy of interaction for
two nanoparticles

b = (exp(-E)-1).*(exp(-U)-1).*R.^2.*sin(theta);
end
```

- Subroutine for calculating the gradient

The program was name as “gradient.m”.

```
function F = gradient(R,theta)
global epsl epsn k T e Y1 Y2 a1 a2 D psi1dim psi2dim model hmmn lamdamn
if model == 1
    %Bell, Levine, and McCartney model

    retardation=1./(1+14.*(R-a1-a2)./lamdamn);
    A = 4.*pi.*epsl.*epsn.*(k.*T./e).^2.*Y1.*Y2.*a1.*a2;
    dd1=-2.*a1.*a2.*2.*R./((R.^2-(a1+a2).^2).^2);
    dd2=-2.*a1.*a2.*2.*R./((R.^2-(a1-a2).^2).^2);
    dd3=2.*R./(R.^2-(a1+a2).^2);
    dd4=-2.*R./(R.^2-(a1-a2).^2);
    vdwf=2.*a1.*a2./(R.^2-(a1+a2).^2)+2.*a1.*a2./(R.^2-(a1-a2).^2)+log((R.^2-
(a1+a2).^2)./(R.^2-(a1-a2).^2));
    F = ((A./(R.^2)).*exp(-D.*(R-a1-a2)) + (A./R).*D.*exp(-D.*(R-a1-
a2))+hmmn./6.*(retardation.*(dd1+dd2+dd3+dd4)+vdwf.*(-
14)./lamdamn.*(retardation.^2))).*cos(theta);

elseif model == 2
    %modified Hogg Healy Fuersteneau model

    A = pi*epsl*epsn*((k*T/e)^2)*a1*a2;
    X = (psi1dim + psi2dim)^2;
    Y = (psi1dim - psi2dim)^2;

    F1 = (A./(R.^2)).*(X.*log(1+exp(-D.*(R-a1-a2))) + Y.*log(1-exp(-D.*(R-a1-
a2))));
    F2 = (A./R).*(((D.*X.*exp(-D.*(R-a1-a2))./(1+exp(-D.*(R-a1-a2)))) -
((D.*Y.*exp(-D.*(R-a1-a2))./(1-exp(-D.*(R-a1-a2)))));

    F = (F1 + F2).*cos(theta);

elseif model == 3
    if (R-a1-a2) <= 0
        F = 0;
    else
        if (R-a1-a2) >= 2e-8
            F = 0;
        else
            F = 2.05709e-16*cos(theta);
        end
    end
end
end
```

- Subroutine for calculating the integration

The program was named as “integrand.m”.

```
function I = integrand(ndim, z)
global a1 rhoinf separation b1 coef;                    %global variables
```

```
E1 = ssenergy(z(1),1);                          %energy of interaction between a
nanoparticle and particle 1

R3 = separation*10^9 + (2*(a1*10^9));       %calculating the distance to
particle 2 from a point in space that
R1 = z(1)*10^9;                             %is a certain distance from
particle 1
R2 = (R3.^2 + R1.^2 - 2.*R3.*R1.*cos(z(2))).^0.5;
Re2 = R2/(10^9);

E2 = ssenergy(Re2,1);                           %energy of interaction between a
nanoparticle and particle 2

G1 = 1e15.*exp(-1e8.*z(1));                 %the Hard Sphere/Hard Wall
portion of the gradient term

G2 = gradient(z(1),z(2));                   %calculating the gradient of the
interaction energy with respect to the surface of particle 1

G = G2;

if coef == 1
    b11 = ppval(b1,z(1));                       %evaluating the 1st virial
coefficient for particles 1 and 2
    b12 = ppval(b1,Re2);
elseif coef == 0
    b11 = 0;
    b12 = 0;
end

I = rhoinf.*exp(-(E1 + E2)).*(1 + (b11 +
b12).*rhoinf).*G.*z(1).^2.*sin(z(2));      %evaluating the integrand

end
```

- Subroutine for calculating equation [3.18]

The program was named as “nrg.m”.

```
function N = nrg(x)
global pp
N = ppval(pp,x);
end
```

- Main program

The program was named as “depletion.m”.

```
clc
tic;                                %keeping track of how long the program
takes to run
```

```
global epsl epsn k T e Y1 Y2 a1 a2 D rhoinf separation x b1 psi1dim psi2dim
model pp debl coef hmmn hmnn lamdamn lamdann;      %sets variables as global
so they can be used in any functions

lamdamn=105e-9;
lamdann=130e-9;
lamdamm=95e-9;

hmmn=0.99e-20;
hmnn=1.36e-20;
hmmm=0.76e-20;

epsl = 78.54;                          %medium dielectric constant
epsn = 8.85418782E-12;                 %permittivity of free space
k = 1.3806503E-23;                     %Boltzmann's constant
T = 298;                               %temperature (K)
e = 1.60217646E-19;                    %charge of a proton
%psi1 = input('Enter the surface potential of the hard sphere in millivolts:
');
psi1 = 30;
%psi2 = input('Enter the surface potential of a macromolecule in millivolts:
');
psi2 = 70;
%if (psi1*psi2) < 0                     %ensuring the potentials have the same
sign
%    fprintf('The surface potentials need to have the same sign.');
%    psi1 = input('--Enter the correct hard sphere surface potential: ');
%    psi2 = inpit('--Enter the correct macromolecule surface potential: ');
%end
psi1 = psi1/1000;
psi1dim = (psi1*e)/(k*T);              %making the potentials dimensionless so
they can be used in the function surfpotential
psi2 = psi2/1000;
psi2dim = (psi2*e)/(k*T);
%a1 = input('Enter the radius of the hard sphere in meters: ');
a1 = 2.5e-6;
if a1 <= 0                             %ensuring the particle radii are correct
    a1 = input('--Enter the correct hard sphere radius: ');
end
%a2 = input('Enter the radius of a macromolecule in meters: ');
a2 = 10e-9;
if a2 <= 0
    a2 = input('--Enter the correct macromolecule radius: ');
end

%debl = input('Enter the Debye length in meters: ');
debl = 9.6e-9;
D = 1/debl;                            %converting the Debye length to the
Debye parameter

Y1 = surfpotential(a1,psi1dim,D);       %finding the effective surface
potentials for both particles
Y2 = surfpotential(a2,psi2dim,D);

%vol = input ('Enter the volume concentration of the macromolecules in
solution (i.e. 1% by volume => 0.01): ');
```

```
vol = 0.01;
macrovol = (4/3)*pi*(a2^3);
rhoinf = vol/macrovol;

%xmin = input ('Enter the minimum separation distance in meters: ');
xmin = 0;
%xmax = input ('Enter the maximum separation distance in meters: ');
xmax = 200e-9;

if xmin < 0 || xmax <= xmin                    %making sure the upper and
lower bounds are acceptable
    xmin = input ('--Enter a correct minimum separation distance: ');
    xmax = input ('--Enter a correct maximum separation distance: ');
end

%num = input ('Enter the number of data points you wish to consider: ');
num = 200;
xintv = (xmax - xmin)/num;          %determines the separation distance step
size
cnt = 0;                            %counter to use in for loop

dist = zeros(1,num+1);              %preallocation of dist and depforce with
zeroes
depforce = zeros(1,num+1);

b = zeros(1,101);                   %preallocation of b and sep with zeros
sep = zeros(1,101);                 %these variables will be used to store
the virial coefficient data

%fprintf('For the Bell, Levine, and McCartney model, enter 1.\n');
%fprintf('For the modified Hogg, Healy, and Fuersteneau model, enter 2.\n')
%model = input('Enter your model choice: ');
model = 1;                          %decision structure for upper and lower
limits of integration, depending on the model used
if model == 1
    lowlim = a1 + a2;
    uplim = 3*a1 + xmax + 50*debl;
elseif model == 2
    lowlim = a1 + a2 + 2e-10;
    uplim = a1 + a2 + 50*debl;
elseif model == 3
    lowlim = a1 + a2;
    uplim = 3*a1 + xmax + 50*debl;
end

%fprintf('If you wish to use virial coefficients, enter 1.\n');
%fprintf('If not, enter 0.\n');
%coef = input('Are you using virial coefficients? ');
coef = 1;                           %coef is used in integrand to decide if
the virial coefficients are going to be used

blowlim = 2*a2 + 1e-10;
buplim = 3*a1 + xmax + 50*debl;
if coef == 1
```

```
    for c1 = lowlim:5e-9:(2*a1)             %for loop to determine the virial
coefficients at a number of separation distances
        cnt = cnt + 1;                      %increment counter
        sep(cnt) = c1;
        x = c1;                             %allows the function 'virial' to
see the separation distance

        b(cnt) = dblquad(@virial,blowlim,buplim,0,pi,1e-27)*2*pi;
                                            %performing the integration in
                                            %equation (13) over all volume
                                            %so the virial coefficient can
                                            %be determined
    end

    b1 = spline(sep,b);                     %the data from the for loop above
is used to create a spline function
                                            %which can then be used to find
                                            %the virial coefficient at any
                                            %R and theta
end

cnt = 0;

c = [lowlim 0];                     %upper and lower limits of integration
for d01fc below
d = [uplim pi];
minpts = int32(0);                  %minimum and maximum number of function
evaluations allowed for d01fc
maxpts = int32(200000);
for c2 = xmin:xintv:xmax
    cnt = cnt + 1;                          %increment counter
    dist(cnt) = c2;
    separation = c2;                        %allows the function 'integrand'
to see the separation distance

    [minpts2, acc, finval, ifail] = d01fc(c, d, minpts, maxpts, 'integrand',
1e-6);
    depforce(cnt) = finval*2*pi;            %multiplying by 2*pi since the
integral is symetrical about the phi axis

end


energy1 = depforce./(k*T);              %creating a spline for the depletion
force so it can be easily integrated
energy = zeros(1,num+1);
pp = spline(dist,energy1);
nlimit = int32(100000);                 %maximum number of function
evaluations allowed for d01ah
for c3 = 1:1:num+1                      %for loop to allow the integration
to proceed over the range of separation distances the user picked

    [result, npts, relerr, ifail] = d01ah(dist(c3), xmax, 1e-5, 'nrg',
nlimit);
    energy(c3) = result;
```

```
end

nmdist = dist.*10^9;
figure('Name','Depletion Interaction Force');
plot(nmdist,depforce)                       %plotting the total force at each
separation distance
xlabel ('Separation Distance (nm)');      %axes labels
ylabel ('Total Interaction Force (N)');

h1=nmdist./(1e9);
sizeh1=size(h1);

for c1=1:sizeh1(2)
    h2=h1(c1);
    R2=h2+2*a1;

    retardation=1./(1+14.*(R2-a1-a1)./lamdamm);
    A = 4.*pi.*epsl.*epsn.*(k.*T./e).^2.*Y1.*Y1.*a1.*a1;
    dd1=-2.*a1.*a1.*2.*R2./((R2.^2-(a1+a1).^2).^2);
    dd2=-2.*a1.*a1.*2.*R2./((R2.^2-(a1-a1).^2).^2);
    dd3=2.*R2./(R2.^2-(a1+a1).^2);
    dd4=-2.*R2./(R2.^2-(a1-a1).^2);
    vdwf=2.*a1.*a1./(R2.^2-(a1+a1).^2)+2.*a1.*a1./(R2.^2-(a1-
a1).^2)+log((R2.^2-(a1+a1).^2)./(R2.^2-(a1-a1).^2));
    F(c1) = (A./(R2.^2)).*exp(-D.*(R2-a1-a1)) + (A./R2).*D.*exp(-D.*(R2-a1-
a1))+hmmm./6.*(retardation.*(dd1+dd2+dd3+dd4)+vdwf.*(-
14)./lamdamm.*(retardation.^2));

    depforce(c1)=depforce(c1)+F(c1);

end

figure('Name','Total Force');
plot(nmdist,energy)                         %plotting the total energy at each
separation distance
xlabel ('Separation Distance (nm)');      %axes labels
ylabel ('Total Interaction Energy (kT)');

data = [nmdist' depforce' energy'];
xlswrite('StraightLineModel_-0.001kT.xls', data);
toc;
```

A4. Matlab Program for the Square Well Model

The program was named as “hardsphere.m”.

```
k = 1.3806503E-23;
T = 298;

R = 2500;
a = 55;

%vol = input ('Enter the volume concentration of the macromolecules in
solution (i.e. 1% by volume => 0.01): ');
vol = 0.05;
macrovol = (4/3)*pi*(a^3);
rhoinf = vol/macrovol;

tau1 = a+20;
tau2 = a+60;
tau3 = a+120;

eps1 = 1096;
eps2 = 0.9996645;

hmin = 0;
hmax = 1000;
hstep = 0.5;

h = zeros(1,5);
F = zeros(1,5);

c = 1;
for cnt = hmin:hstep:hmax
    h(c) = cnt;
    el = cnt + 2*R;

    if (2*R) <= el && el <= (2*(R+tau1))
        T1 = (R+tau1)^2*(1+eps1)*(-1)*(1 - (el/(2*(R+tau1)))^2);
    else
        T1 = 0;
    end

    if (2*R) <= el && el <= (2*R+tau1+tau2)
        if (2*R) <= el && el <= (2*(R+tau1))
            T2 = (R+tau1)^2*(1+eps1)*(eps1)*((el/(2*(R+tau1)))^2 - ((el^2 +
(R+tau1)^2 - (R+tau2)^2)/(2*el*(R+tau1)))^2);
        else
            T2 = (R+tau1)^2*(1+eps1)*(eps1)*(1 - ((el^2 + (R+tau1)^2 -
(R+tau2)^2)/(2*el*(R+tau1)))^2);
        end
    else
        T2 = 0;
    end

    if (2*R) <= el && el <= (2*R+tau1+tau3)
```

```
        if (2*R) <= el && el <= (2*R+tau1+tau2)
            T3 = (R+tau1)^2*(1+eps1)*(-eps2)*(((el^2 + (R+tau1)^2 -
(R+tau2)^2)/(2*el*(R+tau1)))^2 - ((el^2 + (R+tau1)^2 -
(R+tau3)^2)/(2*el*(R+tau1)))^2);
        else
            T3 = (R+tau1)^2*(1+eps1)*(-eps2)*(1 - ((el^2 + (R+tau1)^2 -
(R+tau3)^2)/(2*el*(R+tau1)))^2);
        end
    else
        T3 = 0;
    end

    if (2*R) <= el && el <= (2*R+tau1+tau2)
        T4 = (R+tau2)^2*(-(eps1+eps2))*(-1)*(1 - ((el^2 + (R+tau2)^2 -
(R+tau1)^2)/(2*el*(R+tau2)))^2);
    else
        T4 = 0;
    end

    if (2*R) <= el && el <= (2*(R+tau2))
        if (2*R) <= el && el <= (2*R+tau1+tau2)
            T5 = (R+tau2)^2*(-(eps1+eps2))*(eps1)*(((el^2 + (R+tau2)^2 -
(R+tau1)^2)/(2*el*(R+tau2)))^2 - (el/(2*(R+tau2)))^2);
        else
            T5 = (R+tau2)^2*(-(eps1+eps2))*(eps1)*(1 - (el/(2*(R+tau2)))^2);
        end
    else
        T5 = 0;
    end

    if (2*R) <= el && el <= (2*R+tau2+tau3)
        if (2*R) <= el && el <= (2*(R+tau2))
            T6 = (R+tau2)^2*(-(eps1+eps2))*(-eps2)*((el/(2*(R+tau2)))^2 -
((el^2 + (R+tau2)^2 - (R+tau3)^2)/(2*el*(R+tau2)))^2);
        else
            T6 = (R+tau2)^2*(-(eps1+eps2))*(-eps2)*(1 - ((el^2 + (R+tau2)^2 -
(R+tau3)^2)/(2*el*(R+tau2)))^2);
        end
    else
        T6 = 0;
    end

    if (2*R) <= el && el <= (2*R+tau3+tau1)
        T7 = (R+tau3)^2*(eps2)*(-1)*(1 - ((el^2 + (R+tau3)^2 -
(R+tau1)^2)/(2*el*(R+tau3)))^2);
    else
        T7 = 0;
    end

    if (2*R) <=el && el <= (2*R+tau3+tau2)
        if (2*R) <= el && el <= (2*R+tau1+tau3)
            T8 = (R+tau3)^2*(eps2)*(eps1)*(((el^2 + (R+tau3)^2 -
(R+tau1)^2)/(2*el*(R+tau3)))^2 - ((el^2 + (R+tau3)^2 -
(R+tau2)^2)/(2*el*(R+tau3)))^2);
        else
```

```
            T8 = (R+tau3)^2*(eps2)*(eps1)*(1 - ((el^2 + (R+tau3)^2 -
(R+tau2)^2)/(2*el*(R+tau3)))^2);
        end
    else
        T8 = 0;
    end

    if (2*R) <= el && el <= (2*(R+tau3))
        if (2*R) <= el && el <= (2*R+tau2+tau3)
            T9 = (R+tau3)^2*(eps2)*(-eps2)*(((el^2 + (R+tau3)^2 -
(R+tau2)^2)/(2*el*(R+tau3)))^2 - (el/(2*(R+tau3)))^2);
        else
            T9 = (R+tau3)^2*(eps2)*(-eps2)*(1 - (el/(2*(R+tau3)))^2);
        end
    else
        T9 = 0;
    end

    %fprintf('h = %f        T1 = %f         T2 = %f\n',cnt,T1,T2);

    A = T1+T2+T3+T4+T5+T6+T7+T8+T9;
    B = A*10^9;
    F(c) = pi*rhoinf*k*T*B;
    c = c + 1;
end

h1=h.*(1e-9);
hold off
plot(h,F);
```

A5. Spectra Data Used to Calculate Hamaker Constants with Lifshitz Theory

Table A2. Spectra data for pure water.[100]

Microwave frequencies		
d=74.8	1/τ=6.55e-5 eV	
Infrared frequencies		
ωj/, eV	fj, $(eV)^2$	gj, eV
2.67e-2	6.25e-4	1.5e-2
6.9e-2	3.5e-3	3.8e-2
9.2e-2	1.28e-3	2.8e-2
2.0e-1	5.44e-4	2.5e-2
4.2e-1	1.35e-2	5.6e-2
Ultraviolet frequencies		
ωj/, eV	fj, $(eV)^2$	gj, eV
8.25	2.68	0.51
10.0	5.67	0.88
11.4	12.0	1.54
13.0	26.3	2.05
14.9	33.8	2.96
18.5	92.8	6.26

Table A3. Spectra data for polystyrene.[101]

ωj/, eV	fj, $(eV)^2$	gj, eV
6.4	14.6	0.65
14.0	96.9	5.0
11.0	44.4	3.5
20.1	136.9	11.5

Table A4. Spectra data for silica.[102]

Infrared frequencies	
ωj (e14 rad/s)	fj
1.88	1.71
Ultraviolet frequencies	
ωj (e16 rad/s)	fj
2.033	1.098

References

1. Vincent, B., The Effect of Adsorbed Polymers On Dispersion Stability. *Adv. Colloid Interface Sci.* **1974,** *4,* 193.
2. Napper, D. H., Steric Stabilization. *J. Colloid Interface Sci.* **1976,** *58,* 390.
3. Tohver, V.; Smay, J. E.; Braem, A.; Braun, P. V.; Lewis, J. A., Nanoparticle Halos: A New Colloid Stabilization Mechanism. *PNAS* **2001,** *98,* 8950-8954.
4. Asakura, S.; Oosawa, F., Interaction between Particles Suspended in Solutions of Macromolecules. *J. Polym. Sci.* **1958,** *33,* 183-192.
5. Asakura, S.; Oosawa, F., On Interaction between Two Bodies Immersed in a Solution of Macromolecules. *J. Chem. Phys.* **1954,** *22,* 1255-1256.
6. Feigin, R. I.; Napper, D. H., Stabilization of Colloids by Free Polymer. *J. Colloid Interface Sci.* **1980,** *74*.
7. Mao, Y.; Cates, M. E.; Lekkerkerker, H. N. W., Depletion Force in Colloidal Systems. *Physica A* **1995,** *222,* 10-24.
8. Walz, J. Y.; Sharma, A., Effect of Long Range Interactions on the Depletion Force between Colloid Particles. *J. Colloid Interface Sci.* **1994,** *168,* 485-496.
9. Piech, M.; Walz, J. Y., Effect of Polydispersity and Charge Heterogeneity on the Depletion Interaction in Colloidal Systems. *J. Colloid Interface Sci.* **2000,** *225,* 134-146.
10. Piech, M.; Walz, J. Y., Depletion Interactions Produced by Nonadsorbing Charged and Uncharged Spheroids. *J. Colloid Interface Sci.* **2000,** *232,* 86-101.
11. Fazelabdolabadi, B.; Walz, J. Y.; Tassel, P. R. V., Influence of Charged Nanoparticles on Colloidal Forces: A Molecular Simulation Study. *J. Phys. Chem. B* **2009,** *113,* 13860.
12. Weroński, P.; Walz, J. Y., An Approximate Method for Calculating Depletion and Structural Interactions between Colloidal Particles. *J. Colloid Interface Sci.* **2003,** *263,* 327-332.
13. Trokhymchuk, A.; Henderson, D.; Nikolov, A.; Wasan, D. T., Computer Modeling of Ionic Micelle Structuring in Thin Films. *J. Phys. Chem. B* **2003,** *107,* 3927.
14. Dzubiella, J.; Löwen, H.; Likos, C., Depletion Forces in Nonequilibrium. *Phys. Rev. Lett.* **2003,** *91,* 248301-1.
15. Piech, M.; Weronski, P.; Wu, X.; Walz, J. Y., Prediction and Measurement of the Interparticle Depletion Interaction Next to a Flat Wall. *J. Colloid Interface Sci.* **2002,** *247,* 327-341.
16. Ferreira, P. G.; Dymitrowska, M.; Belloni, L., Mixtures of Charged Colloids and Nonadsorbing Flexible Polyelectrolytes: An Integral Equation Study. *J. Chem. Phys* **2000,** *113,* 9849.
17. Garibay-Alonso, R.; Mendez-Alcaraz, J. M.; Klein, R., Phase Separation of Binary Liquid Mixtures of Hard Spheres and Yukawa Particles. *Physica A* **1997,** *235,* 159-169.
18. Walz, J. Y., Effect of Polydispersity on the Depletion Interaction between Colloidal Particles. *J. Colloid Interface Sci.* **1996,** *178,* 505-513.
19. González-Mozuelos, P.; Alejandre, J., Rogers–Young approximation for the concentration profile of a colloidal suspension in front of a highly repulsive wall. *J. Chem. Phys* **1996,** *105,* 5949.

20. Gonzhlez-Mozuelos, P.; Medina-Noyola, M., Electrostatic Trapping of a Colloidal Monolayer near a Charged Wall. *J. Chem. Phys* **1990,** *94*.
21. Mendez-Alcaraz, J. M.; Klein, R., Depletion Forces in Colloidal Mixtures. *Phys. Rev. E* **2000,** *61,* 4095-4099.
22. Trokhymchuk, A.; Henderson, D.; Nikolov, A.; Wasan, D. T., Depletion and Structural Forces between Two Macrosurfaces Immersed in a Bidisperse Colloidal Suspension. *J. Colloid Interface Sci.* **2001,** *243,* 116-127.
23. Jamnik, A., Effective Interaction between Large Colloidal Particles Immersed in a Bidisperse Suspension of Short-Ranged Attractive Colloids. *J. Chem. Phys.* **2009,** *131,* 1-8.
24. Sharma, A.; Walz, J. Y., Direct Measurement of the Depletion Interaction in a Charged Colloidal Dispersion. *J. Chem. Soc., Faraday Trans.* **1996,** *92,* 4997.
25. Odiachi, P. C.; Prieve, D. C., Effect of Added Salt on the Depletion Attraction Caused by Non-Adsorbing Clay Particles. *Colloids Surf. A* **1999,** *146,* 315-328.
26. Piech, M.; Walz, J. Y., Direct Measurement of Depletion and Structural Forces in Polydisperse, Charged Systems. *J. Colloid Interface Sci.* **2002,** *253,* 117-129.
27. Helden, L.; Koenderink, G. H.; Leiderer, P.; Bechinger, C., Depletion Potentials Induced by Charged Colloidal Rods. *Langmuir* **2004,** *20,* 5662-5665.
28. Tulpar, A.; Walz, J., Simultaneous Measurement of Structural and Hydrodynamic Forces between Colloidal Surfaces in Complex Fluids. *Colloids Surf. A* **2007,** *300,* 268-280.
29. Zeng, Y.; von Klitzing, R., Structuring of Colloidal Suspensions Confined between a Silica Microsphere and an Air Bubble. *Soft Matter* **2011,** *7,* 5329-5338.
30. von Klitzing, R.; Thormann, E.; Nylander, T.; Langevin, D.; Stubenrauch, C., Confinement of Linear Polymers, Surfactants, and Particles between Interfaces. *Adv. Colloid Interface Sci.* **2010,** *155,* 19-31.
31. Verma, R.; Crocker, J. C.; Lubensky, T. C.; Yodh, A. G., Entropic Colloidal Interactions in Concentrated DNA Solutions. *Phys. Rev. Lett.* **1998,** *81,* 4004.
32. Van Winkle, D. H.; Murray, C. A., Layering in Colloidal Fluids near a Smooth Repulsive Wall. *J. Chem. Phys* **1988,** *89,* 3885.
33. Tulpar, A.; Tassel, P. R. V.; Walz, J. Y., Structuring of Macroions Confined between Like-Charged Surfaces. *Langmuir* **2006,** *22,* 2876.
34. Drelich, J.; Long, J.; Xu, Z.; Masliyah, J.; Nalaskowski, J.; Beauchamp, R.; Liu, Y., AFM Colloidal Forces Measured between Microscopic Probes and Flat Substrates in Nanoparticle Suspensions. *J. Colloid Interface Sci.* **2006,** *301,* 511-22.
35. Sharma, A.; Tan, S. N.; Walz, J. Y., Effect of Nonadsorbing Polyelectrolytes on Colloidal Interactions in Aqueous Mixtures. *J. Colloid Interface Sci.* **1997,** *191,* 236.
36. Sober, D. L.; Walz, J. Y., Measurement of Long Range Depletion Energies between a Colloidal Particle and a Flat Surface in Micellar Solutions. *Langmuir* **1995,** *11,* 2352.
37. Rudhardt, D.; Bechinger, C.; Leiderer, P., Direct Measurement of Depletion Potentials in Mixtures of Colloids and Nonionic Polymers. *Phys. Rev. Lett.* **1998,** *81,* 1331-1333.

38. Rudhardt, D.; Bechinger, C.; Leiderer, P., Repulsive Depletion Interactions in Colloid-Polymer Mixtures. *J. Phys.: Condens. Matter* **1999,** *11,* 10073.
39. Prieve, D. C.; Frej, N. A., Total Internal Reflection Microscopy: A Quantitative Tool for the Measurement of Colloidal Forces. *Langmuir* **1990,** *6,* 396-403.
40. Pagac, E. S.; Tilton, R. D.; Pieve, D. C., Depletion Attraction Caused by Unadsorbed Polyelectrolytes. *Langmuir* **1998,** *14,* 5106-5112.
41. Crocker, J. C.; Matteo, J. A.; Dinsmore, A. D.; Yodh, A. G., Entropic Attraction and Repulsion in Binary Colloids Probed with a Line Optical Tweezer. *phys. Rev. Lett.* **1999,** *82,* 4352-4355.
42. Marra, J.; Hair, M. L., Double-Layer Forces in Nonadsorbing Ionic Micellar Solutions and Polyelectrolyte Solutions. *J. Colloid Interface Sci.* **1988,** *128,* 511-522.
43. Richetti, P.; Kékicheff, P., Direct Measurement of Depletion and Structural Forces in a Micellar System. *phys. Rev. Lett.* **1992,** *68,* 1951-1954.
44. Freyssingeas, E.; Thuresson, K.; Nylander, T.; Joabsson, F.; Lindman, B., A Surface Force, Light Scattering, and Osmotic Pressure Study of Semidilute Aqueous Solutions of Ethyl(hydroxyethyl)cellulosesLong-Range Attractive Force between Two Polymer-Coated Surfaces. *Langmuir* **1998,** *14,* 5877.
45. Parker, J.; Richetti, P.; Kékicheff, P.; Sarman, S., Direct Measurement of Structural Forces in a Supermolecular Fluid. *phys. Rev. Lett.* **1992,** *68,* 1955-1958.
46. Milling, A.; Biggs, S., Direct Measurement of the Depletion Force Using an Atomic Force Microscope. *J. Colloid Interface Sci.* **1995,** *170,* 604-606.
47. Milling, A. J.; Vincent, B., Depletion Forces between Silica Surfaces in Solutions of Poly(acrylic acid). *J. Chem. Soc., Faraday Trans.* **1997,** *93,* 3179-3183.
48. Biggs, S.; Burns, J. L.; Yan, Y.-d.; Jameson, G. J.; Jenkins, P., Molecular Weight Dependence of the Depletion Interaction between Silica Surfaces in Solutions of Sodium Poly (styrene sulfonate). *Langmuir* **2000,** *16,* 9242.
49. Piech, M.; Walz, J., The Structuring of Nonadsorbed Nanoparticles and Polyelectrolyte Chains in the Gap between a Colloidal Particle and Plate. *J. Phys. Chem. B* **2004,** *108,* 9177.
50. Xu, W.; Nikolov, A. D.; Wasan, D. T., Role of Depletion and Surface-Induced Structural Forces in Bidisperse Suspensions. *AICHE J.* **1997,** *43,* 3215-3222.
51. Bondy, C., The Creaming of Rubber Latex. *Trans. Faraday Soc.* **1939,** *35,* 1093-1108.
52. Sharma, A.; Tan, S. N.; Walz, J. Y., Measurement of Colloidal Stability in Solutions of Simple, Nonadsorbing Polyelectrolytes. **1997**.
53. Cowell, C.; Li-In-On, R.; Vincent, B., Reversible Flocculation of Sterically-stabilised Dispersions. *J. Chem. Soc. Faraday Trans.* **1977,** *74,* 337-347.
54. Sperry, P. R.; Hopfenberg, H. B.; Thomas, N. L., Flocculation of Latex by Water-Soluble Polymers: Experimental Confirmation of a Nonbridging, Nonadsorptive, Volume-Restriction Mechanism. *J Colloid Interface Sci.* **1980,** *82,* 62-76.
55. Kiratzis, N.; Faers, M.; Luckham, P. F., Depletion flocculation of particulate systems induced by hydroxyethylcellulose. *Colloids and Surfaces a-Physicochemical and Engineering Aspects* **1999,** *151,* 461-471.

56. Seebergh, J. E.; Berg, J. C., Depletion Flocculation of Aqueous, Electrosterically-Stabilized Latex Dispersions. *Langmuir* **1994,** *10,* 454-463.
57. Furusawa, K.; Sato, A.; Shirai, J.; Nashima, T., Depletion flocculation of latex dispersion in ionic micellar systems. *J Colloid Interface Sci* **2002,** *253,* 273-8.
58. Liang, W.; Tadros, T. F.; Luckham, P. F., Flocculation of Sterically Stabilized Polystyrene Latex Particles by Adsorbing and Nonadsorbing Poly(acrylic acid). *Langmuir* **1994,** *10,* 441-446.
59. Sun, X.; Danumah, C.; Liu, Y.; Boluk, Y., Flocculation of bacteria by depletion interactions due to rod-shaped cellulose nanocrystals. *Chemical Engineering Journal* **2012,** *198-199,* 476-481.
60. Tohver, V.; Chan, A.; Sakurada, O.; Lewis, J. A., Nanoparticle Engineering of Complex Fluid Behavior. *Langmuir* **2001,** *17,* 8414-8421.
61. Chan, A. T.; Lewis, J. A., Electrostatically Tuned Interactions in Silica Microsphere-Polystyrene Nanoparticle Mixtures. *Langmuir* **2005,** *21,* 9978-9989.
62. Martinez, C. J.; Liu, J.; Rhodes, S. K.; Luijten, E.; Weeks, E. R.; Lewis, J. A., Interparticle Interactions and Direct Imaging of Colloidal Phases Assembled from Microsphere-Nanoparticle Mixtures. *Langmuir* **2005,** *21,* 9978-9989.
63. Liu, J.; Luijten, E., Generalized Geometric Cluster Algorithm for Fluid Simulation. *Physical Review E* **2005,** *71*.
64. Liu, J.; Luijten, E., Colloidal Stabilization via Nanoparticle Halo Formation. *Phys. Rev. E* **2005,** *72*.
65. Liu, J.; Luijten, E., Rejection-Free Geometric Cluster Algorithm for Complex Fluids. *Physical Review Letters* **2004,** *92*.
66. Liu, J.; Luijten, E., Stabilization of Colloidal Suspensions by Means of Highly Charged Nanoparticles. *Phys. Rev. Lett.* **2004,** *93*.
67. Chan, A. T.; Lewis, J. A., Size Ratio Effects on Interparticle Interactions and Phase Behavior of Microsphere-Nanoparticle Mixtures. *Langmuir* **2008,** *24,* 11399.
68. Chávez-Páez, M.; González-Mozuelos, P.; Medina-Noyola, M.; Méndez-Alcaraz, J. M., Polyion Monolayers and Halos around Large Weakly-Charged Colloids. *Physica A* **2004,** *341,* 1-22.
69. Kong, D.; Yang, H.; Yang, Y.; Wei, S.; Wang, J.; Cheng, B., Dispersion Behavior and Stabilization Mechanism of Alumina Powders in Silica Sol. *Mater. Lett.* **2004,** *58,* 3503-3508.
70. Zhang, F.; Long, G. G.; Jemian, P. R.; Ilavsky, J., Quantitative Measurement of Nanoparticle Halo Formation around Colloidal Microspheres in Binary Mixtures. *Langmuir* **2008,** *24,* 6504-6508.
71. Hong, X.; Willing, G. A., Transition Force Measurement between Two Negligibly Charged Surfaces: A New Perspective on Nanoparticle Halos. *Langmuir* **2009,** *25,* 4929-4933.
72. McKee, C. T.; Walz, J. Y., Interaction Forces between Colloidal Particles in a Solution of Like-Charged, Adsorbing Nanoparticles. *J. Colloid Interface Sci.* **2012,** *365,* 72-80.
73. Tulpar, A.; Tilton, R. D.; Walz, J. Y., Synergistic Effects of Polymers and Surfactants on Depletion Forces. *Langmuir* **2007,** *23,* 4351-4357.

74. Bell, G. M.; Levine, S.; McCartney, L. N., Approximate Methods of Determining the Double-Layer Free Energy of Interaction between Two Charged Colloidal Spheres. *J. Colloid Interface Sci.* **1970,** *33,* 335.
75. Hamaker, H. C., The London—van der Waals Attraction between Spherical Particles. *Physica* **1937,** *4,* 1058.
76. Gregory, J., Approximate Expressions for Retarded van der Waals Interaction *J. Colloid Interface Sci.* **1981a,** *83,* 138.
77. Prieve, D. C.; Russel, W. B., Simplified Predictions of Hamaker Constants from Lifshitz Theory. *J. Colloid Interface Sci.* **1987,** *125,* 1.
78. Bellemans, A., Statistical Mechanics of Surface Phenomena. *Physica* **1962,** *28,* 493-510.
79. Fischer, J., A Fluid in Contact with a Wall: The Percus-Yevick versus the Superposition Approximation. *Molec. Phys.* **1977,** *33,* 75.
80. ANDERSON, J. L.; BRANNON, J. H., Concentration Dependence of the Distribution Coefficient for Macromolecules in Porous Media. *J. Polym. Sci. Polym. Phys. Ed.* **1981,** *19,* 405.
81. GLANDT, E. D., Density Distribution of Hard-Spherical Molecules inside Small Pores of Various Shapes. *J. Colloid Interface Sci.* **1980,** *77,* 512.
82. Binnig, G.; Quate, C. F., Atomic Force Microscope. *Phys. Rev. Lett.* **1986,** *56,* 930-933.
83. Butt, H.-J., Measuring Electrostatic, van der Waals, and Hydration Forces in Electrolyte Solutions with an Atomic Force Microscope. *Biophys. J.* **1991,** *60,* 1438.
84. Ducker, W.; Senden, T., Measurement of Forces in Liquids Using a Force Microscope. *Langmuir* **1992**.
85. Ducker, W. A.; Senden, T. J.; Pashley, R. M., Direct Measurement of Colloidal Forces Using an Atomic Force Microscope. *Nature* **1991,** *353,* 239.
86. Hutter, J. L.; Bechhoefer, J., Calibration of Atomic-Force Microscope Tips. *Rev. Sci. Instrum.* **1993,** *64,* 1868-1873.
87. Butt, H.-J.; Cappella, B.; Kappl, M., Force Measurements with the Atomic Force Microscope: Technique, Interpretation and Applications. *Surf. Sci. Rep.* **2005,** *59,* 1-152.
88. Scales, P. J.; Grieser, F.; Healy, T. W., Electrokinetics of the Silica-Solution Interface: A Flat Plate Streaming Potential Study. *Langmuir* **1992,** *8,* 965.
89. Bergstrom, L.; Meurk, A.; Arwin, H.; Rowcliffe, D. J., Estimation of Hamaker Constants of Ceramic Materials from Optical Data Using Lifshitz Theory. *J. Am. Ceram. Soc.* **1996,** *79,* 339-348.
90. Parsegian, V. A.; Weiss, G. H., Spectroscopic Parameters for Computation of Van Der Waals Forces. *J. Colloid Interface Sci.* **1981,** *81,* 285-289.
91. Piech, M.; Walz, J. Y., Analytical Expressions for Calculating the Depletion Interaction Produced by Charged Spheres and Spheroids. *Langmuir* **2000,** *16,* 7895-7899.
92. James, D.; Thiel, D. V.; Bushell, G. R.; Busfield, W. K.; Mackay-Sim, A., Phase Change and Viscosity Effects on a Quartz Crystal Microbalance. *Analyst* **1994,** *119,* 2005-2007.

93. Liufu, S.; Xiao, H.; Li, Y., Adsorption of Poly(acrylic acid) onto the Surface of Titanium Dioxide and the Colloidal Stability of Aqueous Suspension. *J. Colloid Interface Sci.* **2005,** *281,* 155-163.
94. Luderitz, L. A.; von Klitzing, R., Scanning of Silicon Wafers in Contact with Aqueous CTAB Solutions below the CMC. *Langmuir* **2012,** *28,* 3360-3368.
95. Piech, M. Depletion and Structural Interactions in Charged Colloidal Systems. Dissertation, Yale University, New Haven, Connecticut, 2003.
96. Ji, S.; Walz, J. Y., Synergistic effects of Nanoparticles and polymers on Depletion and Structural Interactions. *Submitted to Langmuir* **2013**.
97. Hunter, R. J., In *Foundations of Colloid Science*, Oxford University Press: New York, 2009; pp 549-552.
98. Feigin, R. I.; Napper, D. H., Depletion Stabilization and Depletion Flocculation. *J. Colloid Interface Sci.* **1980,** *75,* 525-541.
99. Hogg, R.; Yang, K. C., Secondary Coagulation. *J Colloid Interface Sci.* **1976,** *56,* 573-577.
100. Parsegian, V. A., *"Van Der Waals Forces A Handbook for Biologists, Chemists, Engineers, and Physicists,"*. Cambridge Univ. Press: New York, NY, 2006.
101. PAINTER, L. R.; ARAKAWA, E. T.; WILLIAMS, M. W.; ASHLEY, J. C., Optical Properties of Polyethylene: Measurement and Applications. *Rad. Res* **1980,** *83,* 1.
102. Hough, D. B.; White, L. R., The Calculation of Hamaker Constant from Lifshitz Theory with Applications To Wetting Phenomena. *Adv. Colloid Interface Sci.* **1980,** *14,* 3.